Diagnosis of a wind turbine using wireless sensor networks

Lavinius Ioan Gliga

THÈSE EN CO - TUTELLE INTERNATIONALE

Pour obtenir le diplôme de doctorat

Spécialité : Automatique, Signal, Productique, Robotique

Préparée au sein de Université de Rouen Normandie
et de Université « Politehnica » de Bucarest

Diagnostic d'une Turbine Eolienne à Distance à l'aide du Réseau de Capteurs sans Fil

Présentée et soutenue par
Lavinius Ioan GLIGA

Thèse soutenue publiquement le 19.11.2019 devant le jury composé de		
Mme. Cristina MANIU	Professeur à CentraleSupelec, Paris	Rapporteur
M. Radu-Emil PRECUP	Professeur à l'Université « Politehnica » de Timișoara, Timișoara	Rapporteur
M. Moussa BOUKHNIFER	Professeur á l'École Nationale d'Ingénieurs de Metz, Université de Lorraine, Metz	Examinateur
M. Jérôme BOSCHE	MCF-HdR á l'Université de Picardie « Jules Verne », Amiens	Examinateur
M. Dan ȘTEFĂNOIU	Professeur à l'Université « Politehnica » de Bucarest, Bucarest	Examinateur
M. Redouane KHEMMAR	EC á l'ESIGELEC, Rouen	Examinateur
M. Houcine CHAFOUK	EC-HdR á l'ESIGELEC, Rouen	Codirecteur de thèse
M. Dumitru POPESCU	Professeur à l'Université « Politehnica » de Bucarest, Bucarest	Directeur de thèse

Thèse dirigée par

M. Houcine CHAFOUK — Université de Rouen Normandie
M. Dumitru POPESCU — Université « Politehnica » de Bucarest

UNIVERSITY "POLITEHNICA" OF BUCHAREST
NORMANDY UNIVERSITY

DOCTORAL THESIS

Diagnosis of a Wind Turbine using Wireless Sensor Networks

Author:
Lavinius Ioan GLIGA

Supervisors:
Prof. Dumitru POPESCU
Prof. Houcine CHAFOUK

A thesis submitted in fulfillment of the requirements for the degree of Doctor of Philosophy

in the

Doctoral School of Automatic Control and Computer Science
Doctoral School of Mathematics, Information and Systems Engineering

November 19, 2019

Declaration of Authorship

I, Lavinius Ioan GLIGA, declare that this thesis titled, "Diagnosis of a Wind Turbine using Wireless Sensor Networks" and the work presented in it are my own. I confirm that:

- This work was done wholly or mainly while in candidature for a research degree at these universities;
- Where any part of this thesis has previously been submitted for a degree or any other qualification at these universities or any other institution, this has been clearly stated;
- Where I have consulted the published work of others, this is always clearly attributed;
- Where I have quoted from the work of others, the source is always given. With the exception of such quotations, this thesis is entirely my own work;
- I have acknowledged all main sources of help;
- Where the thesis is based on work done by myself jointly with others, I have made clear exactly what was done by others and what I have contributed myself.

Signed:

_____

Date:

_____

"*For you created my inmost being;*
you knit me together in my mother's womb.
I praise you because I am fearfully and wonderfully made;
your works are wonderful,
I know that full well.
My frame was not hidden from you
when I was made in the secret place,
when I was woven together in the depths of the earth.
Your eyes saw my unformed body;
all the days ordained for me were written in your book
before one of them came to be.
How precious to me are your thoughts, God!
How vast is the sum of them!
Were I to count them,
they would outnumber the grains of sand—
when I awake, I am still with you."

Psalm 139:13-18

Acknowledgements

I thank my two supervisors, Mr. Houcine CHAFOUK and Mr. Dumitru POPESCU, for their confidence in me, and for their encouragements during the thesis. I also thank them for their support, especially in untangling the complexities of administrative tasks. Moreover, I am grateful for their guidance and for the discussions we had together. From them, I learnt how to organize and manage my work and my time.

I deeply thank Ms. Cristina STOICA MANIU and Mr. Radu-Emil PRECUP, for the time and energy they devoted to analyzing the manuscript. Only through their critical analysis can I continue to develop, and this work can be polished.

I am grateful towards Mr. Moussa BOUKHNIFER, Mr. Jérôme BOSCHE, Mr. Dan ȘTEFĂNOIU and Mr. Redouane KHEMMAR. Together with the previous two professors, they accepted to devote their time and energy to examine this work and be part of the jury.

I thank the two research and educational institutions where I worked during my thesis: the IRSEEM laboratory from France and the AIS department from Romania. I had the pleasure of conducting this research while meeting friendly and warm people, who helped create a good work environment. Among them, because there are too many to mention, are Mr. Ciprian LUPU, Mr. Nicolas LANGLOIS, Mr. Cătălin PETRESCU, Mr. Vincent SIRCOULOMB, Ms. Janetta CULIȚĂ and Mr. Cristian OARĂ.

Before going forward, I want to express my deepest gratitude towards two other persons who helped me during my thesis: Ms. Kawthar ALAMEH and Mr. Bogdan CIUBOTARU. Their words of encouragements, their advices and their listening were crucial to the success of this thesis.

Thankfully, I also made friends in the two institutions where I worked. Some of them are Severus, Abdelkarim, Cătălin, Ahmad[2], Irina, Jiawei, Florin, Déziré, Andreea, Shirin, Marwa and Houssam. All of them are great persons and researchers. I am happy to have met them and I am grateful for the time spend together.

I am also grateful for my friends, which supported me during these years and with whom I spent memorable moments: Robi, Claudiu, Mihai, Cosmin, Tresti, John, and Valentin. I heard the saying "my brother from another mother", and with them I found out how true it is.

I thank everyone from the Baptist Evangelical Church of Rouen. They were a second family for me. Among the many, I only mention Nathan, Sara and Nathanael.

I am extremely grateful for my family: Sorina, Cristi, Anca and Laurențiu. Without them, I would not exist, and I would not be the person I am today. They have been with me since my birth and they will always be with me. I

know I can always rely on them and that we shall always each other's back. I am also very excited about my future nephew/niece.

Towards the end of my thesis I met a stranger. After some time, I saw her for the shinning brilliant she is. And then I could not help falling in love with her. She has been my inspiration and support ever since. Because to her this thesis is over, and with her I see my future. I thank you, Lina, for you and for your presence. I love you.

Firstly, because He is the most important, I thank God. I had both difficult and happy moments during my thesis. He gave me the difficult moments to push me to grow and He gave the good ones for me to rejoice. He gave me all the people I previously mentioned - after He prepared me, and at the right time. I thank Him for everything He has given and will give me. I know He loves me, and He is always with me.

Contents

List of Figures

List of Tables

List of Abbreviations

a posteriori	(en: from the latter)
a priori	(en: from the former)
AES	**A**dvanced **E**ncryption **S**tandard
AI	**A**rtificial **I**ntelligence
ANT	**A**daptive **N**etwork **T**opology
ARMAX	**A**uto-**R**egressive **M**oving **A**verageeX**o**genous
ARR	**A**nalytic **R**edundancy **R**elation
BLE	**B**luetooth **L**ow **E**nergy
C&C	**C**command **&** **C**ontrol
CM	**C**ondition **M**onitoring
CS	**C**ontrol **S**ystem
DC	**D**irect **C**urrrent
DDoS	**D**istributed **DoS**
DDWT	**D**irect **D**rive **W**ind **T**urbine
de facto	(en: in fact)
DEF	**D**ynamic **E**ccentricity **F**ault
DFIG	**D**oubly-**F**ed **I**induction **G**enerator
DFT	**D**iscrete **F**ourier **T**ransform
DMF	**D**e**M**agnetization **F**ault
DoS	**D**enial **o**f **S**ervice
dq0	**d**irect-**q**uadrature-**zero**
DSSS	**D**irect **S**equence **S**pread **S**pectrum
e.g.	**e**xempli **g**ratia (en: for example)
EC-GSM-IoT	**E**xtended **C**overage - **GSM-IoT**
EKF	**E**xtended **K**alman **F**ilter
EU	**E**uropean **U**nion
FDI	**F**ault **D**etection and **I**dentification
FEI	**F**orward **E**uler **I**ntegrator
FFT	**F**ast **F**ourier **T**ransform
FOC	**F**ield **O**riented **C**ontrol
FTA	**F**ault **T**ree **A**nalysis
GA	**G**oertzel **A**lgorithm
GF	**G**oertzel **F**ilter
GSM	**G**lobal **S**ystem for **M**obile Communications
HAWT	**H**orizontal **A**xis **W**ind **T**urbine

HMI	**H**uman **M**achine **I**nterface
HTTP	**H**yper**T**ext **T**ransfer **P**rotocol
i.e.	**i**d **e**st (en: that is)
HTTPS	**HTTP S**ecure
I/O	**I**nput/**O**utput
I2C	**I**nter- **I**ntegrated **C**ircuit
ICS	**I**ndustrial **C**ommunication **S**ystem
IP	**I**nternet **P**rotocol
IoT	**I**nternet **o**f **T**hings
IrDA	**I**nfra**r**ed **D**ata **A**ssociation
ISCF	**I**nter-turn **S**hort **C**ircuit **F**ault
IWSN	**I**ndustrial **WSN**
JSON	**J**ava**S**cript **O**bject **N**otation
KF	**K**alman **F**ilter
LAIoT	**L**ocal **A**rea **IoT**
LOS	**L**ine **O**f **S**ight
LoRa	**Lo**ng **Ra**nge
LPWA	**L**ong **P**ower **W**ide **A**rea
LTE	**L**ong **T**erm **E**volution
LTE-M	**LTE** for **M**achines
M-Bus	**M**eter-**Bus**
M2M	**M**achine **2** (to) **M**achine
MCSA	**M**achine **C**urrent **S**ignature **A**nalysis
MEF	**M**ixed **E**ccentricity **F**ault
MISO	**M**ultiple **I**input **S**ingle **O**utput
MPPT	**M**aximum **P**ower **P**oint **T**racking
MQTT	**M**essage **Q**ueuing **T**elemetry **T**ransport
NARMAX	**N**onlinear **ARMAX**
NBIoT	**N**arrow **B**and **IoT**
NFC	**N**ear **F**ield **C**ommunication
OLE	**O**bject **L**inking and **E**mbedding
PLC	**P**rogrammable **L**ogic **C**ontroller
PRO	**PRO**fessional
PMSG	**P**ermanent **M**agnet **S**ynchronous **G**enerator
PMSM	**P**ermanent **M**agnet **S**ynchronous **M**achine
PMW	**P**ulse **W**idth **M**odulation
RAT	**R**emote **A**ccess **T**erminal
RF	**R**adio **F**requency
RFID	**RF ID**entification
RL	**R**esistive-Inductive
RPI	**R**aspberry **PI**
RPMA	**R**andom **P**hase **M**ultiple **A**ccess

SBC	**S**ide-**B**and **C**omponents
SCADA	**S**upervisory **C**ontrol **A**nd **D**ata **A**cquisition
SEF	**S**tatic **E**ccentricity **F**ault
SHM	**S**tructural **H**ealth **M**onitoring
SQL	**S**tructured **Q**uery **L**anguage
SRUKF	**S**quare **R**oot **UKF**
SVM	**S**upport **V**ector **M**achine
SVPWM	**S**pace **V**ector **PWM**
SWFFT	**S**liding **W**indow **FFT**
TSE	**T**aylor **S**eries **E**xpansion
TSO	**T**ransmission **S**ystem **O**perator
TV	**T**ele**V**ision
UKF	**U**nscented **K**alman **F**ilter
USB	**U**niversal **S**erial **B**us
UT	**U**nscented **T**ransform
VAWT	**V**ertical **A**xis **W**ind **T**urbine
VPN	**V**irtual **P**rivate **N**etwork
W-SVM	**W**eighted-**SVM**
WECS	**W**ind **E**nergy **C**onversion **S**ystem
WF	**W**ind **F**arm
WAN	**W**ide **A**rea **N**etwork
WiMAX	**W**orldwide **i**nteroperability for **M**icrowave **A**ccess
WirelessHART	**Wireless H**ighly **A**ddressable **R**emote **T**ransducer
WSN	**W**ireless **S**ensor **N**etwork
WT	**W**ind **T**urbine
ZSVC	**Z**ero **S**equence **V**oltage **C**omponent

Dedicated to Lina and my wonderful family.

Introduction

Context

WIND Farm (WF) numbers are on the rise in the European Union. From the potential electrical energy generation capacity, using wind power, of about 500GW, only 178.8GW are currently harvested using Wind Energy Conversion Systems (WECS) (Walsh and Pineda, 2019). Wind Turbines (WTs) are expected to become the primary source of electrical energy in the EU by 2019. They offer a very good combination between power generation capacity and cost. Therefore, they are attractive to investors. With this future growth in perspective, there are certain challenges that still need to be solved.

There are different types of WTs, depending on the generator type and on the presence or lack of a gearbox. Direct Drive Wind Turbines (DDWTs) are considered in this work. They do not have a gearbox and are usually equipped with Permanent Magnet Synchronous Generators (PMSG). They are widely used in offshore installations and their market share is increasing in both offshore and onshore WFs, due to their higher energy yield and reliability (Carroll, McDonald, and McMillan, 2015).

Monitoring of WFs is not trivial. Offshore WFs can lie several kilometers away from the shore and they can be made of hundreds of WTs. The largest offshore WF in the world, which is currently under extension, is the Walney Offshore WF, in the United Kingdom. It comprises 189 WTs which cover an

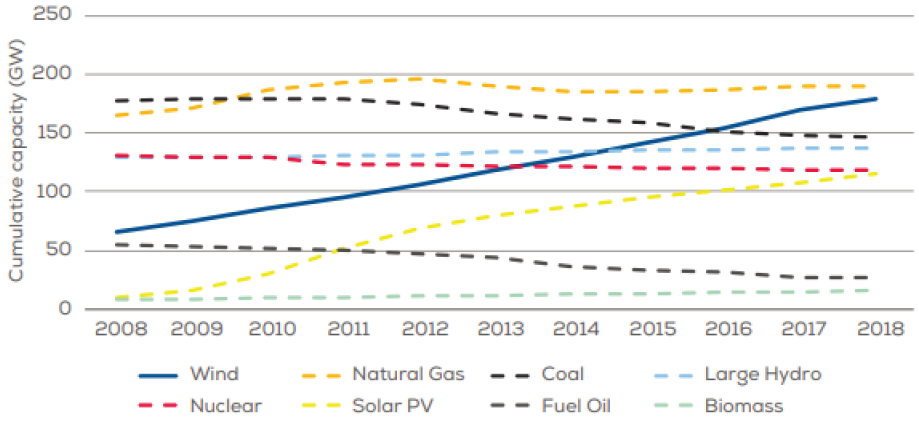

FIGURE 1: Power generation capacity in the EU, by source (Walsh and Pineda, 2019).

area of around $73km^2$ (Ørsted, 2017). The largest onshore WF is the Gansu WF in China, which comprises around 7000 WTs (Vyas, 2018).

Usually, a WT is equipped with a Supervisory Control and Data Acquisition (SCADA) system. It can also be monitored using Condition Monitoring (CM) and/or Structural Health Monitoring (SHM) systems. The data acquired and sent by these systems is usually transmitted through copper cables, inside each WT. Although no official statistic could be found, it can be reasonably assumed that the number of signals transmitted inside each WT is, at least, in the order of hundreds. Therefore, when considering the number of WTs of the previously mentioned WFs, the cost generated by the installation and maintenance of the cables becomes significant.

Moreover, WF operators need to remotely monitor their assets. Thus, fiber-optic cables are laid between the different WTs in a WF, and from the gateway of the WF to the operator. These data transmission lines run along the three-phase power cables (in case of AC transmission) which are laid from the WF to the grid. The dedicated line used for the communication between the dispatch center and the WF is maintained by a separate company, for a fee. This tax is relatively high, and depending on the availability and redundancy requirements, it can amount to tens of thousands of euros per year.

Although DDWTs are more reliable nowadays than those in previous generations, they can still break down, so they require automatic diagnosis systems. The different components which can fail in a DDWT are the blades, the generator, the main shaft, the hydraulic systems, etc., (Qiao and Lu, 2015a). These impairments can lead to lower power generation, asset damage and even downtime. The generator is considered in this work, as it is responsible for almost 25% of the total downtime of a DDWT. The distribution of faults and downtime, due to each component of a DDWT is shown in Table 1.

Objectives

The PMSG of the DDWT should be diagnosed, and the most common faults which can affect it should be detected and isolated. These impairments should be detected as early as possible, even in incipient stages. The Fault Detection and Identification (FDI) tools should be precise, but also simple to use and implement. Therefore, the accent should lie on simpler methods which can be understood and utilized by engineers with only bachelor-level studies.

The feasibility of using Wireless Sensor Networks (WSNs), to eliminate the wired communication network, should be investigated. The current communication architecture of a WT should be studied, together with different

TABLE 1: Failure Percentages of WT Systems (Pinar Pérez et al., 2013).

Component	Failures [%]	Downtime [%]
Hub	10.08	17.76
Pitch and Yaw	17.22	8.88
Generator	14.7	24.42
Electronic Subsystems	35.7	25.53
Shaft and Bearings	3.36	8.88
Sensors	8.4	3.98
Brake	0	0
Hydraulics	0.84	0.56
Other	9.7	9.99

wireless communication technologies. A short guide should be developed, to help choose a suitable wireless protocol for a given application.

Description of the Chapters

The state of the art, related to the diagnosis and to surveys of wireless communication, is presented in Chapter I.

The mathematical model of the PMSG is presented in Chapter II. Its mathematical model is continuous and non-linear, therefore it is difficult to discretize. A comparison is made between different discretization techniques. A continuous model with a discrete integrator is shown to be the best solution. Then, the nominal closed-loop control of the WT is presented.

In Chapter III, there is presented a new method to compute the covariance matrix of the process noise. This procedure is shown in the context of an Extended Kalman Filter (EKF). However, it does not use any of the matrices of the filter and is therefore independent of it. The method uses a constant covariance matrix for the measurement noise and, at each iteration, it re-computes the values of the process noise covariance matrix. The proposed method and two other ones, selected from the scientific literature, are tested to estimate the current generated by the PMSG. All three methods are tested in the context of the EKF. The obtained results are compared and discussed to highlight the strengths and weaknesses of the proposed approach. Then, the Kalman Filter (KF), the Extended Kalman Filter (EKF) and the Unscented Kalman Filter (UKF) are compared. The results are presented and it is shown that the EKF is the most suitable one for this application. This is followed by a discussion regarding the behavior of the filters, where all are shown to act like proportional controllers.

The different faults which can affect a PMSG are shown in Chapter IV. The most common ones are the rotor demagnetization, eccentricity (static, dynamic and mixed) and inter-turn short circuit. Their effect is noticeable on the spectrum of the stator currents, which is computed using the Fast Fourier Transform (FFT). However, for a WT, the spectrum of the currents changes with the wind speed. Therefore, the obtained results may not be accurate. In this chapter, the residuals, computed using the currents estimated with the EKF and the measured ones, are proposed to be used for FDI, together with the FFT. The spectrum of the residuals is invariant to changes in the wind speed, but sensitive to faults. However, the FFT computes the whole spectrum, while the number of possible faults and the number of introduced harmonics is very low. The Goertzel Algorithm (GA), implemented as a filter - the Goertzel Filter (GF), is also presented in this chapter as a more efficient alternative to the FFT. The GF was tested and simulation results prove that it can return the squared magnitude of these harmonics. This information can be used to set thresholds for fault detection, within a FDI algorithm.

WFs can be located in isolated areas, or the WTs may be distributed geographically. Therefore, the necessary communication infrastructure can be expensive to install and maintain. In Chapter V, WSNs and the Internet of Things (IoT) are presented as solutions for these problems. WSNs are quick to install, easy to maintain and they scale up easily. The requirements for a potential WSN, for both a WT and a WF, are studied in this chapter. Different wireless communication technologies are thoroughly compared. Both long-range low-power protocols and short-range high-speed ones are considered. A possible LoRa-based architecture of a WF communication system is presented. The integration of a power generation facility in the IoT raises security concerns. Potential dangers and vulnerabilities are listed, to increase awareness of the necessity of security in Industrial Communication Systems (ICS).

Chapter 1

State of the Art

1.1 About Wind Turbines

WIND Turbines (WTs) have changed over the years. The earlier models were designed to produce electrical energy while the rotor was moving at constant angular velocities. In time, these were replaced by variable-speed WTs, which are currently in use. Gearboxes were used in variable-speed WTs to maintain a near-constant speed for the generator. This near-constant velocity which would be one or two order of measures higher than the angular speed of the propeller.

In time, gearboxes proved to be an unreliable and expensive component to replace. Therefore, the design of WTs was again refined, and doubly-fed induction generators were replaced by permanent magnet synchronous ones.

The rotor of a PMSG is usually constructed from rare-earths, such as neodymium. It is rotated by the shaft which connects it directly to the rotor. According to Faraday's Law of induction, when the rotor is moving, a current appears in the windings of the stator. Thus, the kinetic energy of the wind is converted into electrical energy.

The Wind Energy Conversion System (WECS), located inside the nacelle of the WT, comprises:

- the rotor, which is made up of the propeller and the hub;

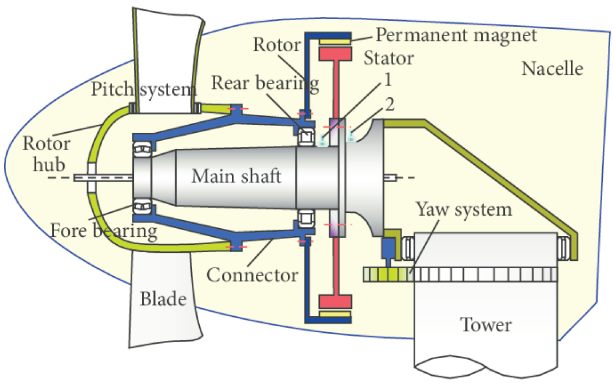

FIGURE 1.1: Schematic of a DDWT (Teng et al., 2016).

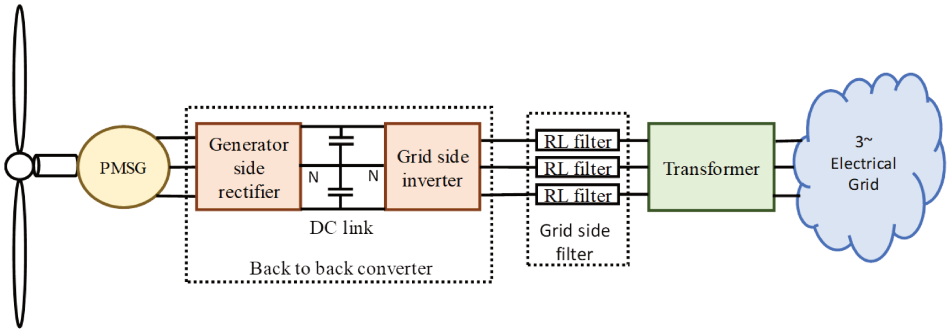

FIGURE 1.2: Schematic of a WECS.

- the main shaft which connects the rotor to the generator;
- the PMSG, which converts the mechanical energy into electrical one;
- a capacitor to smooth out the current;
- a back-to-back converter, which is made up of:
  - a rectifier;
  - a DC link with a capacitor used to smooth out the DC voltage (it may also contain a chopper circuit);
  - an inverter;
- a bank of resistive-inductive filters which are used to smooth out the resulting sinusoid;
- a transformer which changes the voltage and intensity of the generated energy to be compliant with grid requirements;
- the connection to the electrical grid.

The different systems of the WECS were simulated in Matlab/Simulink, using the Simscape Power Systems Toolbox. More details about the modeling and the mathematical relations which describe their behavior are presented in Chapter II. In the same chapter, the Control Systems (CSs), which are relevant for this work, are shown.

As mentioned in the Introduction, the component of interest of this work is the PMSG. The different faults which can affect the PMSG are (Alameh et al., 2015) the rotor demagnetization, inter-turn short circuit and the three types of eccentricity: dynamic, static and mixed. There faults are presently in detail in Chapter IV.

1.2 Existing Monitoring Systems for Wind Turbines

Four systems are used to monitor a WT and, by extension, a Wind Farm (WF). These are the:

- Supervisory Control and Data Acquisition (SCADA) system, which is used to:
  - acquire the data required by the control systems;
  - process the information according to some algorithms;
  - send the resulting commands to the different actuators;
- Condition Monitoring (CM) system, which gathers information used to determine the health-state of the equipment (e.g. the generator, the converter, the transformers, etc.);
- Structural Health Monitoring (SHM) system, which acquires data and asses the state of the structural elements of the WT (e.g. the blades, the tower, the foundation, etc.);
- Safety system, which is not considered in this work. This system can stop the WT if a catastrophic failure occurs.

According to the survey in (Yang et al., 2014), there are more than 15 commercially available SCADA systems specifically designed to monitor a WT. The number of CM systems, for a WT, available for purchase is 23. The survey was published in 2014, so the number of commercially available systems is expected to have increased. Not all CM systems supervise the whole WT - most of them are designed to monitor a specific component, such as the generator or the main bearing (which connects the rotor to the main shaft). Although it is not mentioned in (Yang et al., 2014) whether the different systems use wireless communication or not, they are assumed to be wired. Considering that "wireless" is a strong selling point and that the use of this technology would be interesting from a scientific and industrial point of view, the lack of any mention means that cables are used.

Since more than a decade ago, different proposals have surfaced in the literature about the possibility of using wireless communication for the different systems of a WT. Such proposals can be seen in (Xingzhen et al., 2008), (Meng and Gong, 2012) and (A. Ahmed and E. Ahmed, 2016). However, no experimental implementation has been reported.

The first step towards an experimental demonstration lies in studying the requirements of such a system and the different available solutions. Because the information about different industrial systems is confidential, the requirements have to be estimated from the publicly available information (e.g. the one from (Enjie, 2018)). On the other hand, information about different wireless technologies is widespread.

In (B. K. Singh et al., 2013) it is presented a short survey on communication technologies, which can be used for WF installations. The focus is on wired protocols such as Modbus, Profibus, fiber optics, etc. and only three

wireless technologies are discussed: Wi-Fi, Zigbee and WiMAX (the latter now being obsolete). However, no comparison is made between the different communication technologies. The standard communication architecture of a WF is also not presented - just various experimental implementations shown in different papers. In the conclusions of the article, the need for a comprehensive review of new communication technologies is highlighted.

The design procedure for a WF communication system, and a possible structure for a data package which would be used in this Industrial Communication System (ICS), are shown in (M. A. Ahmed and Kim, 2014). The proposed multi-level communication network is based on wired protocols like CAN or Ethernet Passive Optical Network, while wireless protocols (like Zigbee) are mentioned as back-up solutions. The focus is on the link layer of the OSI model. Again, this paper stressed the need for a thorough comparison of communication technologies.

Two communication technologies for long distance transmission using low power are compared in (Sinha, Wei, and S. H. Hwang, 2017). These are LoRa and NB-IoT, which is currently under roll-out.

WirelessHART and other protocols are shown in (Queiroz et al., 2017). This paper is mostly focused on wireless standards and on classifications. Therefore, no technical specifications are presented.

Different wireless technologies, for smart grid communication, are presented in (Mahmood, Javaid, and Razzaq, 2015). The considered technologies are ZigBee, Wi-fi, Bluetooth, 6LowPan, Z-wave, WiMAX and cellular networks. A brief comparison is made between them, to recommend the best one.

The survey from (Ali et al., 2017) is more detailed. It presents both long-range communication technologies such as Lora, NB-IoT, Sigfox, WiMAX and LTE, but also short-range high-speed ones, such as Zigbee, Wi-Fi and Bluetooth. However, more protocols are reviewed in this work and the results are summarized, to lower the time necessary for a comparison.

In (Moness and Moustafa, 2016), both WTs and WFs are presented as cyber-physical systems, being made up of physical components such as the blades, generator, nacelle etc. and cyber components such as the SCADA and CM systems. Their integration in the Internet of Energy is also discussed. The authors focused on presenting concepts, without many recommendations for practical implementations. There is no discussion about different communication technologies, just a very brief mention of general security aspects for cyber-physical systems.

Different attack vectors directed against WFs are presented in (Staggs, Ferlemann, and Shenoi, 2017). The emphasis is on physical attacks, i.e. destroying or adding equipment. A Raspberry PI is added to the ICS to acquire data from it and to serve as an entry-point in the system. The authors

give several recommendations at the end of the paper, to help mitigate these risks.

Security aspects are also considered in this thesis. Due to the connectedness of industrial systems and the internet, attackers can take control of equipment and shut it down, with serious consequences. These aspects are mentioned, to increase awareness about the dangers, and the methods to mitigate them.

1.3 Fault Detection and Identification

According to (Venkatasubramanian, Rengaswamy, Yin, et al., 2003) there are three types of diagnostic methods:

1. qualitative model-based, which consider the interconnections between the different components to identify the faulty one and the cause of the fault;
2. process history based, which use signal processing or artificial intelligence.
3. quantitative model-based, which use observers and state estimators;

1.3.1 Qualitative-Model Based Methods

In (Kang, Sun, and Guedes Soares, 2019) is presented a Fault Tree Analysis (FTA) for offshore WTs. Only the structure, the pitch and hydraulic systems, the gearbox and the generator were considered in the paper. However, the common generator faults were not mentioned. All the causes of the failures were external, like human error, anchor failure, storm, plane crash, etc. No FTA could be found in the literature for a Permanent Magnet Synchronous Machine (PMSM).

Faults were detected in (Badoud et al., 2014) using Bond Graphs and Analytic Redundancy Relations (ARRs). A DDWT equipped with a PMSG was selected as a case study. However, only sensor faults were considered.

In (Echavarria et al., 2008) is presented a model of an offshore WT. This model was obtained using qualitative physics, which describe, abstractly, the behavior of the WT without modelling it according to specific laws of physics. A WT equipped with a gearbox was considered, and, again, the focus was on sensor faults.

It is difficult to use qualitative model-based methods for FDI. Firstly, a WT is a complex system, which consists of multiple interconnected subsystems. Moreover, this approach requires very good knowledge of the functioning of a WT, which is nigh impossible to obtain without working in a

company which produces WTs. Therefore, attention was turned towards methods based on the history of the process.

1.3.2 The Case for Using the Fast Fourier Transform

Diagnosis based on signal processing is common for PMSMs. The usual tools of diagnosis are the Discrete Fourier Transform (DFT), through the Fast Fourier Transform (FFT) algorithm. Other methods used in the literature are the Wavelet Decomposition (Gritli et al., 2012), the Hilbert-Huang Transform (Espinosa et al., 2010), Wiegner-Ville Distribution and Empirical Mode Decomposition (Zhifu et al., 2014), among others.

The Fast Fourier Transform (FFT) is the most used signal processing technique. It is recommended when faults introduce additional harmonics into the signals acquired from the process. However, it is also not precise. The spectrum of the currents changes with wind speed, so the threshold values used for a FFT-based detection algorithm might not be sensitive enough for different wind speeds (Faiz and Nejadi-Koti, 2016).

The latter methods previously mentioned are insensitive to variations in the wind speed, but at the same time they are more complex and require more computational power.

The cyclostationarity (Napolitano, 2016) of the process can be used to enable the usage of the FFT. The spectrum of the currents changes with wind speed, but the same wind speed determines a similar spectrum in the currents. However, this approach suffers from several drawbacks:

- The wind speed is stochastic, because it is affected by noise. This perturbation might introduce unwanted harmonics, which could trigger false-positive alarms;
- Because the spectrum of the generated currents can change with the physical parameters of the WT (i.e. blade span, etc.) the fault detection threshold should be different for each type of WT;
- The variation of the wind speed should be split into intervals, where the spectrum of the currents remains (almost) constant. Then, detection thresholds should be defined on each interval. The number of intervals could be large, and problems might arise when the speed of the wind changes from one interval to another.

Classification algorithms (Duviella, Serir, and Sayed-Mouchaweh, 2013) are used to estimate the operating point of each turbine in a park. When the operating point of one or more turbines strays too far away from the expected estimation, a fault is detected. The exact fault is discovered by applying the parity space method on the residuals obtained between the real output and the one estimated using a nonlinear model. A similar approach

was developed for only one turbine (Fernandez-Canti et al., 2013), but the model is computed within a Bayesian framework.

Data mining techniques can be used for FDI, as they search for specific patterns or values, in data. The behavior of the process can be described using weighted support vector machines (W-SVM) (Lopez Pulgarin and Sofrony Esmeral, 2016). The operating point of the process is again estimated. When it strays outside a hyperplane, a fault is detected. One set of W-SVMs is utilized for fault detection, while another set for isolation. The histogram of the data can also be analyzed (S. Wang et al., 2016) for offline FDI.

A probabilistic change detection method, such as the Dynamic Cumulative Sum algorithm can also be used (Borcehrsen, Larsen, and Stoustrup, 2014). Faults are detected by monitoring the power output of each turbine and of the whole farm. Other similar methods, which may be employed, are the Page – Hinkley Test and the Generalized Likelihood Ratio.

Diagnosis based on Artificial Intelligence (AI) is not commonly used to diagnose WT or PMSM faults, due to the following disadvantages:

- The AI should be trained using data acquired in both healthy and faulty scenarios. Due to the high cost of a WT, companies prefer not to damage them;
- Researchers do not know exactly what happens during the functioning of some AI algorithms, such as neural-networks (Reddi, Kale, and Kumar, 2019). Accordingly, they are reluctant to use them in critical applications.

The problems of the FFT can be solved if the spectrum of the signal, is constant regardless of the different wind speeds. During this work, it was discovered that the spectrum of the residuals, computed between the generated currents and an estimation obtained using model-based approaches, can be considered constant.

1.3.3 The Case for the Goertzel Filter

Although the FFT is widely used as a signal processing technique, its performance can be overshadowed, in certain circumstances, by the Goertzel Algorithm (GA) (Goertzel, 1958). The GA is usually implemented as a two-stage filter, called the Goertzel Filter (GF). If the number of frequencies of interest, that should be monitored using the FFT, is very low, then the GA is a better alternative.

In (Bocca et al., 2011), wireless nodes are used to monitor the acceleration of a structure. The FFT would normally be used to monitor changes in the spectrum, due to faults. Because the sensors are battery-powered, they should use very efficient algorithms to minimize the amount of energy that

they require. The GA is presented as a replacement for the FFT, because the number of frequencies of interest is very low.

The GA is also used in (Koziy, Bei, and Aslakson, 2013) to compute the Total Harmonics Distortion (THD) of the electrical current flowing through a section of a smart grid. Only a few supplementary harmonics can appear, so the FFT would be inefficient in that application. The GA is implemented on a low power smart meter.

A fault tolerant implementation of the GA is shown in (Gao et al., 2014). Two GAs are used in parallel and they run on different equipment, in case one hardware unit breaks down. In this case, the GAs are not used for FDI, but this implementation may be useful in critical applications such as nuclear power plants, where equipment redundancy is mandatory.

In (Reljic, Tomic, and Kanovic, 2015), the GA is used to find eccentricity-type faults for a three-phase induction motor. The application is similar to the one presented in this paper, as the authors also used Machine Current Signature Analysis (MCSA). However, in this work, five faults are considered (compared to three in (Reljic, Tomic, and Kanovic, 2015) and they will affect a PMSG.

In (Sapena-Bano et al., 2018), the FFT is replaced by a sliding-window FFT (SWFFT), its design being based on the GA. The SWFFT computes the magnitude for just one frequency component of the signal, as does the GA. The SWFFT is again used to diagnose eccentricity-type faults which can appear in an induction motor.

1.3.4 The Case for Using the Extended Kalman Filter

Different model-based approaches can be used to obtain the residuals needed for the signal-processing based diagnosis.

Nonlinear parameter varying equations can be used to model the process (Blesa, Jimenez, et al., 2014). They are used to extract residuals for the parity space method. The equations define NARMAX models. The static characteristic of each turbine is split into regions, and a model is computed for each one. The models are identified by minimizing a constrained optimization problem (Gliga, Mihai, et al., 2015) (Gliga, Mihai, et al., 2017) around each operating point. An approach using linear equations also exists (Chouiref et al., 2015), where the models are of type ARMAX.

A set of MISO fuzzy models can be obtained for the wind farm (Simani, Farsoni, and Castaldi, 2015). A group of Takagi – Sugeno observers are used to estimate the output of each WT. Luenberger interval observers can also be used (Blesa, Nejjari, et al., 2013). Each observer is valid on an interval around an operating point.

Different types of state observers may be used, such as the sliding-mode observer (Y. Feng et al., 2009), the unknown input observer (Alahakoon et al., 2013) and the Luenberger observer mentioned earlier.

However, the decision was taken to use a Kalman-type filter for residual generation, namely the Extended Kalman Filter, because:

- these are widely used in the monitoring of PMSMs (e.g. (Dhaouadi, Mohan, and Norum, 1991) and (Foo, X. Zhang, and M. D. Vilathgamuwa, 2013));
- they are widely taught in universities worldwide;
- they have proven their capabilities (e.g. their usage in the Apollo 11 guidance computer, in the localization system on smartphones, etc.).

Current Methods to Estimate the Process Noise Covariance

Even in such an old algorithm as a Kalman-type filter, there are still problems that can be addressed. Among them, is the classical challenge of selecting the covariance matrices for the process and for the measurement noise. While a constant matrix can be selected for the measurement noise (Levy, 2016), the estimation of the other matrix is more difficult.

In the scientific literature, different methods are presented to estimate the covariance matrix of the noise affecting a process. However, most of them are designed for the linear Kalman Filter (KF), and they are not usable in an EKF. In other cases, their design limits their applicability.

A similar estimation procedure, to the one proposed in this work, is presented in (B. Feng et al., 2014). That method is explicitly derived for the KF, and it is not applicable for the EKF. Moreover, the authors of (B. Feng et al., 2014) used the following equation to compute the covariance of the estimation error:

$$\hat{cov}\left(\epsilon_{k+1}, \epsilon_{k+1}\right) = \frac{k}{k+1}\hat{cov}\left(\epsilon_k, \epsilon_k\right) + \frac{1}{k+1}\epsilon_{k+1}\epsilon_{k+1}^T, \tag{1.1}$$

where $\epsilon \in \mathbb{R}^{n_y}$ is the error between the real outputs of the process and the estimated outputs of the model and $\hat{cov}(\epsilon_k, \epsilon_k) \in \mathbb{R}^{n_y * n_y}$ is the covariance matrix of the error at the k^{th} time step. In (1.1) it is assumed that the mean of the noise is zero. The new method presented in this work also considers non-zero average values for the noise. Therefore is can be used when sensor faults are present, namely bias Gliga, Chafouk, et al., 2017.

The authors of (Z. Liu and He, 2017) present an iterative procedure to compute the covariance matrices of the process and of the measurement

noises. The method is simple to implement, and it is designed for the EKF:

$$S_k = \frac{1}{N} \sum_{j=k-N+1}^{k} \epsilon_k \epsilon_k^T, \tag{1.2}$$

$$Q_k = K_k S_k K_k^T, \tag{1.3}$$

$$R_k = S_k + H_k P_k H_k^T, \tag{1.4}$$

where K_k is the Kalman gain obtained in the update phase of the EKF. N is chosen arbitrarily, with no suggestion being provided in (Z. Liu and He, 2017). Different values were tested, from the set $\{1, 10, 100, 1000, 10000\}$, to find the most suitable one. There is no universal value, and it should be changed according to the uncertainty affecting the process.

Another iterative method, shown in (Akhlaghi, Zhou, and Huang, 2017), can be used to compute the process and the measurement noises covariances. This procedure is similar to an optimization method with a forgetting factor:

$$Q_k = \alpha Q_{k-1} + (1 - \alpha) \left(K_k d_k d_k^T K_k^T \right), \tag{1.5}$$

$$R_k = \alpha R_{k-1} + (1 - \alpha) \left(\epsilon_k \epsilon_k^T + H_k P_k H_k^T \right), \tag{1.6}$$

where $\alpha \in [0, 1]$ is the forgetting factor and $d_k = y_k - h(\hat{x}_k)$ is the a priori estimation error. $\epsilon_k = y_k - h(\hat{x}_k^*)$ is the a posteriori estimation error. In the rest of this work, the phrase "estimation error" refers to the a posteriori estimation error.

In (Xi et al., 2018), a procedure is presented to compute the covariance of the process noise. It only uses the estimation error and its covariance. However, the authors assume that the diagonal elements of the covariance matrix of the process noise are equal. In practice, there is no guarantee that the noise has the same linear behavior across all measurement channels. Moreover, the amplitude of the noises might be different, thus the resulting variances - the diagonal elements of the covariance matrix, might not be equal. For example, the engine of a car is influenced differently by the quality of the fuel and the ruggedness of the road.

Another method, shown in (Qiu, Qian, and G. Wang, 2018), is used to determine the covariance matrix of the process noise. The authors assume that the covariance matrix is split, by the anti-diagonal, into two halves: each half has equal elements on its first diagonal, but the values are different between the two halves. While this is a generalization from the previous case, it is still a particular one.

An EKF with three stages is presented in (Xiao et al., 2018). The second and the third stages are used to improve the estimation obtained from the first one. The method used to compute the process noise covariance matrix

has no constraints, compared to the previous two approaches. However, it is very complex as there are three EKFs connected in series. The process and measurement noises covariances are estimated in each stage. As it will be shown in Chapter III, even one EKF is very accurate, so the increase in complexity is not necessary (at least for a PMSG).

The procedure presented in this work was compared with the methods presented in (Z. Liu and He, 2017) and (Akhlaghi, Zhou, and Huang, 2017). The algorithm to estimate the measurement noise covariance is not published in a peer-reviewed scientific paper. The authors decided to test it, together with the proposed method, against the established ones.

1.4 Contributions

A new procedure to estimate the covariance matrix of the process noise is presented in Chapter III. It only uses information related to the model of the process, and therefore it can be utilized for any state estimator and observer. Moreover, when compared with other methods from the literature, it is proven to be faster and just as precise.

In Chapter IV, an EKF is used to estimate the generated currents. The spectrum of the residuals computed between this estimation and the real currents is nearly constant. Therefore, simpler signal processing tools, such as the Fast Fourier Transform, can be used. In the same chapter, the FFT is replaced by the Goetzel Filter, which is more efficient when the number of frequencies of interest is low.

In Chapter V, many wireless communication technologies are compared. This can help engineers quickly choose the most suitable one for their application.

Chapter 2

Generator Modelling and Nominal Control

2.1 Introduction

As it was previously presented, a Wind Turbine (WT) is made up of a multitude of components. The behavior of the WT has to be represented using a mathematical model, which can then be used in simulations.

The mechanical part of the wind turbine, which comprises the rotor hub and the rotor shaft, can be modeled using the equations shown in Appendix B. The parameters of this model are shown in Appendix A, together with the other parameters used in the simulations.

In this chapter, the model of the Permanent Magnet Synchronous Generator (PMSG) is presented in Section 2.2. Because the model is nonlinear and continuous, it must be approximated by a discrete one. The discretization is presented in Section 2.3. Before any fault symptoms are introduced and any diagnosis is performed, the WT should be controlled, in nominal operation. The control of the WT is presented in Section 2.4.

2.2 The Model of the Generator

The PMSG is simulated in Matlab, Simulink, using the Simscape/Power Systems toolbox. The equations of the PMSG are (Gliga, Chafouk, et al., 2018a):

$$\hat{I}_d(t) = -\frac{R_s I_d(t)}{L_s} + \frac{n_p \omega_m(t) L_s I_q(t)}{L_s} + \frac{V_d(t)}{L_s}, \tag{2.1}$$

$$\hat{I}_q(t) = -\frac{R_s I_q(t)}{L_s} - \frac{n_p \omega_m(t) L_s I_d(t)}{L_s} - \frac{n_p \omega_m(t) \phi}{L_s} + \frac{V_q(t)}{L_s}, \tag{2.2}$$

where I_d, I_q, V_d and V_q are the currents (in A) and the voltages (in V) in the dq0 rotor frame. R_s and L_s are the stator resistance (in Ω) and inductance (in H) in the dq0 frame. ω_m is the angular velocity of the generator shaft

(in rpm), and ϕ is flux linkage between the permanent magnet rotor and the stator (in Wb).

The states of the model are the currents, and the inputs are the voltages and the angular velocity. The model is nonlinear due to the product between a state and an input, in each state equation. The equipment was simulated in nominal operation, when no faults are present.

Another equation can be added in the model, to capture the behavior of the angular velocity. The complete model is (Pillay and Krishnan, 1989):

$$\begin{aligned} \dot{I}_d(t) &= \frac{V_d(t) - R_s I_d(t) + n_P \omega_m(t) L_s I_q(t)}{L_s}, \\ \dot{I}_q(t) &= \frac{V_q(t) - R_s I_q(t) - n_P \omega_m(t) L_s I_d(t)}{L_s} - \\ &\qquad \frac{n_p \omega_m(t) \phi}{L_s}, \\ \dot{\omega}_m(t) &= \frac{T_e(t) - T_m(t) - B * \omega_m(t)}{J}, \end{aligned} \tag{2.3}$$

where B is the viscous damping of the generator shaft and J is the inertia coefficient of the rotor. T_e is the electrical torque

$$T_e(t) = 1.5 n_P \phi I_q(t), \tag{2.4}$$

and T_m is the mechanical torque, which can be estimated using the equations from Appendix B.

The PMSG is connected to a system which simulates the small capacity wind turbine, as shown in Appendix D. The generator is connected to the grid through a two-level back-to-back converter and an RL filter. The transformer was not considered in this work, because it does not directly affect the PMSG.

A word of caution when using the SimScape Power Systems library in Simulink. Although the recommended solver is ode23tb, the simulation might return different results on minor modifications done to the code. This problem can be avoided by using a fixed-step solver with a very low time step. For the simulations presented in this work, the authors utilized the ode1 solver (MathWorks, 2018) with a time step of 10^{-6}.

2.3 Model Discretization

It is difficult to discretize a nonlinear function. So, the most suitable option is to use the Taylor Series Expansion (TSE) to obtain a linear model

(Morel et al., 2009)

$$\begin{bmatrix} i_{d_{k+1}} \\ i_{q_{k+1}} \end{bmatrix} = F_k * \begin{bmatrix} i_{d_k} \\ i_{q_k} \end{bmatrix} + G_k * \begin{bmatrix} V_{d_k} \\ V_{q_k} \end{bmatrix} + H_k \tag{2.5}$$

where

$$F_k = \begin{bmatrix} 1 - \frac{R_s T_s}{L_s} & T_s n_P \omega_{m_k} \\ -T_s n_P \omega_{m_k} & 1 - \frac{R_s T_s}{L_s} \end{bmatrix}$$

$$G_k = \begin{bmatrix} \frac{T_s}{L_s} & 0 \\ 0 & \frac{T_s}{L_s} \end{bmatrix} \; and \; H_k = \begin{bmatrix} 0 \\ -\frac{T_s n_P \omega_k}{L_s} \phi \end{bmatrix}$$

and T_s is the sampling period.

However, any linearization may introduce errors in the model. In (Shahriari et al., 2016), it is suggested to use the continuous model, but with the following discrete integrator

$$x_k = x_{k-1} + \dot{x} * Ts;$$

where x is the state vector of the process.

However, this integrator differs from the one used in Simulink, in the Power Systems Toolbox. There, when the PMSG is simulated in discrete mode, the continuous model is used with a Forward Euler Integrator (FEI) (TransÉnergie Technologies Inc, 2003)

$$y_k = x_k$$

$$x_{k+1} = x_k + T_s * u_k$$

where y is the output of the integrator, x is its internal state and u is its input, i.e. the derivative of the system states.

The simulation results are presented in Table 2.1. The errors obtained with the continuous integrator and the FEI are similar, because the sampling period was chosen to be very small, 10^{-6}. This is to prevent numerical instability in the simulation. In Fig. 2.3 and Fig. 2.4, the methods appear to return the same results, but this is out of coincidence. The simulations was checked, and the same results were obtained. Although Fig. 2.1 and 2.2 are identical, they show that the discrete integrator behaves like the continuous one, for the chosen sampling period (10^{-6} s).

A small error appears in the case of the continuous model with a continuous integrator, because of how Simulink compiles the schematic. Any collection of Power Systems blocks is approximated by a state space model (TransÉnergie Technologies Inc, 2003).

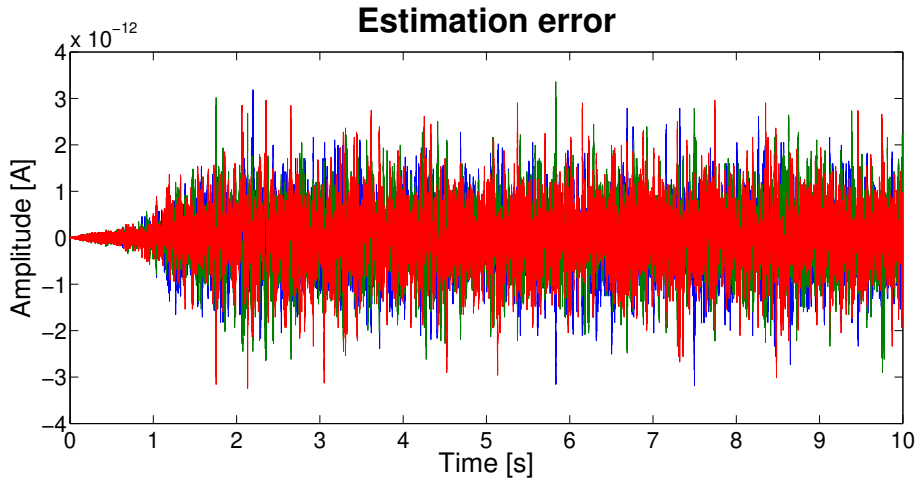

FIGURE 2.1: The continuous model with a continuous integrator.

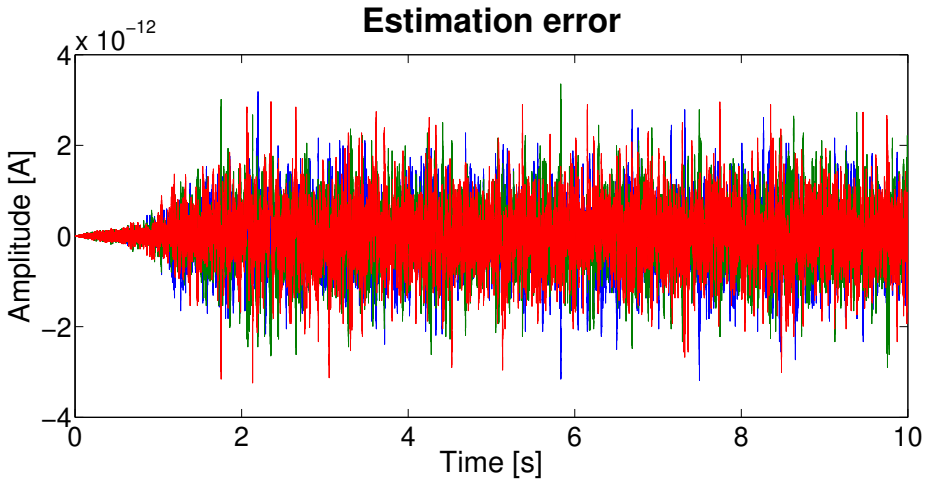

FIGURE 2.2: The continuous model with the discrete FEI.

2.4 Nominal Control of the Wind Turbine

There are multiple Control Systems (CSs) used to control a WT (Yan et al., 2014):

- the pitch CS, which changes the angle-of-attack of each blade;
- the yaw CS, which changes the orientation of the nacelle, to align the propeller according to the direction the wind is blowing;
- the rectifier CS, which is used to control the angular velocity/torque of the shaft, and through it the generated currents;
- the inverter CS, which controls the active and reactive powers of the energy injected into the grid;
- the cooling system of the nacelle;

TABLE 2.1: Comparison of the discretization methods.

Model	Integrator type	Order of error
Continuous	Continuous	$\approx 10^{-13}$
Continuous	Discrete - FEI	$\approx 10^{-13}$
Continuous	Discrete - from (Shahriari et al., 2016)	≈ 4
Linearised	N/A	≈ 4

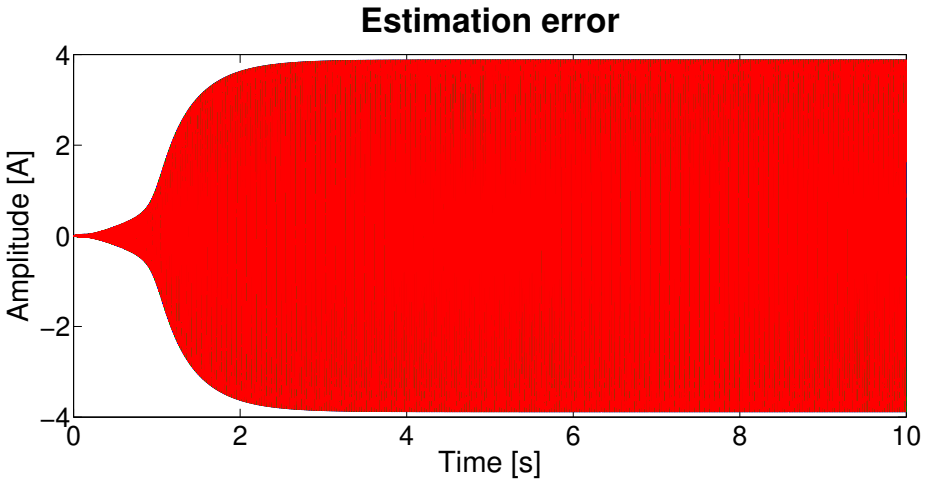

FIGURE 2.3: The continuous model with the discrete integrator from (Shahriari et al., 2016).

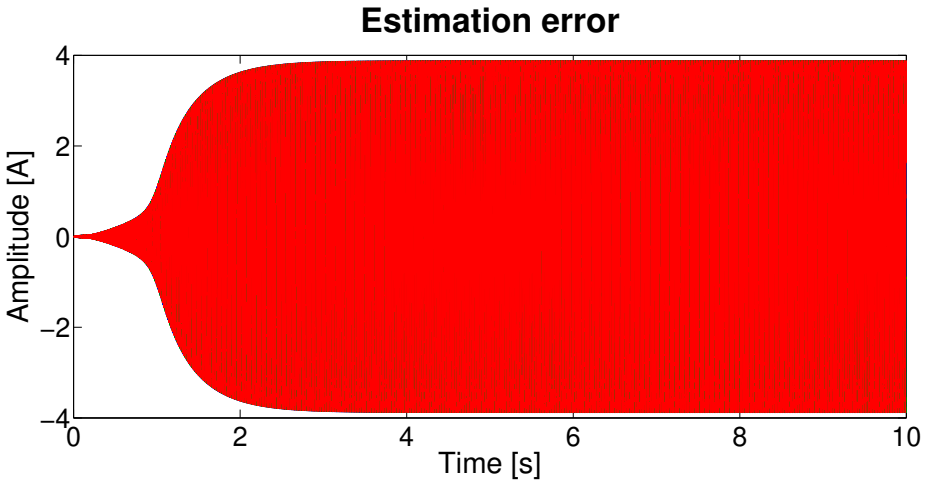

FIGURE 2.4: The linearized model.

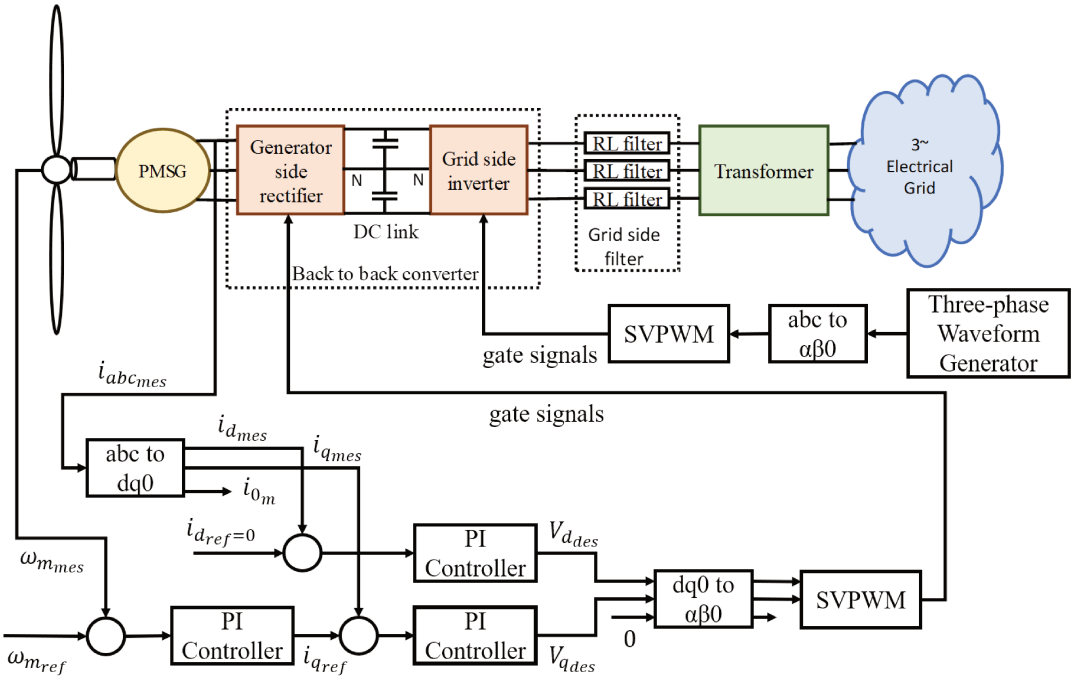

FIGURE 2.5: The control systems used in this work (Bin et al., 2014).

- the mechanical break of the rotor;
- etc.

The setpoints for the pitch and rectifier control systems are usually computed by a Maximum Power Point Tracking (MPPT) controller (Errami et al., 2018). They are calculated using optimization methods, which try to maximize the power coefficient of the WT.

This work is focused on the diagnosis of the PMSG, therefore the only considered control systems are the ones which can affect the behavior of the generator. These systems are shown in Figure 2.5, and they are the rectifier and the inverter control systems.

The rectifier is controlled in closed-loop, using Field Oriented Control (FOC) (Damiano et al., 2012) (Ed-dahmani et al., 2018). FOC is used to change the angle of the magnetic field inside the electrical machine. The desired angle should be 90^o further than the current one, to keep the rotor turning at a desired frequency.

Classical PI controllers are used in many works in the literature. These controllers are utilized after the currents are transformed from the three-phase abc frame to the dq0 frame, using the Park Transform (Mohan, 2012). After the required voltages are computed in the dq0 frame, they are transformed in the alpha-beta frame using the Inverse Clarke Transform (Mohan, 2012). More details about the Park and Clarke Transforms can be found in Appendix C.

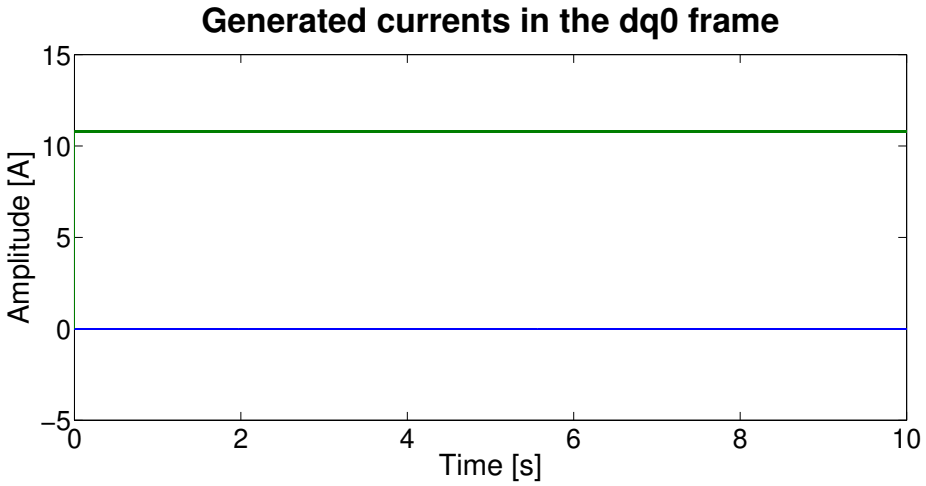

FIGURE 2.6: The generated currents in the dq0 frame.

The rectifier and the inverter receive the gate control signals from a Space-Vector Pulse-Width Modulation block. The input of the block are the voltages, in the alpha-beta frame, which point to the desired location of the voltage phasor (Mohan, 2012).

The PI controller which assured a certain angular velocity was designed considering the third equation from (2.3). However, the other two were tuned using Ziegler-Nichols (Popescu et al., 2006).

Feedforward control is sufficient for the inverter. As long as it operates in the nominal mode, its behavior does not directly influence the generator. It only considers the grid-side voltages and currents. Therefore, it would react to grid disturbances, not to changes in the wind speed. The three-phase setpoints selected for the inverter were AC currents with an amplitude of $230V$ and a frequency of $50Hz$.

The currents obtained in the dq0 frame, using the rectifier and inverter control systems described earlier, are shown in Figure 2.6.

2.5 Conclusions

In the first part of this chapter, it was proven the necessity for using a nonlinear model, in the case of a PMSG. A nonlinear model has an insignificant estimation error, while a linear one has an error with a amplitude around four. Moreover, it was shown that using a discrete integrator with a continuous model is the best approach to discretize the PMSG. Therefore, the resulting system is hybrid, having both a continuous part (the model) and a discrete one (the state estimator).

Among the different control systems which are present in a WT, feedback control system was implemented for the rectifier and feedforward control for

the inverter. The generated currents, transformed in the dq0 frame, are stable, proving the effectiveness of the control structure.

Chapter 3

State Estimation

3.1 Introduction

STATE estimators are one of the two possible approaches to assure sensor redundancy - the other being state observers. This redundancy is critical for the monitoring of sensors and different equipment, and for constructing residuals which may be later used in fault diagnosis. The purpose of this chapter is to lay a foundation for the latter.

The main difference between state observers and estimators is that the latter consider the statistical properties of the process. They can use the covariance matrices of the process and the measurement noises. They also do not require a priori knowledge of the process uncertainties or the impact of faults. They can also be more insensitive to noises.

The best-known state estimator is the Kalman Filter (KF). It is an optimal estimator for linear systems affected by Gaussian noises, and is widely used. The Extended Kalman Filter (EKF) is the first nonlinear extension of the classical KF. It is widely used in localization and navigation, being the de facto standard. The Unscented Kalman Filter (UKF) is a further nonlinear extension of the Kalman Filter. It is used in military and aeronautic applications, as it can have superior performance to the EKF, in the presence of strong nonlinearities (Kulikov and Kulikova, 2017).

The objective of this chapter is to study the differences between these three state estimators. The selected case study is the Permanent Magnet Synchronous Generator (PMSG). These are used in direct drive wind turbines (Gliga, Lupu, et al., 2017), and their motor counterparts are widely used in hybrid electric vehicles Alameh et al., 2015. Multiple faults can affect such a machine (Alameh et al., 2015) (Niu and S. Liu, 2018), the most common being inter-turn short circuit, rotor demagnetization and eccentricity. These faults are usually detected and identified through signal processing techniques, by monitoring the vibrations of the generator shaft or of the stator. Nonetheless, dedicated sensors raise the cost of the equipment. Research was conducted on generator fault diagnosis and performance monitoring via currents or voltages (Ogidi, Barendse, and Mohamed

A. Khan, 2016) (Q. Zhang, Tan, and Xu, 2018), to eliminate the need for dedicated sensors. However, these electrical signals are affected by the change in wind speed and the results obtained from signal processing methods like the Fast Fourier Transform can be erroneous (Faiz and Nejadi-Koti, 2016).

A possible solution is to generate residuals between the real currents and the estimated ones Gliga, Chafouk, et al., 2018b. A state estimator can be used to ensure the required redundancy. The challenge, when using a state estimator, is to find out the covariance matrices for the process and for the measurement noises. If the matrices are not properly chosen, the estimated states might not converge to the real ones. The values of these matrices must be close to the real covariances to ensure the consistency of the estimation. The covariance matrix of the measurement noise can be easily found out using the procedure presented in (Levy, 2016). It is difficult to select a constant matrix for the process noise, since it is very hard, if not impossible, to estimate the process noise. Even if a good constant covariance matrix could be chosen, one which would guarantee the consistency of the estimated states, it would only be suited for certain values of the noise. If the environmental conditions or the degradation of the equipment would change the intrinsic uncertainties of the process, the covariance would change, and the estimation consistency would no longer be ensured.

The proposed solution is to use an iterative method which could be implemented online. The covariance matrix would be automatically adapted to always ensure the consistency of the estimated states. The method is simple to utilize, but its usage is constrained to certain non-linear systems. Its advantages and limitations are discussed in the conclusions.

This chapter is organized as follows: The algorithms of the KF, EKF and UKF are presented in Section 3.2. The estimation method is explained in Section 3.3, together with the obtained results. The three Kalman filters are compared in Section 3.4. The conclusions close this chapter.

3.2 Kalman Filters

3.2.1 The Kalman Filter

Although the linear model from (2.5) introduces significant modelling errors, it is interesting to see if a KF, which integrates this model, would achieve better results. The Kalman Filter uses a linear model of the form

$$\begin{aligned} \hat{x}_{k+1} &= A_k * \hat{x}_k + B_k * u_k, \\ \hat{y}_k &= C * \hat{x}_k \qquad\quad , \end{aligned} \tag{3.1}$$

where $x \in \mathbb{R}^{n_x}$ are the states of the process. $u \in \mathbb{R}^{n_u}$ are the inputs and $y \in \mathbb{R}^{n_y}$ are the outputs of the process. $A \in \mathbb{R}^{n_x * n_x}$ is the state matrix, $B \in$

$\mathbb{R}^{n_x * n_u}$ is the input matrix and $C \in \mathbb{R}^{n_y * n_x}$ is the output matrix. The number of states is n_x, the number of inputs is n_u and the number of measurements is n_y. The sampling time is k. The "^" denotes an estimation.

The model from (2.5) can be put into this form by combining the matrices G and H and using a vector with three elements for the inputs,

$$\begin{bmatrix} i_{d_{k+1}} \\ i_{q_{k+1}} \end{bmatrix} = A_k * \begin{bmatrix} i_{d_k} \\ i_{q_k} \end{bmatrix} + B_k * \begin{bmatrix} V_{d_k} \\ V_{q_k} \\ \phi \end{bmatrix}, \tag{3.2}$$

where

$$A_k = F_k = \begin{bmatrix} 1 - \frac{R_s T_s}{L_s} & T_s n_P \omega_k \\ -T_s n_P \omega_k & 1 - \frac{R_s T_s}{L_s} \end{bmatrix},$$

$$B_k = \begin{bmatrix} \frac{T_s}{L_s} & 0 & 0 \\ 0 & \frac{T_s}{L_s} & -\frac{T_s n_P \omega_k}{L_s} \end{bmatrix},$$

$$C = \begin{bmatrix} 1 & 0 \\ 0 & 1 \end{bmatrix}.$$

Then, the classical KF algorithm can be used (Ștefănoiu and Culiță, 2009)

- Prediction phase:

$$\hat{P}_k = A_k \hat{P}_k^* A_k^T + Q_k; \tag{3.3}$$

- Update phase:

$$K_k = \hat{P}_k C^T (C \hat{P}_k C^T + R_k)^{-1}; \tag{3.4}$$

$$\hat{x}_{k+1}^* = \hat{x}_k + K_k (y_k - C \hat{x}_k); \tag{3.5}$$

$$\hat{P}_k^* = (I - K_k C) \hat{P}_k; \tag{3.6}$$

where $P \in \mathbb{R}^{n_x * n_x}$ is the covariance matrix of the estimation error, $Q \in \mathbb{R}^{n_x * n_x}$ and $R \in \mathbb{R}^{n_y * n_y}$ are the covariance matrices of the process and the measurement noises. $K \in R^{n_x * n_y}$ is the Kalman gain and $y \in R^{n_y}$ are the measurements acquired from the process. The "*" denotes the corrected estimation.

3.2.2 The Extended Kalman Filter

The EKF also introduces a linearization, through the Taylor Series Expansion (TSE) of the state function. This linearization is used to estimate the covariance matrix of the estimation error. However, these linearizations are computed only around the current estimated state, so the introduced error should be small.

The EKF uses the most general formulation of a nonlinear model

$$\hat{x}_{k+1} = f(\hat{x}_k, u_k), \tag{3.7}$$

$$y_k = h(\hat{x}_k), \tag{3.8}$$

where the state function is $f : \mathbb{R}^{n_x+n_u} \to \mathbb{R}^{n_x}$ and the measurement function is $h : \mathbb{R}^{n_x} \to \mathbb{R}^{n_y}$. For the EKF, the model presented in (2.3) is already written in the required form. The algorithm of the EKF is (Foo, X. Zhang, and D. M. Vilathgamuwa, 2013):

- Prediction phase:

$$\hat{P}_k = F_k \hat{P}_{k-1} F_k^T + Q_k; \tag{3.9}$$

- Update phase:

$$K_k = \hat{P}_k H_k^T (H_k \hat{P}_k H_k^T + R_k)^{-1}; \tag{3.10}$$

$$\hat{x}_k^* = \hat{x}_k + K_k * (y_k - \hat{y}_k); \tag{3.11}$$

$$\hat{P}_k^* = (I - K_k H_k)\hat{P}_k; \tag{3.12}$$

where $F \in \mathbb{R}^{n_x * n_x}$ and $H \in \mathbb{R}^{n_y * n_x}$ are the Jacobians of the state and measurement functions.

3.2.3 The Unscented Kalman Filter

The UKF uses the Unscented Transform (UT) (Althof and Ferber, 2017) to account for the nonlinearity in the model. The current estimation of the state is treated as the mean value of a probability distribution, which has the same covariance as the estimation error. Depending on the implementation, either $2n_x + 1$ (for a full order UT) or $n_x + 1$ (for a reduced order UT) points are chosen around the current mean. Each sigma point has a certain weight associated with it. There are multiple ways to choose the sigma points (Van der Merwe and Wan, 2001) (Terejanu, 2008).

The UKF uses the same model shown in (2.3). The chosen (sigma) points are propagated through the state function. The new points are used to compute the new estimate of the mean, i.e. the state, and its covariance. The new points are also propagated through the measurement function, and their mean is the estimated output of the system (Van der Merwe and Wan, 2001). The next steps are similar, in concept, to the algorithm of the EKF.

The classical formulation of the UKF uses the square root of the covariance matrix of the estimation error to compute the sigma points. To calculate the square root, the covariance matrix must be at least positive semi-definite, which is not guaranteed by the algorithm. A more stable version of the UKF, with a similar degree of complexity is the Square Root UKF (SRUKF). Its algorithm is (Van der Merwe and Wan, 2001):

- Choose the sigma points:
  - Select the weights of the sigma points, (Terejanu, 2008)

$$W_i = \frac{1 - W_0}{2n_x}, \tag{3.13}$$

    where W_0 is chosen arbitrarily. A positive value moves the sigma points further away from the previous estimate of the state, while a negative one brings them closer to the previous average. However, the weights must obey the condition

$$\sum_{i=0}^{2n_x} W_i = 1.$$

  - Compute the scaling parameters

$$\eta_i = \sqrt{\frac{n_x}{1 - W_i}}. \tag{3.14}$$

  - Choose the actual sigma points

$$, \chi_{k-1_0|k} = \hat{x}^*_{k-1}, \tag{3.15}$$

$$\chi_{k-1_i|k} = \hat{x}^*_{k-1} + \eta_i \hat{S}^*_{k-1}, \tag{3.16}$$

    where $i = \overline{1, n_x}$

$$\chi_{k-1_i|k} = \hat{x}^*_{k-1} - \eta_i \hat{S}^*_{k-1}, \tag{3.17}$$

    where $i = \overline{n_x + 1, 2n_x}$;

- Prediction phase:
  - Propagate the sigma points through the state function

$$\chi_{k_i|k} = f(\chi_{k-1_i|k}); \tag{3.18}$$

  - Compute the new state estimation

$$\hat{x}_k = \sum_{i=0}^{2n_x} W_i \chi_{k_i|k}; \tag{3.19}$$

  - Calculate and then update the square root of the state covariance matrix

$$\hat{S}_{x_k} = qr([\sqrt{W_i}(\chi_{k_i|k} - \hat{x}_k) \quad \sqrt{Q_k}]); \tag{3.20}$$

    for $i = \overline{1, 2n_x}$. "qr" refers to the QR decomposition.

$$\hat{S}_{x_k} = cholupdate(S_{x_k}, \chi_{k_0|k} - \hat{x}_k, sign(W_0)); \tag{3.21}$$

"cholupdate" is the rank 1 update. The rank update formula is $A1 = A \pm x * x^T$ where A is the matrix obtained through a Cholesky factorization (replaced by a QR one in this case) and x is a column vector. The sign to be used in the update is the one of W_0.

- Propagate the "state" sigma points through the measurement function

$$\mathcal{Y}_{k_i} = h(\chi_{k_i|k}); \tag{3.22}$$

- Compute the new measurement estimation

$$\hat{y}_k = \sum_{i=0}^{2n_x} W_i \mathcal{Y}_{k_i}; \tag{3.23}$$

- Update phase
  - Compute and then update the square root of the output covariance matrix

$$\hat{S}_{y_k} = qr([\sqrt{W_i}(\mathcal{Y}_{k_i} - \hat{y}_k) \quad \sqrt{R_k}]); \tag{3.24}$$

for $i = \overline{1, 2n_x}$

$$\hat{S}_{y_k} = cholupdate(S_{y_k}, \mathcal{Y}_{k_0} - \hat{y}_k, sign(W_0)); \tag{3.25}$$

  - Calculate the covariance between the states and the measurements

$$\hat{P}_{xy_k} = \sum_{i=0}^{2n_x} W_i(\chi_{k_i|k} - \hat{x}_k)(\mathcal{Y}_{k_i} - \hat{y}_k)^T; \tag{3.26}$$

  - Find out the Kalman gain

$$\mathcal{K}_k = (\hat{P}_{x_k y_k} / \hat{S}_{y_k}^T) / \hat{S}_{y_k}; \tag{3.27}$$

  - Update the state estimation

$$\hat{x}_k^* = \hat{x}_k + \mathcal{K}_k(y_k - \hat{y}_k); \tag{3.28}$$

  - Correct the square root of the state covariance matrix

$$S_{x_k} = cholupdate(S_{x_k}, \mathcal{K}_k S_{\hat{y}_k}, -1). \tag{3.29}$$

3.3 Covariance Estimation

The measurement noise covariance matrix can be easily estimated (Levy, 2016). The measurement noise affects the data through the sensors. Information about this perturbation is available in the sensor datasheet, as

the sensor tolerance or precision. This is the standard deviation of the measurements of the sensor. Thus, the covariance matrix can be computed as:

$$R = \begin{bmatrix} \sigma_1^2 & 0 & \dots & 0 \\ 0 & \sigma_2^2 & \dots & 0 \\ \vdots & \vdots & \ddots & \vdots \\ 0 & 0 & \dots & \sigma_n^2 \end{bmatrix},$$

where $\sigma_i, i = \{1, 2, ..., n_y\}$ is the standard deviation on each measurement channel. This matrix is diagonal because there is a single sensor on each measurement channel. Therefore, the data acquired by each sensor is only affected by the noise which perturbs that channel.

One possible counter argument to the above reasoning might be that R is constant and the noise covariance might change due to sensor faults or degradation of the equipment. Firstly, sensors are routinely calibrated, at intervals specified by the legislation of each country, or by the manufacturer. This calibration frequency is also mentioned in international standards, such as ISO:9001 (DNV GL, 2015). Therefore, the tolerance should remain within the limits specified on the datasheet and the covariance matrix should be constant. Secondly, if the sensor is faulty, it should be replaced. A sensor fault can be quickly diagnosed using an EKF (Idrissi, El bachtiri, and Chafouk, 2017).

Thus, only the process noise covariance matrix Q remains to be computed. The nonlinear state-space model of the real process is

$$x_k = f(x_{k-1}, u_k) + w_k, \tag{3.30}$$

$$y_k = h(x_k) + v_k, \tag{3.31}$$

where $w_k \in \mathbb{R}^{n_x}$ is the noise or uncertainty which affects the process and $v_k \in \mathbb{R}^{n_y}$ is the perturbation of the measurements. These noises are assumed to be independent and normally distributed. The lack of symbols over the variables means that all of them are the real states and outputs of the process.

The estimation error is

$$\epsilon_k = y_k - \hat{y}_k = h(x_k) + v_k - h(\hat{x}_k), \tag{3.32}$$

which can be re-written as

$$\epsilon_k = h(f(x_{k-1}, u_k) + w_k) + v_k - h\left(f\left(\hat{x}^*_{k-1}, u_k\right)\right). \tag{3.33}$$

Assumption 1: $h : R^{n_x} \to R^{n_y}$ is a linear function defined as $h(x) = Ax+b$,

where $A \in R^{n_y * n_x}$ is an invertible matrix and $b \in R^{n_y}$ is a vector. Since A is invertible, it is a square matrix and $n_y = n_x$. For simplicity, A and b will be considered constant.

This assumption is restrictive. The number of measurements is usually higher than the number of states and the measurement function is generally nonlinear. There are workarounds around these constraints, which will be the focus of future research. The possible solutions are:

- For a linear measurement function with a non-invertible matrix A, the pseudoinverse can replace the inverse of the matrix;
- A non-linear measurement function can be approximated using Taylor Series Expansion (TSE). For simplicity, it can be linearized by considering only the first term of the TSE, namely the Jacobian matrix. The same reasoning was used to design the EKF. If the Jacobian is not invertible, its pseudoinverse can be used. This Jacobian can be either pre-computed or estimated online using cvasi-Newton methods.

Equation (3.33) becomes

$$\epsilon_k = h\left(f\left(x_{k-1}, u_k\right)\right) + h\left(w_k\right) + v_k - h\left(f\left(\hat{x}^*_{k-1}, u_k\right)\right). \tag{3.34}$$

Assumption 2: The estimation error between the real and the estimated states tends to zero, i.e. $\lim_{k\to\inf}\left(x_k - \hat{x}_k\right) = 0$.

This assumption is also restrictive, since it implies that the covariance matrix of the error tends to zero. However, in usual applications, the covariance may tend to a non-zero value or even non-constant values. In the second case, it would oscillate around a certain set of values for its elements, and the amplitude and frequency of these oscillations would depend on the uncertainties affecting the process. Therefore, the system should have a high observability index, in order to use this method.

Equation (3.34) can be reduced to

$$\epsilon_k = h\left(w_k\right) + v_k. \tag{3.35}$$

The covariance matrix of the error can be computed as

$$c\hat{o}v\left(\epsilon_k, \epsilon_k\right) = c\hat{o}v\left(h\left(w_k\right) + v_k, h\left(w_k\right) + v_k\right), \tag{3.36}$$

$$c\hat{o}v(\epsilon_k, \epsilon_k) = c\hat{o}v(Aw_k + v_k + b, Aw_k + v_k + b). \tag{3.37}$$

b is a constant vector, therefore

$$c\hat{o}v\left(\epsilon_k, \epsilon_k\right) = c\hat{o}v\left(Aw_k + v_k, Aw_k + v_k\right). \tag{3.38}$$

The previous equation can be re-written using the bilinearity property of the covariance (Culiță and Ștefănoiu, 2008)

$$\hat{cov}\left(\epsilon_k, \epsilon_k\right) = \hat{cov}\left(Aw_k, Aw_k\right) + \hat{cov}\left(v_k, v_k\right) + \hat{cov}\left(Aw_k, v_k\right) + \hat{cov}\left(v_k, Aw_k\right). \quad (3.39)$$

The noises are independent even when they are propagated through the linear transformation A. Therefore, the covariance of the estimation error is equal to

$$\hat{cov}\left(\epsilon_k, \epsilon_k\right) = \hat{cov}\left(Aw_k, Aw_k\right) + \hat{cov}\left(v_k, v_k\right). \quad (3.40)$$

The previous equation can be rewritten as

$$\hat{cov}\left(\epsilon_k, \epsilon_k\right) = A \cdot \hat{cov}\left(w_k, w_k\right) \cdot A^T + \hat{cov}\left(v_k, v_k\right), \quad (3.41)$$

which can be reformulated using the specific notations of the EKF

$$\hat{cov}\left(\epsilon_k, \epsilon_k\right) = AQ_kA^T + R. \quad (3.42)$$

The estimation of the process noise covariance matrix is

$$Q_k = A^{-1}\left(\hat{cov}\left(\epsilon_k, \epsilon_k\right) - R\right)\left(A^{-1}\right)^T. \quad (3.43)$$

The covariance matrix of the estimation error can be computed online using (Burkholder, 2013)

$$\hat{cov}\left(\epsilon_k, \epsilon_k\right) = \hat{cov}\left(\epsilon_{k-1}, \epsilon_{k-1}\right) - \frac{\hat{cov}\left(\epsilon_{k-1}, \epsilon_{k-1}\right) - \left(\epsilon_k - \bar{\epsilon}_k\right)\left(\epsilon_k - \bar{\epsilon}_k\right)^T}{k}, \quad (3.44)$$

where $\bar{\epsilon}_k$ is the mean of the estimation error, computed at sampling time k.

3.3.1 Simulation of the proposed method

The proposed method was tested for an EKF, which was used to estimate the currents generated by the PMSG of a direct drive wind turbine. To use (2.1) and (2.2) in the EKF, the authors used the continuous model with a discrete-time integrator, as shown in Chapter II. This approach is also used by the Simscape/Power Systems toolbox to discretize the model of the generator, when the user selects a discrete-time simulation.

The proposed method was compared with two other ones from the literature, namely the ones presented in (Z. Liu and He, 2017) and (Akhlaghi, Zhou, and Huang, 2017).

In a real implementation, the noise cannot be directly measured. The quantifiable measure of performance is the error between the generated and the estimated currents.

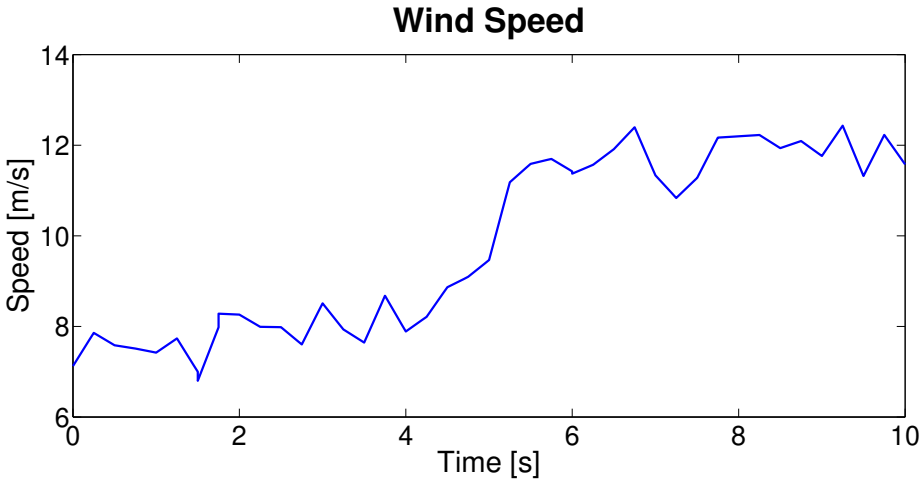

FIGURE 3.1: The profile of the wind speed

In the simulation, the wind speed changes from $8m/s$ to $12m/s$, and it is disturbed by a gaussian noise with a mean of zero and a variance of 0.2. The profile of the wind speed is shown in Figure 3.1.

To test the proposed method, the sensor noise covariance matrix was initialized with the values

$$R = \begin{bmatrix} 0.0001 & 0 \\ 0 & 0.0001 \end{bmatrix},$$

and was kept constant throughout the simulations. These values correspond to a current sensor with a tolerance of 1% (LEM, n.d.). The EKF was implemented to estimate the currents in the dq0 reference frame. However, the estimation error is presented in the abc reference frame.

Initially, no noise was added to the measurements and the parameters of the model were considered constant. The results obtained are shown in Figures 3.2, 3.3, and 3.4.

There is a small error around 10^{-13} for all the three methods, due to the way Simscape Power Systems library works: the electrical model is approximated with either a state space model (for continuous or discrete simulations) or with a transfer function model (for phasor simulation) (TransÉnergie Technologies Inc, 2003).

Due to the limitations of the Simscape/Power System toolbox, the parameters of the blocks, which are used to model the electrical components such as the generator, cannot be changed while the simulation is running. Therefore, all possible 27 combinations of parameter values were considered - maximum, minimum and nominal for each one, in the absence of perturbations. The results are similar for many combinations. The system was simulated when R_s is 10% lower, L_s is 7% higher and Φ is 2.5% lower than their nominal values, and no noise is added.

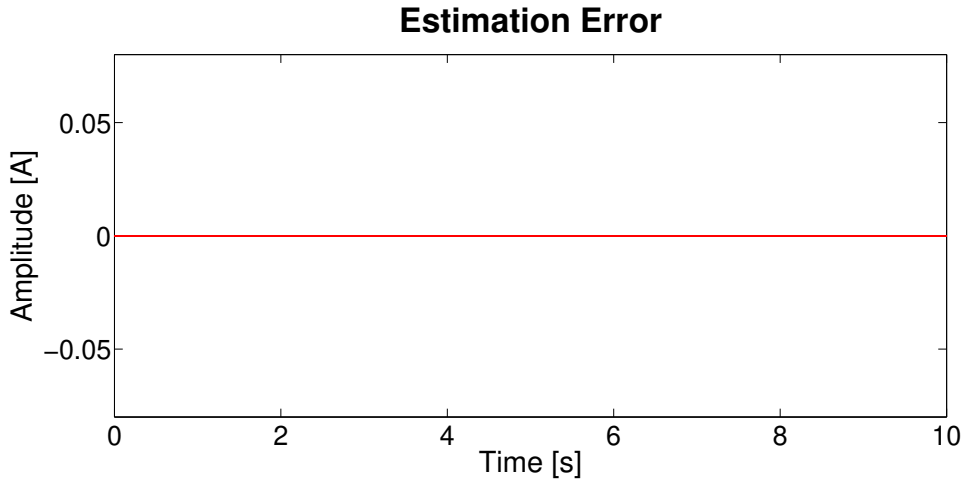

FIGURE 3.2: The estimation error using the EKF with the proposed method.

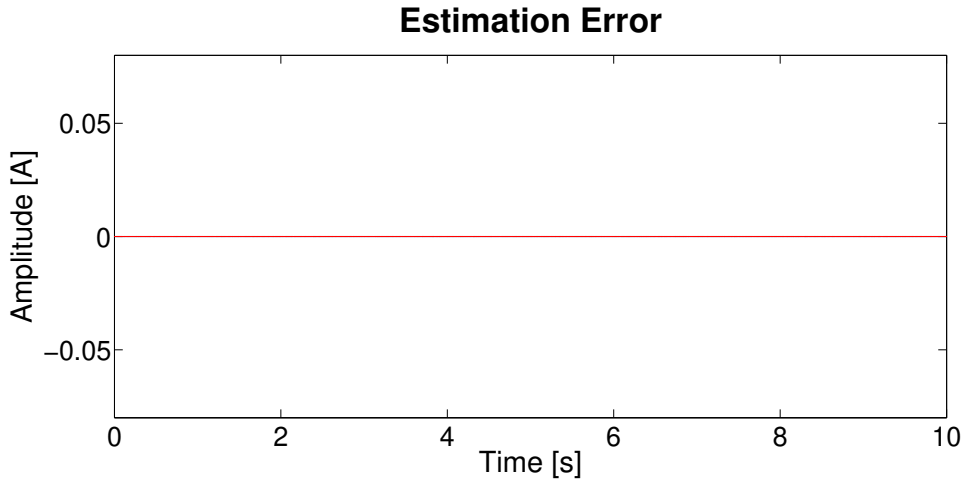

FIGURE 3.3: The estimation error using the EKF with the method from (Z. Liu and He, 2017).

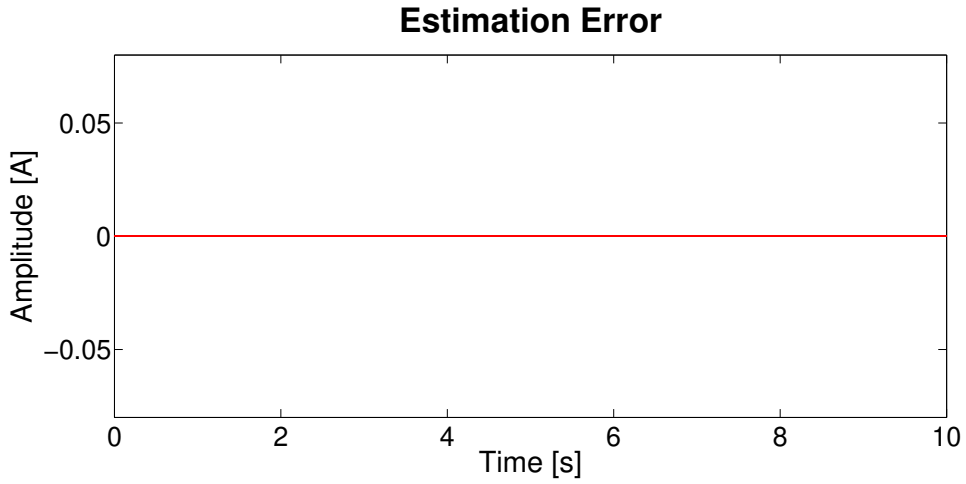

FIGURE 3.4: The estimation error using the EKF with the method from (Akhlaghi, Zhou, and Huang, 2017).

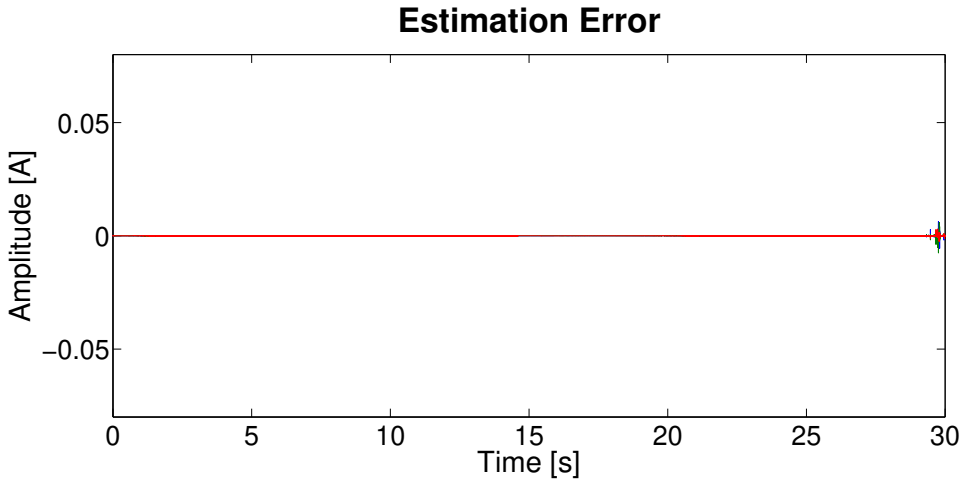

FIGURE 3.5: The estimation error using the EKF with the proposed method. The parameters are different from the nominal case.

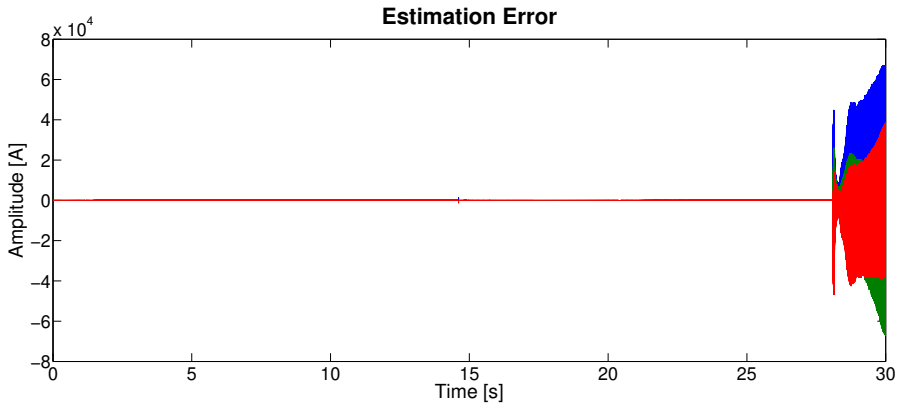

FIGURE 3.6: The estimation error using the EKF with the method from (Z. Liu and He, 2017). The parameters are different from the nominal case.

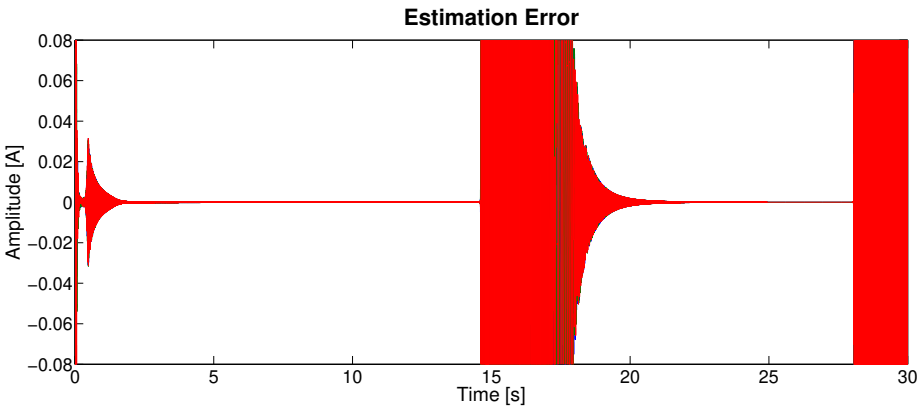

FIGURE 3.7: Zoom in on the estimation error computed using the EKF with the method from (Z. Liu and He, 2017). The parameters are different than in the nominal case.

The results obtained, when the parameters of the process are different

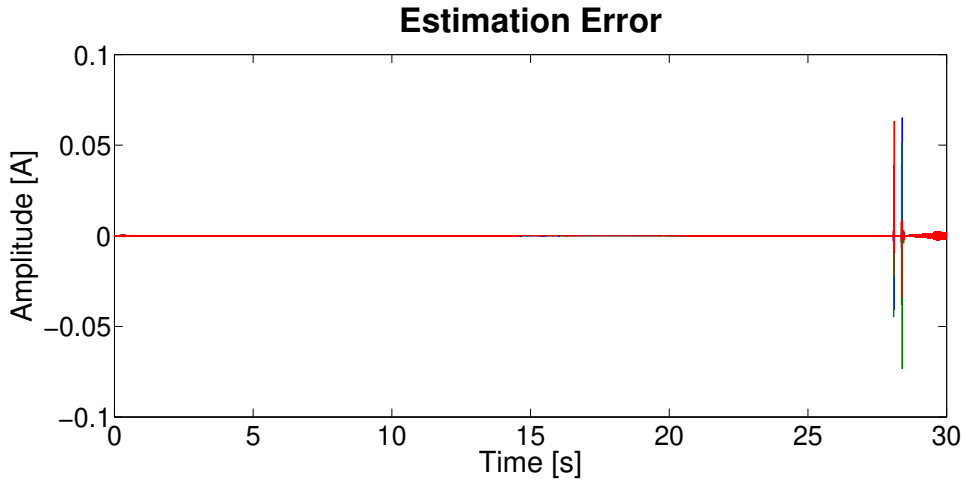

FIGURE 3.8: The estimation error using the EKF with the method from (Akhlaghi, Zhou, and Huang, 2017). The parameters are different from the nominal case.

than the ones of the model, are shown in Figures 3.5, 3.6 and 3.8. Due to the large estimation error of the method from (Z. Liu and He, 2017), a zoomed in version is shown in Figure 3.7. During a 10 sec simulation, the output is continuously increasing, therefore the simulation duration was changed to 30 sec, to completely observe the behavior. Because of the very low sampling period, 10^{-6}, the computer would run out of memory for longer simulations.

When the process has different parameters than the model, the EKF which uses the proposed method has the lowest error, less than $0.1A$. It is followed by the EKF which utilizes the procedure from (Akhlaghi, Zhou, and Huang, 2017). The method from (Z. Liu and He, 2017) causes the EKF to become unstable.

Zero-Mean Noises (ZMNs) was added to the signals used by the EKFs. These noises were introduced by the sensors measuring the voltages, the angular velocity of the shaft and the currents. The voltage was perturbed by a noise with a variance of 2, to correspond to a sensor tolerance of 0.5% (LEM, 2013). The noise affecting the current had a variance of 3.5, as a sensor with a tolerance of 1% (LEM, n.d.). The angular velocity was affected by a perturbation with a variance of 14, to simulate a sensor with a tolerance of 1%. The values of the variances were chosen using the assumed tolerance and the maximum amplitudes of these signals. The results are presented in Figures 3.9, 3.10, and 3.11.

In Figures 3.12 to 3.15 are presented the estimation errors in the presence of Non-Zero Mean Noises (NZMN). The noise affecting the voltages has a mean of 1, the one perturbing the angular velocity has a mean of 2 and the current perturbation has a mean of 3. Although these values were chosen arbitrarily, they can represent sensor biases. In this case, there is a

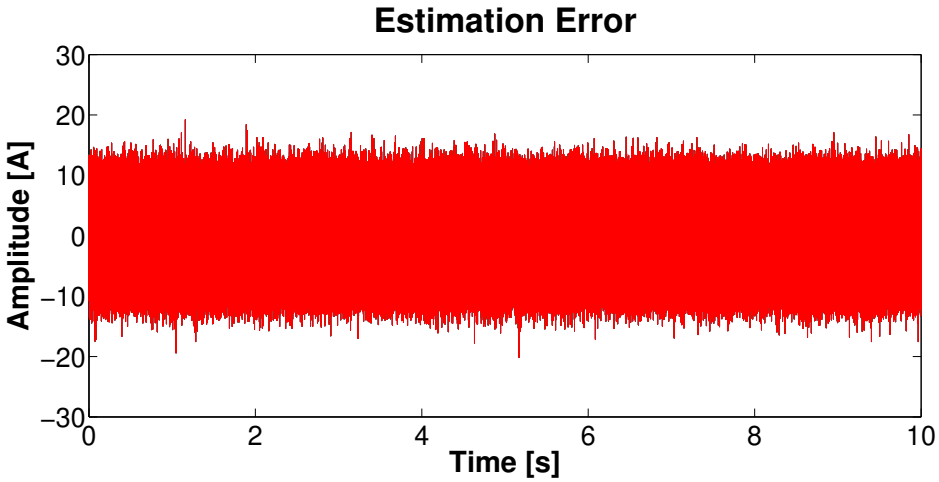

FIGURE 3.9: The estimation error using the EKF with the proposed method, in the presence of zero mean noises.

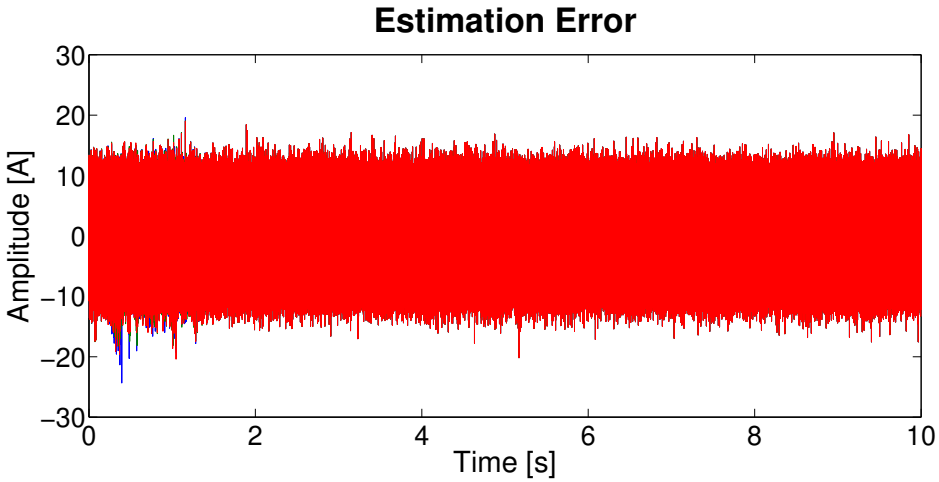

FIGURE 3.10: The estimation error using the EKF with the method from (Z. Liu and He, 2017), in the presence of zero mean noises.

DC component in the error in this case. The mean of the error can be used to detect sensor faults. Machine faults can be detected through signal processing techniques applied on the residuals.

The results of all the simulations are summarized in Table 3.1.

None of the methods seems to be affected by the variation in the wind speed. The only significant difference between them is the speed. The proposed method is the fastest. It is followed by the one from (Akhlaghi, Zhou, and Huang, 2017) and then the procedure from (Z. Liu and He, 2017). The speed of each method was found out by observing the increments of the simulation time, in Simulink. Their values were: 10 for the proposed method, 2 for the one from (Z. Liu and He, 2017) and 6.66 for the one from (Akhlaghi,

[1]Zero Mean Noises
[2]Non-Zero Mean Noises
[3]Different Parameters

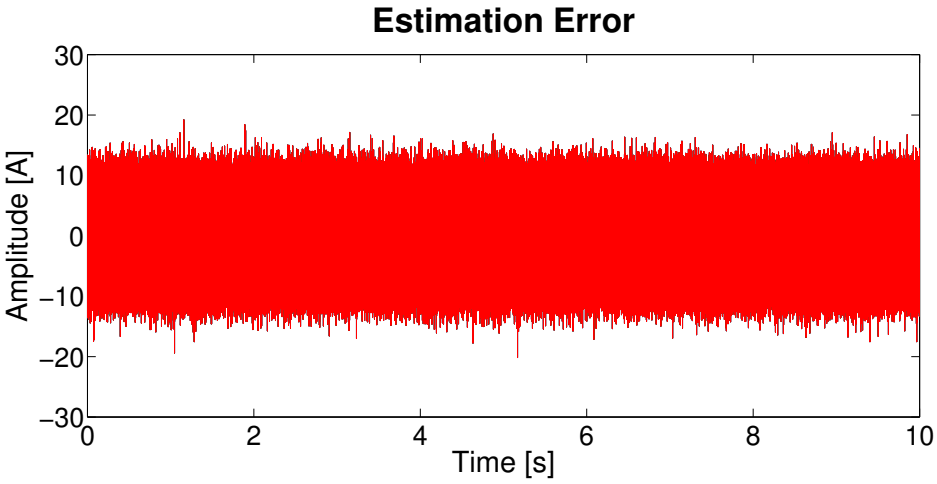

FIGURE 3.11: The estimation error using the EKF with the method from (Akhlaghi, Zhou, and Huang, 2017), in the presence of zero mean noises.

TABLE 3.1: Comparison of the different methods.

Method	**RMS Error in presence of**				**Speed** [%]	**Applicability**
	no noise	ZMNs [1]	NZMNs [2]	DP [3]		
Proposed	$\approx 10^{-14}$	3.5004	11.0669	$\approx 10^{-6}$	100	Any Algorithm
(Z. Liu and He, 2017)	$\approx 10^{-14}$	3.5051	347.9036	$\approx 10^{+3}$	20	Only the EKF
(Akhlaghi, Zhou, and Huang, 2017)	$\approx 10^{-14}$	3.5004	11.0669	$\approx 10^{-4}$	66.6	Only the EKF

Zhou, and Huang, 2017). They were later converted to percentage of the speed of the proposed method. These results were obtained using the "Normal" simulation mode in Simulink.

The maximum amplitude of the generated current is around 400 Amperes. In the presence of noises, the proposed method has an estimation error of 3.68%, as the one from (Akhlaghi, Zhou, and Huang, 2017).

The proposed method is very easy to implement, but it requires the covariance matrix of the measurement noise. It is at least as precise as the method from (Akhlaghi, Zhou, and Huang, 2017), but it is faster, because of the lower complexity. Moreover, it is completely independent of the EKF, and can be used for any algorithm. The potential disadvantage of the proposed method is its reliance on the precomputed covariance matrix of the measurement noise. If this matrix does not closely approximate the real covariance, the estimation of the EKF might not be accurate and precise.

The procedure from (Z. Liu and He, 2017) is the slowest. Its accuracy and precision are lower than the other two. It can only be applied for the EKF.

The method from (Akhlaghi, Zhou, and Huang, 2017) can be used only for the EKF. In simulation, the forgetting factor α was chosen equal to 0.5.

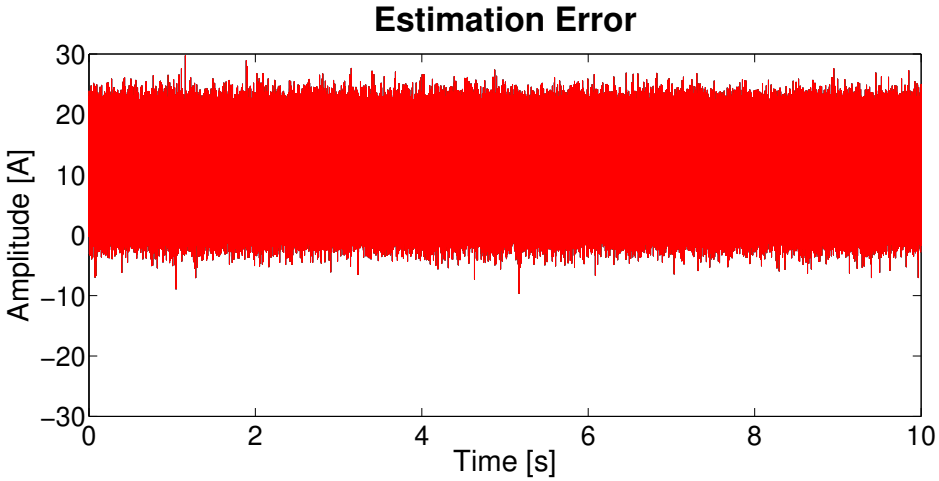

FIGURE 3.12: The estimation error using the EKF with the proposed method, in the presence of non-zero mean noises.

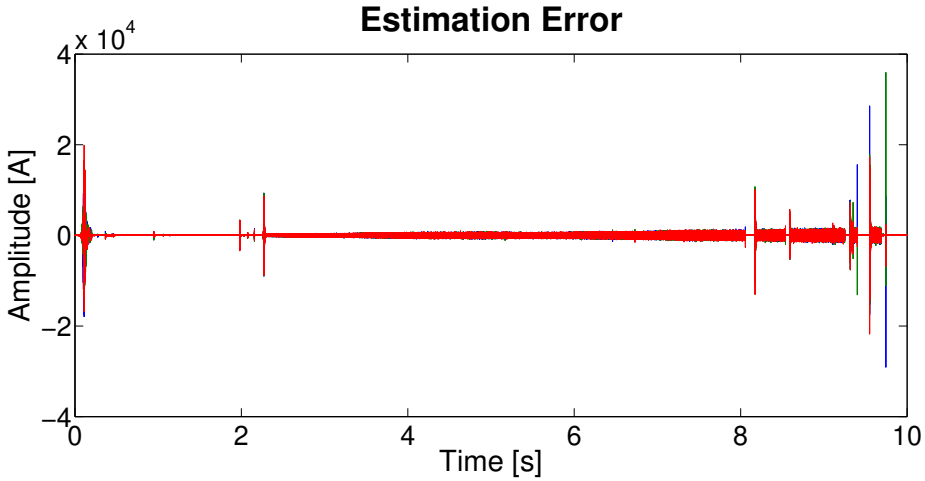

FIGURE 3.13: The estimation error using the EKF with the method from (Z. Liu and He, 2017), in the presence of non-zero mean noises.

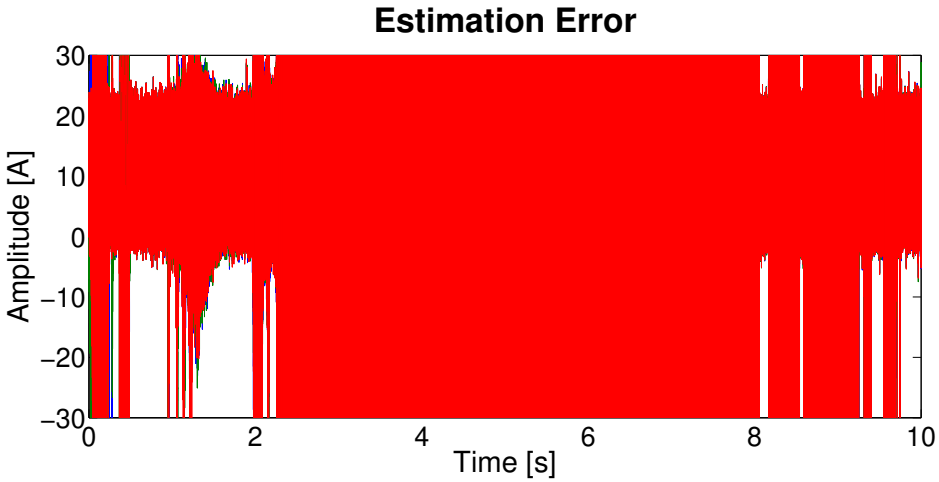

FIGURE 3.14: Zoom in on the estimation error using the EKF with the method from (Z. Liu and He, 2017), in the presence of non-zero mean noises.

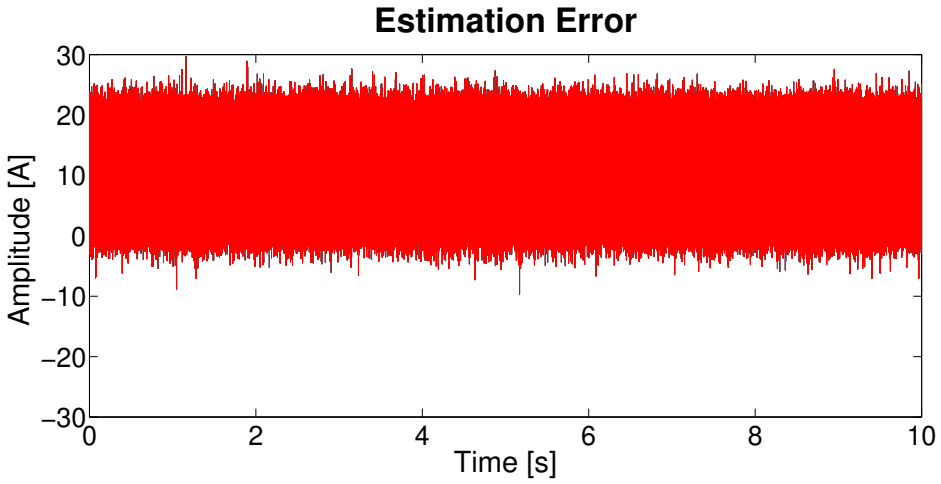

FIGURE 3.15: The estimation error using the EKF with the method from (Akhlaghi, Zhou, and Huang, 2017), in the presence of non-zero mean noises.

The frequency of the errors is mainly due to the very small sampling period used for the simulation, 10^{-6}. In the simulation, noise is generated at each sampling moment, while the parameters of the process have their nominal values. Due of the lack of a filter, the noise was directly propagated in the current. Moreover, the simulation duration is $10s$, and the frequency of the generated current is $50Hz$. In each figure, expect Figures 3.5 to 3.8, are shown three phases, therefore 5000 oscillations of the currents.

The estimations of the noise covariance matrices, in the nominal case, are:

- For the simulations without perturbations:
  - The proposed method:
    - The elements on the main diagonal of Q have negative values in the order of 10^{-4} while the elements on the anti-diagonal have negative values in the order of 10^{-25}.
  - The method from (Z. Liu and He, 2017):
    - The elements of Q are zero.
    - The elements of R have values in the order of 10^{-35} on the diagonal and in the order of 10^{-36} on the anti-diagonal.
  - The method from (Akhlaghi, Zhou, and Huang, 2017):
    - The elements on the main diagonal of Q have positive values in the order of 10^{-24} and 10^{-22}, while the elements on the anti-diagonal have positive values in the order of 10^{-23}.
    - The elements of R have values in the order of 10^{-3} on the diagonal and a negative element in the order of 10^{-23} together with another positive one in the order of 10^{-24} on the anti-diagonal.

- For the simulations with zero mean noises:
  - The proposed method:
    - The elements on the main diagonal of Q have positive values in the order of 10^5 while the elements on the anti-diagonal have negative values in the order of 10^5.
  - The method from (Z. Liu and He, 2017):
    - The elements on the main diagonal of Q have positive values in the order of 10^{11} while the elements on the anti-diagonal have negative values in the order of 10^9.
    - The elements of R have values in the order of 10^1, namely 10.4 and 33.46 on the main diagonal and 18.65 on the anti-diagonal.
  - The method from (Akhlaghi, Zhou, and Huang, 2017):
    - The elements on the main diagonal of Q have positive values in the order of 10^6 while the elements on the anti-diagonal have negative values in the order of 10^6.
    - The elements of R have values in the order of 10^{-3}, with negative elements, of the same order, on the anti-diagonal.
- For the simulations with non-zero mean noises:
  - The proposed method:
    - The elements on the main diagonal of Q have positive values in the order of 10^{10} while the elements on the anti-diagonal have negative values in the order of 10^{10}.
  - The method from (Z. Liu and He, 2017):
    - The elements on the main diagonal of Q have positive values in the order of 10^{11} while the elements on the anti-diagonal have negative values in the order of 10^8.
    - The elements of R have the values 0.7655 and 40.26 on the diagonal, respectively 5.552 on the anti-diagonal.
  - The method from (Akhlaghi, Zhou, and Huang, 2017):
    - The elements on the main diagonal of Q have positive values in the order of 10^{11} while the elements on the anti-diagonal have negative values in the order of 10^{11}.
    - All the elements of R have values in the order of 10^{-1}, with a negative element on the anti-diagonal.
- For the simulation without perturbations, but with different parameters for the process:
  - The proposed method:

    - The elements on the main diagonal of Q are $\approx 10^{18}$ and $\approx 10^{12}$, while the elements on the anti-diagonal are both $\approx 10^{15}$.
  - The method from (Z. Liu and He, 2017):
    - Both Q and R have values that are not numbers (NaNs in Matlab), hence the instability of the EKF which uses this method.
  - The method from (Akhlaghi, Zhou, and Huang, 2017):
    - The elements on the main diagonal of Q have positive values in the order of 10^{19} and 10^{14}, while the elements on the anti-diagonal have negative values in the order of 10^{17}.
    - The elements of the first row of R are $\approx -10^{7}$ and $\approx -10^{4}$, while the elements on the second row are -1215 and -4735.

The results of the proposed method are very similar the ones obtained using the procedure presented in (Akhlaghi, Zhou, and Huang, 2017). The values of the process noise covariance matrices tend to have similar orders of magnitude. The measurement noise covariance matrix estimated using the method from (Akhlaghi, Zhou, and Huang, 2017) tends to have lower values than the constant covariance matrix used in the proposed method. This may explain their similar behaviors and results.

3.4 Comparison between the state estimators

The results of the comparison are shown and Figures 3.16 - 3.18 and they are summarized in Table 3.2. No noises were introduced, to test their behavior in the ideal case.

The initial error of the SRUKF is not zero but is close to 10^{-4}. However, in time it quickly converges to $\approx 10^{-13}$. This is due to improper initialization, so the initial error is ignored.

As complexity, the KF and the EKF are the same. This is because the Jacobian of the state function can be computed in advance. It depends on ω_{m_k}, but so does the state matrix of the linear model. The SRUKF is by far the most complex.

The EKF is the fastest of the three filters, being closely followed by the KF and then, by a large margin, the SRUKF. The sigma point selection, the propagation of the $2n_x + 1$ points through the state function, the QR decompositions and the Cholesky rank update slow it down considerably. The slowdown of the KF might seem surprising. The linear model requires the computation of more mathematical operations - 27, in comparison with the nonlinear one - 21. As the rest of the algorithms are the same, the slowdown is due only to the model.

All filter present oscillations. While the EKF and UKF assure a very low modelling error, the KF is plagued by rather large spikes. To understand

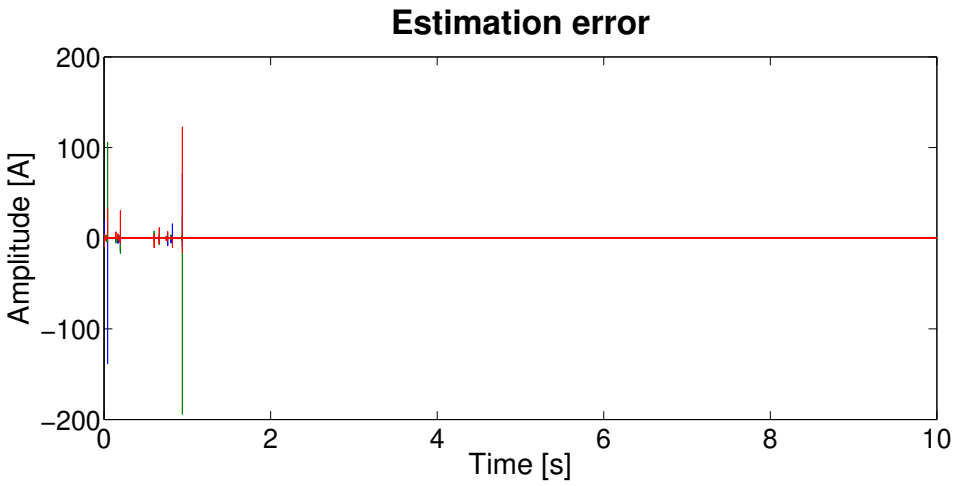

FIGURE 3.16: Estimation error using the Kalman Filter.

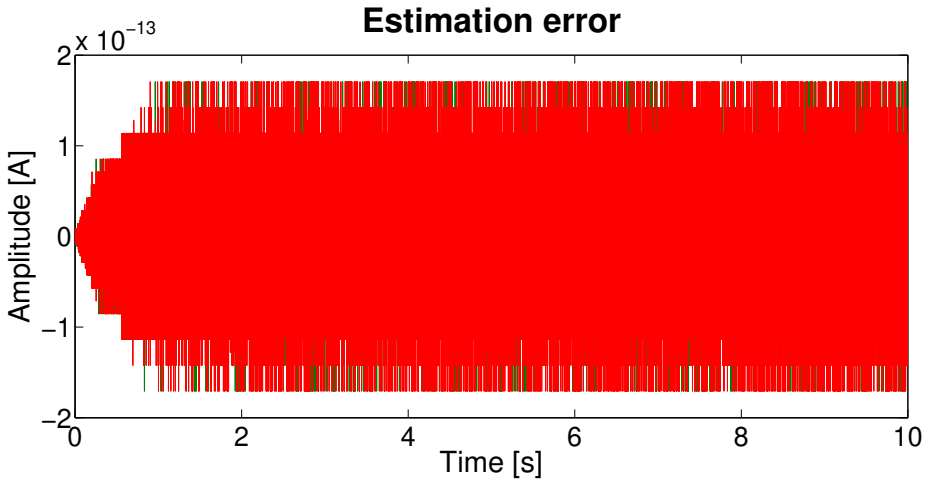

FIGURE 3.17: Estimation error using the Extended Kalman Filter.

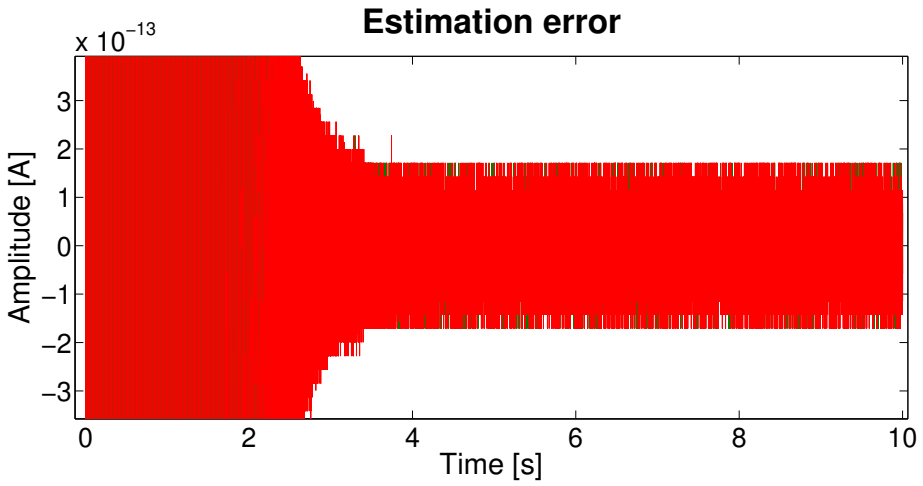

FIGURE 3.18: Estimation error using the Square Root Unscented Kalman Filter.

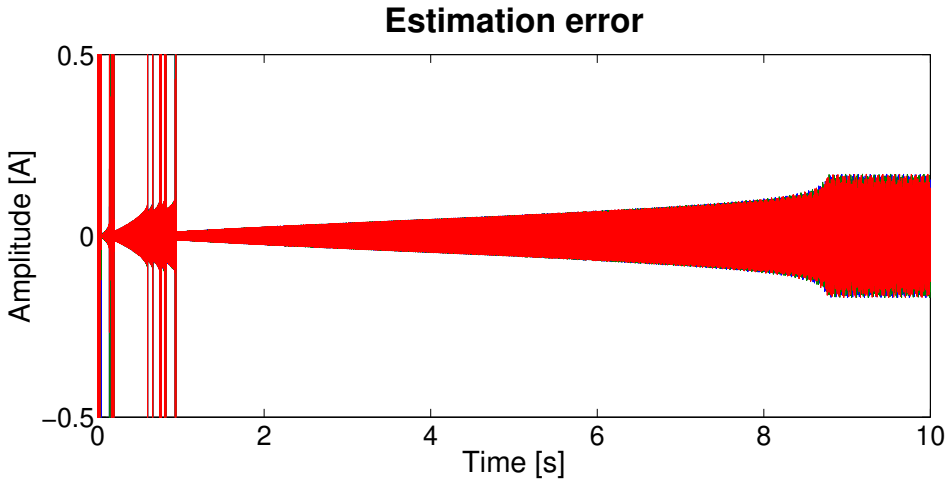

FIGURE 3.19: Zoom in of the estimation error using the KF.

what is happening, a zoomed in view of the estimation error of the KF is presented in Figure 3.19.

Before the large spike, the error of the KF oscillates but fairly slow, with certain pauses between each oscillation. In time, due to accumulation of energy, large oscillations appear, like the great spikes. After the large spike, the oscillation frequency has increased, so all the energy causing the previous large spikes is dissipated more quickly. A similar phenomenon can be seen for the EKF and UKF, where very small oscillation are present, but with a very high frequency.

The cause of these oscillations is the approximation made by Simulink. The electrical model of the wind turbine was made using the Simscape / PowerSystems toolbox. When the Simulink diagram is compiled, the electrical model is approximated by a state space model. This introduces differences between the model used in the state estimators and the one used by Simulink. All filters try to compensate for this difference in a similar manner, as a P controller. As the KF uses a linearized model which is even further away from the one used by Simulink, it is harder for it to achieve and maintain a null error. However, because both the state matrix used by the KF and the Jacobian of the state function used by the EKF depend

TABLE 3.2: Comparison of the state estimators.

Estimator	Speed [% of EKF]	Maximum error	Complexity
KF	97.5	≈ 194	Low
EKF	100	$\approx 10^{-13}$	Low
SRUKF	40	$\approx 10^{-13}$	High

on time, together with the intrinsic design (varying amplification and state covariance matrix) of the two filters, they manage to minimize the error. The UT transform helps the SRUKF to minimize the error. The EKF and SRUKF, as they use the nonlinear model, are better.

One might argue that both the EKF and the nonlinear model with a discrete integrator produce a similar estimation error (in the order of 10^{-12} and 10^{-13}), so the added complexity of the EKF is useless. However, when noise is added, the utility of the EKF is obvious (Figures 3.20 and 3.21). Zero mean noise with a variance of one was added to the measurement of the voltages, which are used as inputs for the model.

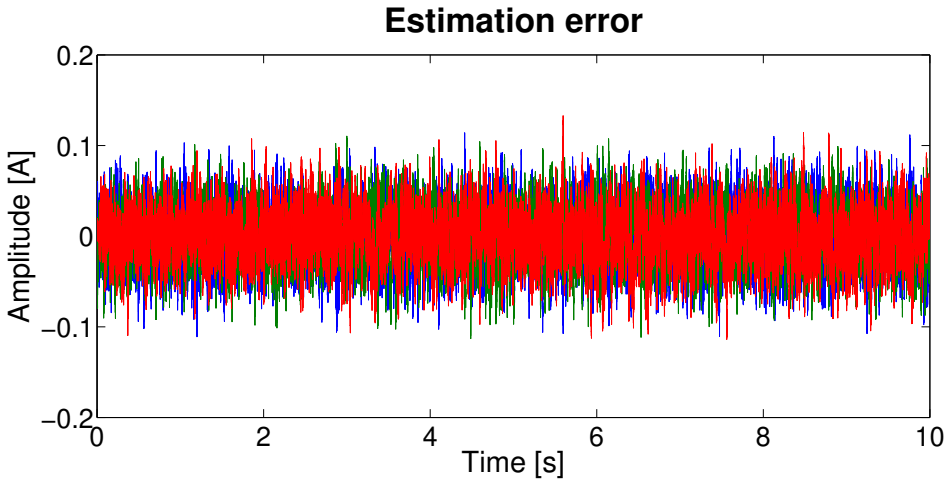

FIGURE 3.20: Estimation error using the nonlinear model, in the presence of gaussian noise.

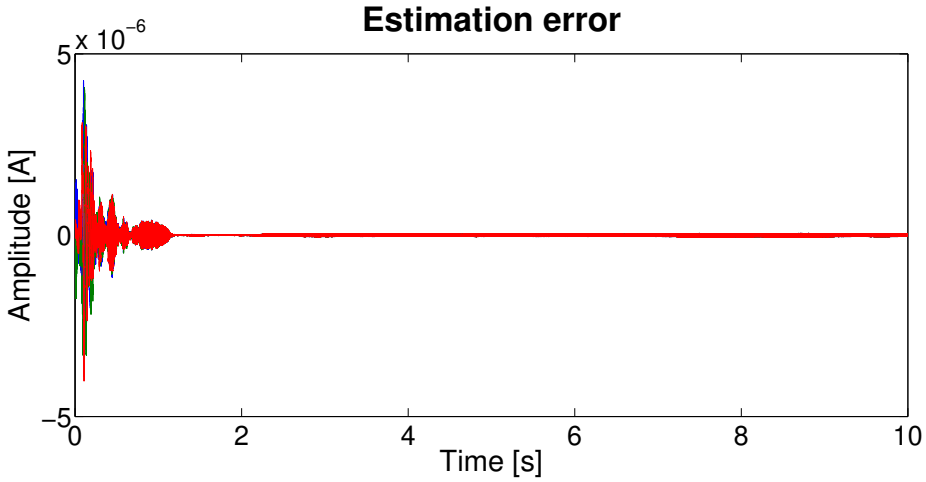

FIGURE 3.21: Estimation error using the EKF, in the presence of gaussian noise.

3.5 Conclusions

A new method, for the estimation of the process noise covariance matrix, was presented in this chapter. Although it is shown in the context of an EKF, is it independent from it and can be used with any other type of algorithm. It only uses the measured and estimated signals, and the model of the process.

The procedure only needs an estimation of the covariance matrix of the measurement noise. This can be easily obtained from the datasheets of the sensors, by considering the sensor tolerance as the standard deviation of the data acquired on each channel.

The proposed method was compared with two other ones, and the simulation results proved its effectiveness. The procedure is simple, fast and precise. The estimation error can be lowered if the measurement signals are filtered before they are input in the EKF. Filters were not used in the simulation.

Moreover, this method can be used for linear systems.

The disadvantages of the proposed method are:

- The measurement function has to be linear, of the form $h(x) = Ax + b$ where the matrix A has to be invertible;
- The number of inputs has to be equal to the number of states;
- The internal states have to be observable.

Three state estimators were compared: the KF, the EKF and the SRUKF. The EKF is about 2.5 times faster than the SRUKF and its error is in the order of 10^{-13}, as the SRUKF, which can be reasonably approximated by 0. The KF could not compensate completely for the linearization of the model. Because the new model required more mathematical operations, it was also slower than the EKF.

The behavior of the different filters in the presence of the uncertainties generated by the functioning of Simulink and of the Simscape/PowerSystems toolbox was also examined. It was shown that the behaviors of the filters are similar to a proportional controller.

Chapter 4

Diagnosis of the Permanent Magnet Synchronous Generator

4.1 Introduction

DIRECT Drive Wind Turbines (DDWTs) are widely used in the renewable energy industry, especially in offshore installations. They eliminate the need for a gearbox, which is the component most prone to faults (Qiao and Lu, 2015a). They are usually equipped with Permanent Magnet Synchronous Generators (PMSGs) (Gliga, Lupu, et al., 2017), a type of Permanent Magnet Synchronous Machines (PMSMs). PMSMs are widely used as motors in electric vehicles (Alameh et al., 2015).

Most of the research is focused on Permanent Magnet Synchronous Motors (PMSMs), which, physically, are identical to PMSGs. Because there will be used results from the research on motors, the terms PMSG and PMSM will be used interchangeably.

Although a great deal of research was conducted on the fault diagnosis and identification of PMSMs, they are still prone to faults. PMSG faults represent 14.7% of all faults in a WT, and they account for 24.42% of the downtime (Pinar Pérez et al., 2013).

Fault Diagnosis and Identification (FDI) methods are usually split into three large categories, depending on what approach they are based on: signal processing, mathematical modelling and artificial intelligence (Venkatasubramanian, Rengaswamy, Yin, et al., 2003), (Venkatasubramanian, Rengaswamy, Kavuri, and Yin, 2003), (Venkatasubramanian, Rengaswamy, and Kavuri, 2003). This work will focus on FDI methods based on signal processing, as they are used in commercial Condition Monitoring (CM) and Structural Health Monitoring (SHM) systems for wind turbine installations (Yang et al., 2014).

Signal processing is commonly used in the diagnosis of PMSM faults (Qiao and Lu, 2015b) (Riera-Guasp, Antonino-Daviu, and Capolino, 2015).

Spectrum analysis of the stator currents is a common diagnosis method, through The Fast Fourier Transform (FFT). However the diagnosis is hindered, because the harmonics of the current change with the wind speed (Faiz and Nejadi-Koti, 2016), and so does the spectrum. The Wavelet Transform or the Hilbert Transform are some of the methods used to solve this problem (Alameh et al., 2015), but they are computationally intensive and more complex.

The Extended Kalman Filter (EKF) is presented in this chapter, as a solution to enable the use of the FFT. If the residuals between the estimated currents, using the EKF, have the same spectrum regardless of the change in wind speed, they can be used for signal processing-based diagnosis. However, the impact of the faults must be noticeable in the residuals or in their spectrum.

The FFT computes the spectrum of a given signal over all possible frequencies, which is not efficient when only few frequencies are of interest. To counteract this drawback, the authors turned to the Goertzel Algorithm (GA) (Goertzel, 1958). It is implemented using a Finite Impulse Response (FIR) filter connected in series with an Infinite Impulse Response (IIR) filter. The GA can be used to evaluate the magnitude of a signal at a specific frequency. The GA is used in voice communication, in dual-tone multi-frequency signaling (DMTF), to recognize the key which was pressed by the user on the phone, when dialling a number (R. G. Lyons, 2010), (Oppenheim, Schafer, and Buck, 1999). Because of the low number of frequencies of interest in the diagnosis of a PMSG, it is appropriate for this application as well.

In this chapter, the GA will be tested for the FDI of a PMSG. A diagnosis procedure is also presented, which can detect and identify the different faults which can affect a PMSG.

The methodology which will be followed in this chapter is:

1. Find out the possible faults which can affect a PMSG;
2. List the symptoms they induce into the generated currents;
3. Simulate the functioning of a DDWT cloat different wind speeds;
4. Introduce the symptoms of the faults in the generated currents;
5. Estimate the currents using an EKF;
6. Compute the residuals between the estimations and the measured currents;
7. Apply the FFT to calculate the spectrum of the residuals;
8. Check if the spectrum remains constant at different wind speeds and if the faults influence the spectrum;

9. Construct a bank of Goertzel Filters (GFs) to monitor the harmonic content inside different frequency bins;

10. Analyze the outputs of the GFs to determine if they can be used for FDI.

In Section 4.2, the most common generator faults will be described, together with the fault signature matrix and the symptoms they induce into the generator currents. In Section 4.3, the generation of the residuals, using the EKF, will be presented. The effect of the different faults on the spectrum of the residuals will also be shown. The Goertzel Algorithm will be presented in Section 4.4. The FDI procedure for a PMSG will be explained in Section 4.5. Simulation results and their discussion will follow in section 4.6. The conclusions will be presented at the end of this chapter.

4.2 PMSG Faults

The most common faults which can affect a PMSM are the demagnetization of the rotor, eccentricity and inter-turn short circuit (Alameh et al., 2015).

Demagnetization Fault (DMF) (Faiz and Nejadi-Koti, 2016) means that the rotor loses some or all of the residual magnetic flux. The main factors which contribute to DMF are high temperatures or cracks which had appeared during the manufacturing process. Another possible cause can even be the magnetic field of the stator. The stator currents and voltages are controlled to maintain a certain angular velocity or/and a torque in the rotor. When the rotor is slowed slowed down, the magnetic field of the stator acts like a brake. This effect can damage the rotor. There are 2 types of DMF:

- Partial DMF means that just parts (or areas) of the rotor are affected;
- Complete DMF means that the whole rotor is affected.

Inter-turn Short Circuit Fault (ISCF) (Hang et al., 2015) appears when an unwanted current passes between two turns of the stator winding, usually of the same phase. It is produced by faulty insulation, high temperatures or high voltages which can affect the stator. This is considered an incipient fault, as it can lead to inter-phase short circuits and DMFs.

The Eccentricity Fault (Ebrahimi et al., 2014) means that the rotation axis of the rotor is deviated from the center. This deviation means that the air gap between the stator and the rotor is not uniform. This fault can lead to unbalanced voltages and currents in the different phases and, if left unchecked, can allow the rotor and the stator to rub against each other. It is a mechanical fault, which can appear during the manufacturing process,

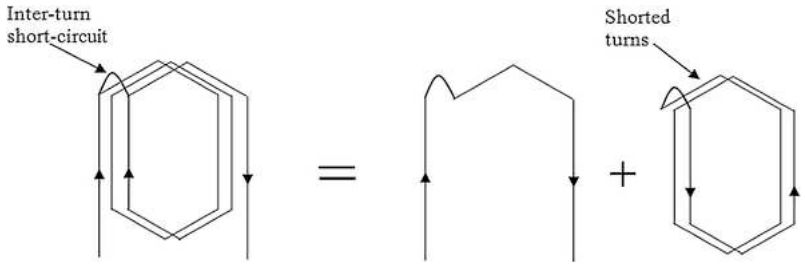

FIGURE 4.1: The ISCF (Sahraoui et al., 2014).

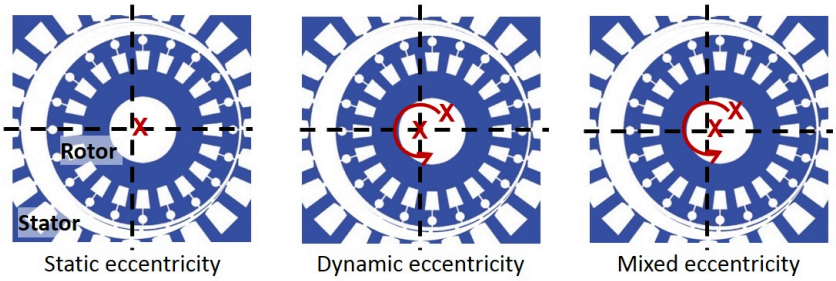

FIGURE 4.2: The different types of eccentricity faults (Marché, 2017).

during the installation or during operation (because of an unbalanced load, i.e. the rotor). The different types of eccentricity faults are:

- Static Eccentricity Fault (SEF) - the deviation in the air gap is constant in time;
- Dynamic Eccentricity Fault (DEF) - the deviation in the air gap changes in time;
- Mixed Eccentricity Fault (MEF) - both of the above.

TABLE 4.1: PMSG Fault Signature Matrix for MCSA.

Faults	Frequencies				
	$(1 \pm \frac{3}{n_P})f_s$	$(1 \pm \frac{1}{n_P})f_s$	$(1 \pm \frac{3}{n_P})f_s$ & $(1 \pm \frac{1}{n_P})f_s$	$(1 \pm \frac{2k-1}{n_P})f_s$	$(2k \pm 1)f_s$
SEF	x	x	x	x	
DEF		x	x	x	
MEF			x	x	
DMF	x	x	x	x	
ISCF					x

All the previous faults affect different signals acquired from the generator, namely the torque, voltages, currents, temperature, vibrations, etc. Therefore, diagnosis through signal processing is a common.

Although widely used, vibrations measurements require the presence of accelerometers. Their elimination would lower the costs of WT installation and maintenance. The temperature inside the generator tends to change

slowly. Therefore, if the FDI system would monitor it, incipient or fault evolving faults might be hidden.

Together with the voltages, currents are signals acquired by the Supervisory Control and Data Acquisition (SCADA) system of the WT (Schlechtingen, Santos, and Achiche, 2013). Therefore, no additional sensors are necessary. The focus on this work will lay on Machine Current Signature Analysis (MCSA), as it is a well-proven technique for the diagnosis of electrical machines (Qiao and Lu, 2015b).

According to (Hang et al., 2015) (Ebrahimi et al., 2014) (Roux, Harley, and Habetler, 2007) (Faiz and Nejadi-Koti, 2016) (Yassa and Rachek, 2018) the previous faults introduce different harmonics into the ABC currents. This is summarized in the fault signature matrix, shown in Table 4.1. There, f_s is the fundamental frequency of the signal and k is an integer.

4.3 Diagnosis using the EKF and the FFT

The EKF can be used to estimate the generated currents. In Chapter III it is shown that it is as good as the Unscented Kalman Filter to estimate the currents generated by a PMSG, but it is faster. The signal which is proposed to be used for diagnosis is made up of the residuals between the estimated and the simulated currents.

The EKF and the computed residuals were tested to see if they are usable for diagnosis. The following steps were taken:

1. Check if the spectrum of the residuals is constant when the wind speed changes;

2. Introduce faults in the model and check if the EKF does not hide them.

The behavior of the residuals, for different wind speeds, is shown in Figures 4.3 and 4.4. The wind speeds are perturbed with a Gaussian noise of zero mean and with a variance equal to 1. For both wind speeds, the residuals are similar, in the range of 10^{-14}, so they can be approximated by 0. The values of the wind speed were chosen to account for both zones of the WT power curves: the transient increase in generated power and the stationary one.

Because the PMSM block of the Simscape/Power Systems library is used, the PMSG is modelled in the dq0 reference frame. Therefore, the faults cannot be simulated directly, i.e. introduced in the model. Instead, the symptoms of the faults are introduced in the signals "acquired" from the simulated process. The EKF uses the fault-affected signals, and the residuals are computed using the perturbed signals.

The SEF fault is simulated by introducing a harmonic at the frequency $f_{SE} = 25Hz$ and with an amplitude of 0.1. The results are shown in Fig. 4.5

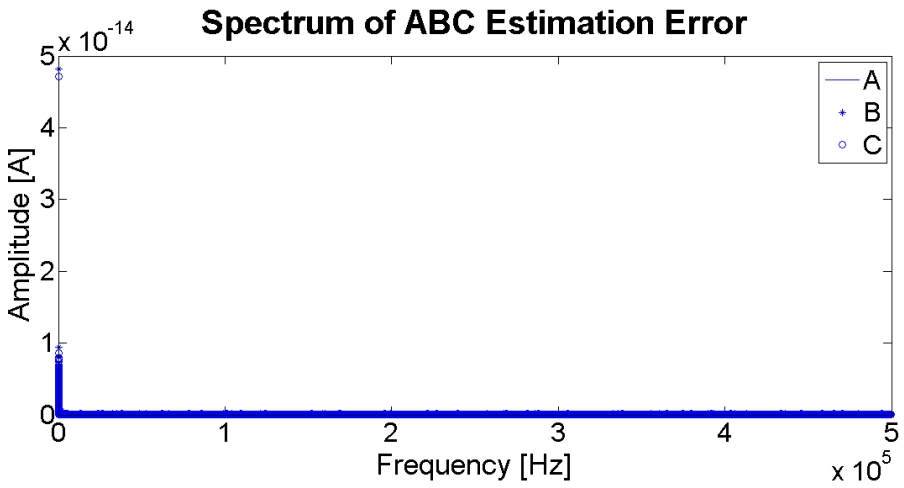

FIGURE 4.3: Spectrum of the residuals for a wind speed around $10m/s$.

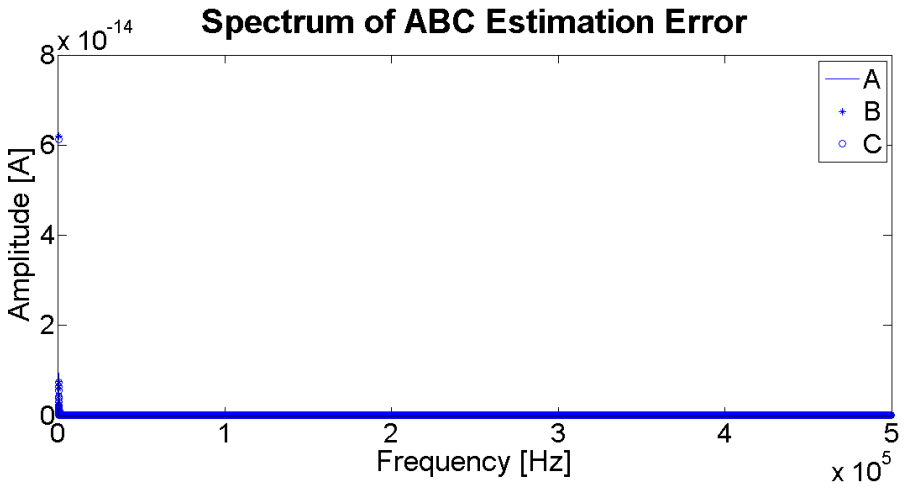

FIGURE 4.4: Spectrum of the residuals for a wind speed around $18m/s$.

and 4.6. The harmonic is visible in the frequency domain, although it is attenuated by the EKF.

A harmonic with a frequency of $f_{DE} = 58.3333Hz$ and an amplitude of 0.2 is introduced in each phase of the ABC current, to simulate the DEF fault. The effect can be seen in Fig. 4.7 and 4.8. Again, the harmonic is clearly visible in the frequency domain.

The amplitude in the frequency domain seems to depend linearly on the amplitude of a harmonic, with a inverse ratio of 2.5.

Until now, harmonics were introduced only in the current. According to (Faiz and Nejadi-Koti, 2016), the DMF fault affects the currents, voltages, torque and magnetic flux. The symptoms which can be simulated in a dq0 model are the harmonics in the current, the zero-sequence voltage component (ZSVC) and the harmonics in the torque. Because of the limitation of the model in the dq0 reference frame, the effect on the magnetic flux and

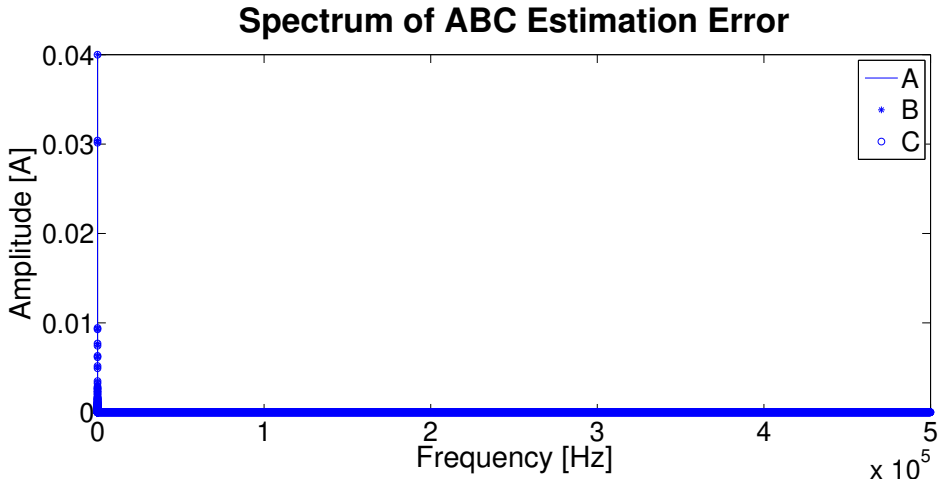

FIGURE 4.5: Spectrum of the residuals for the SEF.

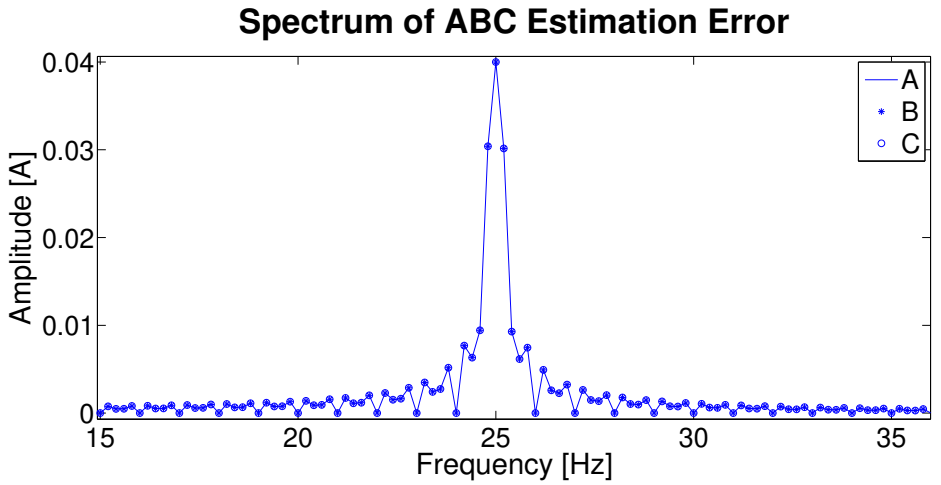

FIGURE 4.6: Zoomed in spectrum of the residuals for the SEF.

electromotive force cannot be simulated. The torque is affect by harmonics with the frequency

$$(\lambda \pm \frac{\epsilon}{n_P}) f_s, \tag{4.1}$$

where λ and ϵ are arbitrarily chosen integers.

In the simulation, $\lambda = 2$ and $\epsilon = 4$, so the frequency of the harmonic added to the torque is $f_{DM_T} = 133.33Hz$. The amplitude of the harmonic is 0.3. The zero sequence voltage component (ZSVC) is also modified.

$$ZSVC = \frac{1}{3}(V_a + V_b + V_c) \tag{4.2}$$

A constant value of 10 is used to simulate a ZSVC introduced by a DMF fault. A harmonic with an amplitude of 0.1 is added to the current, at the frequency $f_{SE} = 25Hz$, because the DMF and eccentricity-type faults introduce the same harmonics into the current. The results are presented in Fig. 4.9 and 4.10.

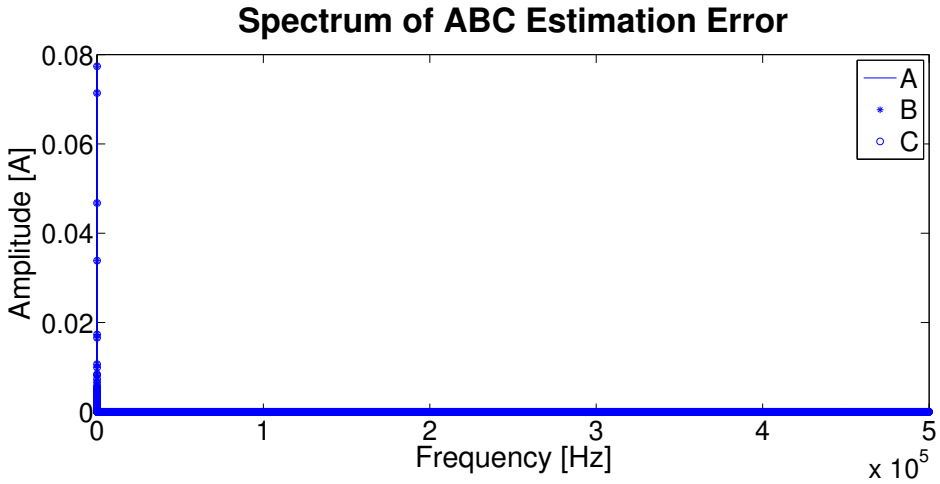

FIGURE 4.7: Spectrum of the residuals for the DEF.

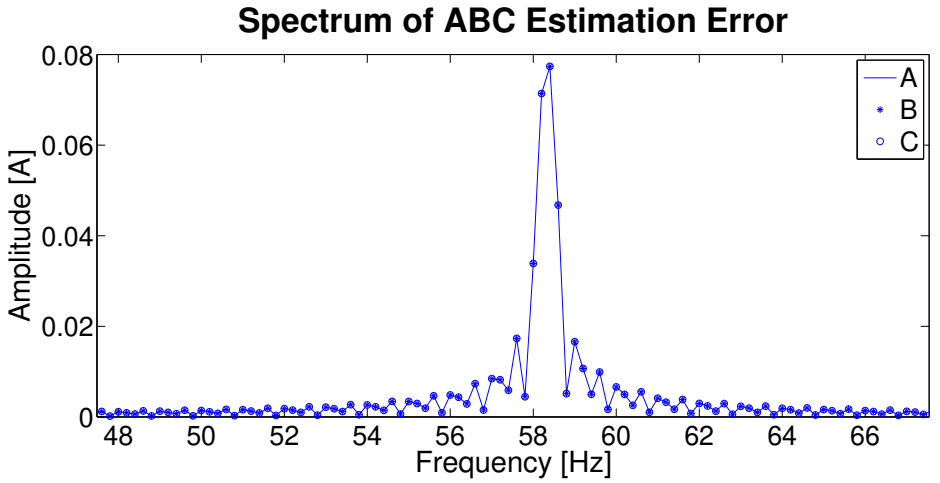

FIGURE 4.8: Zoomed in spectrum of the residuals for the DEF.

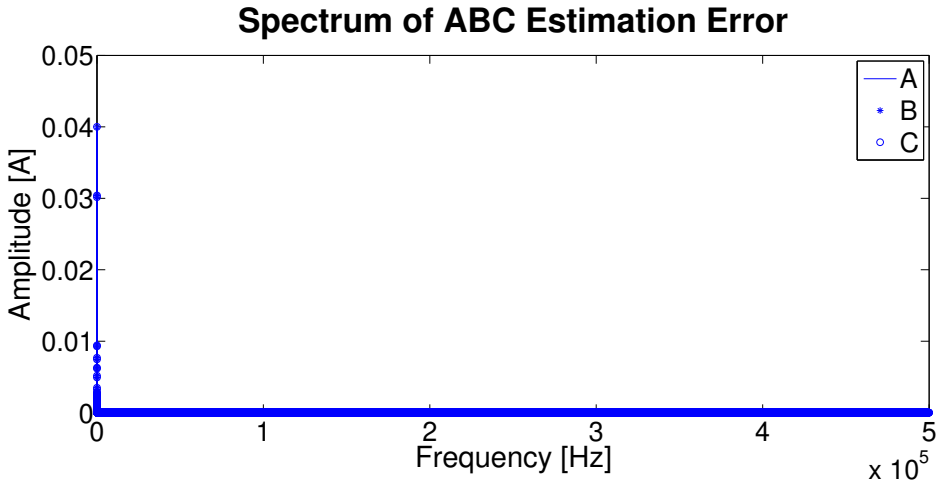

FIGURE 4.9: Spectrum of the residuals for the DMF.

It can be seen from Fig. 4.10 and 4.6 that the DMF and SEF faults completely overlap, and cannot be distinguished from one another. No significant change happens in the spectrum of the currents, although the voltage

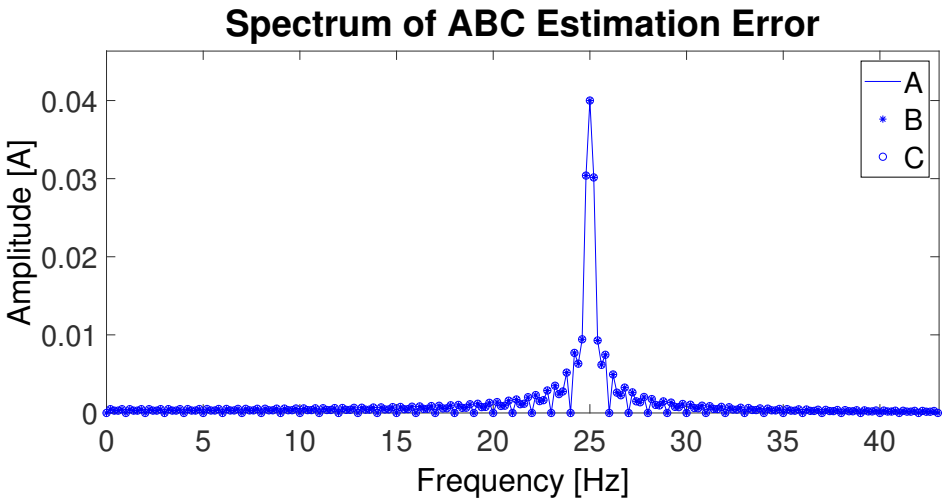

FIGURE 4.10: Zoomed in spectrum of the residuals for the DMF.

and the torque are also modified. Therefore, currents cannot be used to identify these faults. The results were identical to the ones predicted using the fault signature matrix, so the simulation methodology was correct.

The ISCF fault was simulated by introducing a harmonic in the current at the frequency $f_{ISC} = 250Hz$, with an amplitude of 0.05. However, it was introduced together with the DM fault, to check if simultaneous faults hide each other.

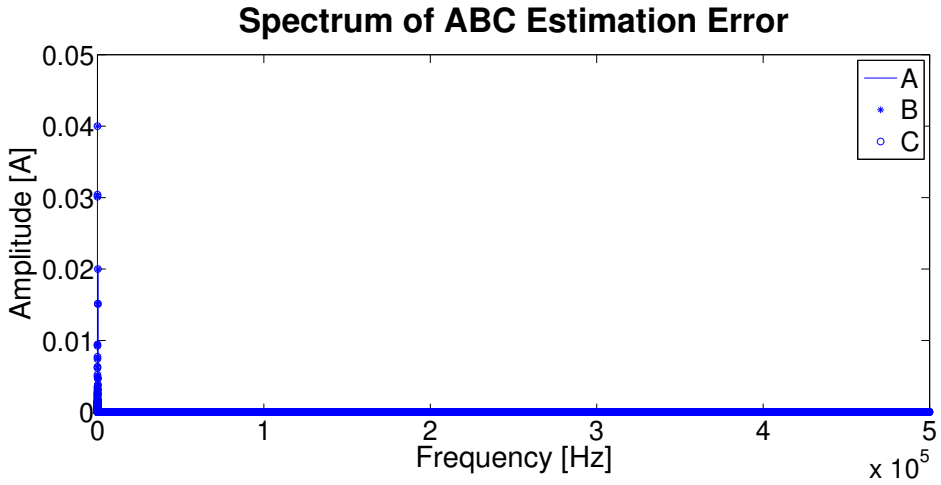

FIGURE 4.11: Spectrum of the residuals for the DMF and ISCF.

The effects of both faults can be distinguished separately, and each of them can be identified from the other using MCSA.

4.4 The Goertzel Algorithm

The GA is used to compute the Discrete Fourier Transform (DFT) inside a single frequency bin, i.e., an interval between two frequencies.

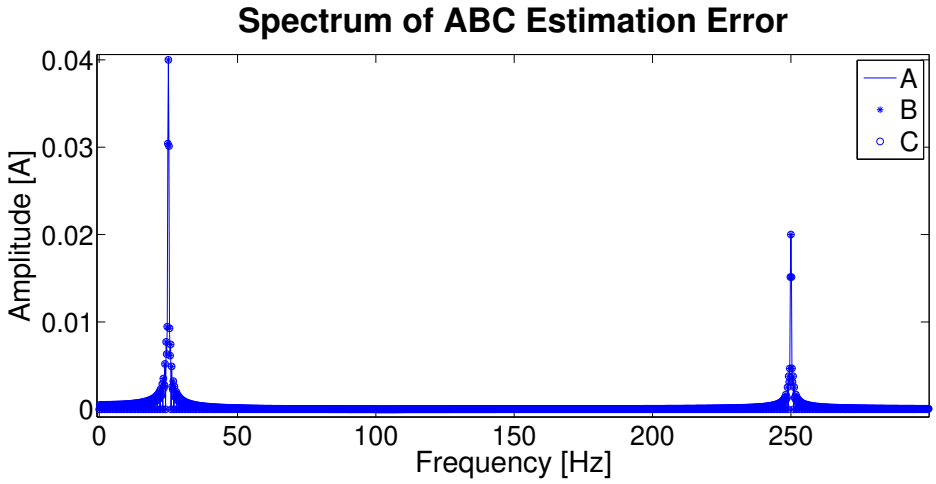

FIGURE 4.12: Zoomed in spectrum of the residuals for the DMF and ISCF.

The basic form of the GA is (R. G. Lyons, 2010)

$$H_{GA}(z^{-1}) = \frac{1}{1 - e^{j2\pi\frac{k}{N}}z^{-1}}, \tag{4.3}$$

where N is the number of frequency bins and k is the bin of interest, i.e., the interval which contains the frequency of the harmonic of interest; N is also the resolution of the DFT and the block size which will be used to compute it (unlike the FFT, it does not need to be a power of two, nor an integer (Sysel and Rajmic, 2012)). This transfer function has one pole which lies on the unit circle, at $e^{j2\pi\frac{k}{N}}$, so it is only marginally stable. Because of the finite-precision representation of numbers in digital computers and microprocessors, the poles of the filter might lie outside the unit circle (R. G. Lyons, 2010) and it might become unstable.

An improved version of the GA, where the stability problem is solved, is obtained when the previous fraction is multiplied and simplified by $(1 - e^{-j2\pi\frac{k}{N}}z^{-1})$ (R. G. Lyons, 2010), respectively

$$H_{GA}(z^{-1}) = \frac{1 - e^{-j2\pi\frac{k}{N}}z^{-1}}{(1 - e^{j2\pi\frac{k}{N}}z^{-1})(1 - e^{-j2\pi\frac{k}{N}}z^{-1})}, \tag{4.4}$$

which leads to

$$H_{GA}(z^{-1}) = \frac{1 - e^{-j2\pi\frac{k}{N}}z^{-1}}{1 - 2\cos\left(2\pi\frac{k}{N}\right)z^{-1} + z^{-2}}. \tag{4.5}$$

Another form of this transfer function is (Bocca et al., 2011)

$$H_{GA}(z^{-1}) = \frac{1 - e^{2\pi\frac{f_i}{f_s}}z^{-1}}{1 - 2\cos\left(2\pi\frac{f_i}{f_s}\right)z^{-1} + z^{-2}}, \tag{4.6}$$

where f_s is the sampling frequency and f_i is the frequency of interest.

The transfer function from (4.5) will be used throughout this work, as that is the standard representation. It has one zero at $e^{-j2\pi\frac{k}{N}}$ and two conjugate poles located at $e^{\pm j2\pi\frac{k}{N}}$. One of the poles is cancelled by the zero. All poles and zeros are located on the unit circle. A common misconception is that (4.5) is marginally stable and can become unstable if the numerical precision used for implementation is low - the same problem as with (4.3). However, it can be proven that the filter is always stable (Sysel and Rajmic, 2012), (R. Lyons, 2015) and only large round-off errors (which can appear when filtering a very large number of samples) can destabilize it.

The GA is implemented as a two stage discrete-time filter. Its difference equations are

$$v[n] = 2\cos\left(2\pi\frac{k}{N}\right)v[n-1] - v[n-2] + x[n], \tag{4.7}$$

$$y[n] = v[n] - e^{-j2\pi\frac{k}{N}}v[n-1], \tag{4.8}$$

where v is an internal variable, x is the input signal, y is the output of the filter and n is the current sampling moment. Equation (4.7) describes an IIR filter, while (4.8) shows a FIR filter.

The intermediate variable has to be computed at every sampling moment, but the output of the filter is equal to the result of an equivalent single-bin DFT only at every N^{th} sample

$$y[n]|_{n=N} = X(k), \tag{4.9}$$

where $X[k]$ is the result of the DFT computed in the k^{th} frequency bin for the x input signal. Therefore, (4.8) can be computed more rarely.

The discrete transfer functions of (4.7) is

$$\frac{v[n]}{x[n]} = \frac{1}{1 - 2\cos\left(2\pi\frac{k}{N}\right)z^{-1} + z^{-2}}, \tag{4.10}$$

which is equal to

$$\frac{v[n]}{x[n]} = \frac{1}{(1 - e^{j2\pi\frac{k}{N}}z^{-1})(1 - e^{-j2\pi\frac{k}{N}}z^{-1})}. \tag{4.11}$$

The discrete transfer function of (4.8) is

$$\frac{y[n]}{z[n]} = 1 - e^{-j2\pi\frac{k}{N}}z^{-1}. \tag{4.12}$$

If (4.11) would be multiplied by (4.12), to compute the equivalent series filter, the obtained result would be equal to (4.4), the stable GA. This short demonstration was given as it is frequently skipped in works introducing

the GA, such as (R. G. Lyons, 2010) and (Oppenheim, Schafer, and Buck, 1999).

To eliminate the complex number multiplication from (4.8), the output of the filter is modified to compute the square of the magnitude from the bin of interest.

First, (4.8) is rewritten to compute the magnitude of the frequencies from the k^{th} bin, respectively

$$y[n]|_{n=N} = v[n] - v[n-1]\cos\left(2\pi\frac{k}{N}\right) + \\ + jv[n-1]\sin\left(2\pi\frac{k}{N}\right), \quad (4.13)$$

and the square of the magnitude will be

$$y[n]|_{n=N} = v^2[n-1] + v^2[n] - \\ - 2v[n-1]v[n]\cos\left(2\pi\frac{k}{N}\right). \quad (4.14)$$

The implementation of the GA using the difference equations, which describe two filters connected in series, is called the Goertzel Filter (GF). To preserve the stability of the filter when processing a very large numbers of samples, the internal variable of the GF is reset to 0 after each computation of its output.

4.5 The FDI Procedure

In MCSA, the FFT is used to monitor the harmonics introduced, by faults, into the generated currents. However, the previously described GF can also be used. Specifically, a bank of GFs must be used, one GF for each frequency of interest (Idrissi, El bachtiri, and Chafouk, 2017). Three filters have to be utilized: one to monitor the harmonic introduced by the SEF, another one for the sinusoid inserted by the DEF and a last one for the harmonic introduced by the ISCF.

An algorithm which can identify the previously discussed faults can be formalized as follows:

1. Design the GFs and mark the sampling periods when each of their output equals the output of the equivalent single-bin DFT.

2. While the PMSG is running, count the sampling moments:

   (a) At the correct sampling moment, check the magnitude of the harmonic which may be introduced by the SEF.

i. If it is lower than a threshold, the SEF is not present.
ii. Else, the PMSG is affected by the SEF. If DEF is also present, then the actual fault is the MEF.

(b) At the right sampling moment, check the magnitude of the harmonic which may be introduced by the DEF.
i. If it is lower than a threshold, the DEF is not present.
ii. Else, the PMSG is affected by the DEF.

(c) If a SEF or MEF is present, check the DC component of the voltage.
i. If it is zero, the DMF is not present.
ii. Else, the PMSG is actually affected by the DMF, and not by SEF or MEF.

(d) At the correct sampling moment, check the magnitude of the harmonic which may be introduced by the ISCF.
i. If it is lower than a threshold, the ISCF is not present.
ii. Else, the PMSG is affected by the ISCF.

Between steps (2.a) and (2.d), the results of the algorithm should be hidden from the operator. A possible change in the detected fault, e.g., from SEF to DMF, might confuse the user.

This algorithm only allows the identification of DEF from DMF, but it cannot detect SEF or MEF when they appear together with the DMF. Another downside of the algorithm is that when SEF is present, DEF can no longer be detected. However, it can detect any fault which appears while the PMSG is affected by the ISCF.

SEF can be identified by monitoring only the first harmonic presented in Table 4.1 . DEF can be identified by monitoring the first two harmonics from Table 4.1, but it does not cause a significant change in the first harmonic.

When both the previous faults are present, it means that the MEF affects the PMSG. Both the previous harmonics appear during DM faults. So, the DM fault cannot be distinguished from eccentricity-type faults.

The ISCF can be detected by monitoring harmonics of the type $(2k+1)f_s$, so ISCF faults can be discerned from the rest.

4.6 Simulation and Results

The symptoms which were introduced by the faults are the same as in the previous case.

Several constants were precomputed to fasten the GFs:

- The sampling period was chosen to be $1e^{-6}$ sec to ensure the stability of the electrical model of the wind turbine (a constraint imposed by the Simscape/Power Systems toolbox).

- Different numbers of frequency bins were selected for the different impairments:
  - $N = 100000$ bins were used for SEF and DEF. Each resulting bin contains 10 frequencies which can be represented by integers;
  - $N = 10000$ bins were used for ISCF. Each resulting bin covers 100 frequencies which can be represented by integers.
- The bins of interest were selected at $k = \left[0.5 + \frac{N*f_i}{f_s}\right]$, where k is rounded to the nearest integer.
- The cosine from (4.7) was precomputed, as its value depends only on the number of frequency bins and the bin of interest.

The results obtained from the simulation when SEF is introduced in the PMSG are presented in Figures 4.13 to 4.15. The squared magnitude of the introduced harmonic is very visible on the output of the GF dedicated to SEF detection, where its value is almost 1500. The other two filters of the bank report a squared magnitude of only around 150 and almost 30.

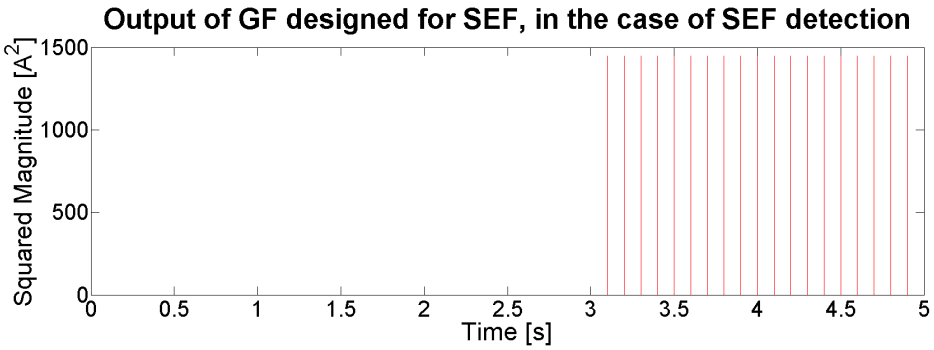

FIGURE 4.13: The output of the GF designed for SEF, when the PMSG is affected by SEF.

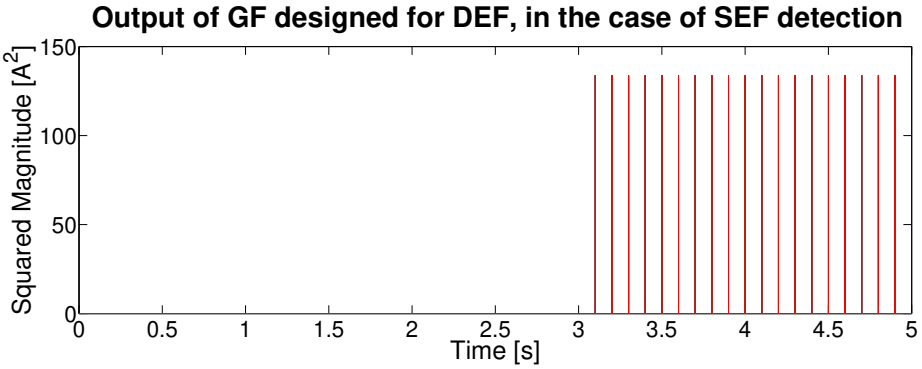

FIGURE 4.14: The output of the GF designed for DEF, when the PMSG is affected by SEF.

The outputs of the bank of GFs, when the PMSG is affected by DEF, are presented in Figures 4.16 to 4.18. The output of the second GF is in the

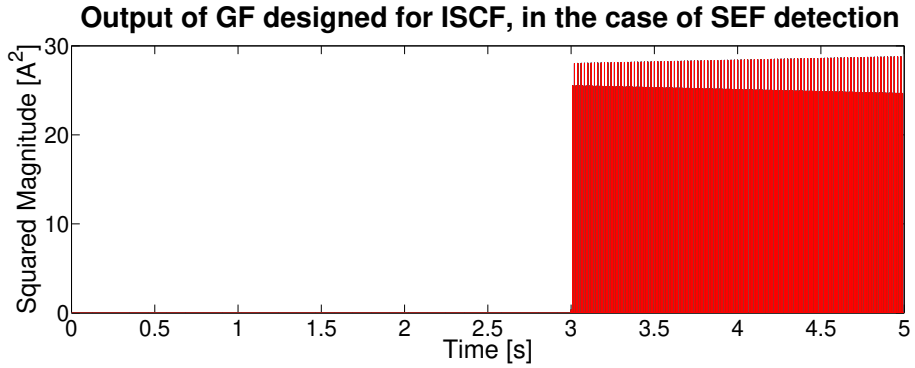

FIGURE 4.15: The output of the GF designed for ISCF, when the PMSG is affected by SEF.

order of thousands, while the other two filters show squared magnitudes of hundreds and respectively tens of Ampers.

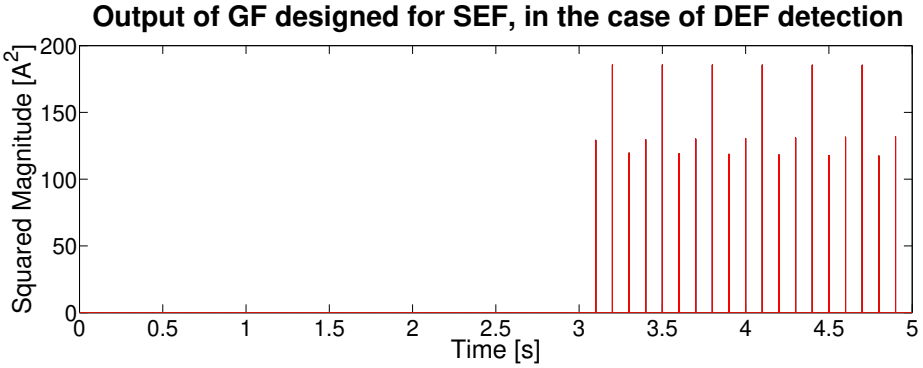

FIGURE 4.16: The output of the GF designed for SEF, when the PMSG is affected by DEF.

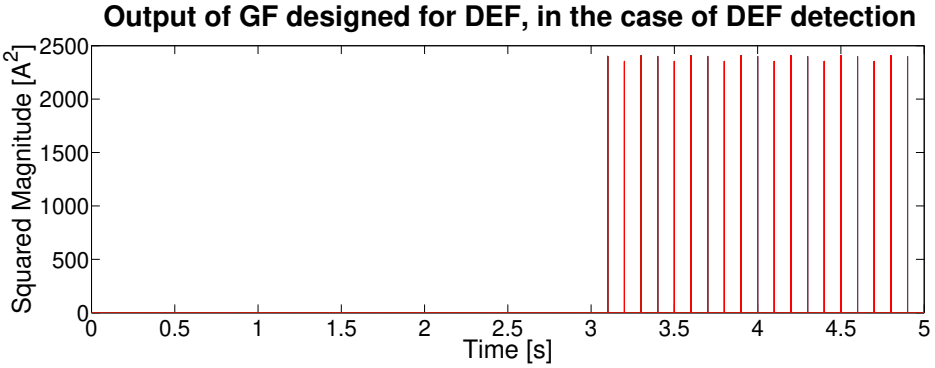

FIGURE 4.17: The output of the GF designed for DEF, when the PMSG is affected by DEF.

The ISCF was simulated together with the DEF, to test the FDI algorithm presented in Section 4.5. While the first GF from the bank reports a squared magnitude in the order of hundreds, the output of the second one is in the order of thousands, while the output of the third one is in the order of hundreds.

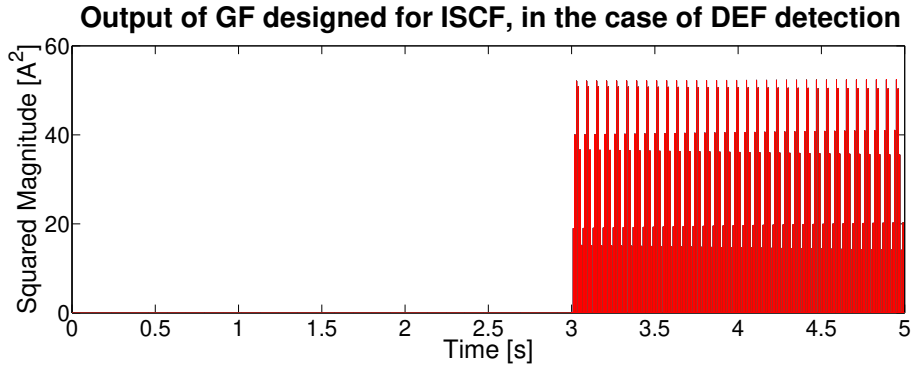

FIGURE 4.18: The output of the GF designed for ISCF, when the PMSG is affected by DEF.

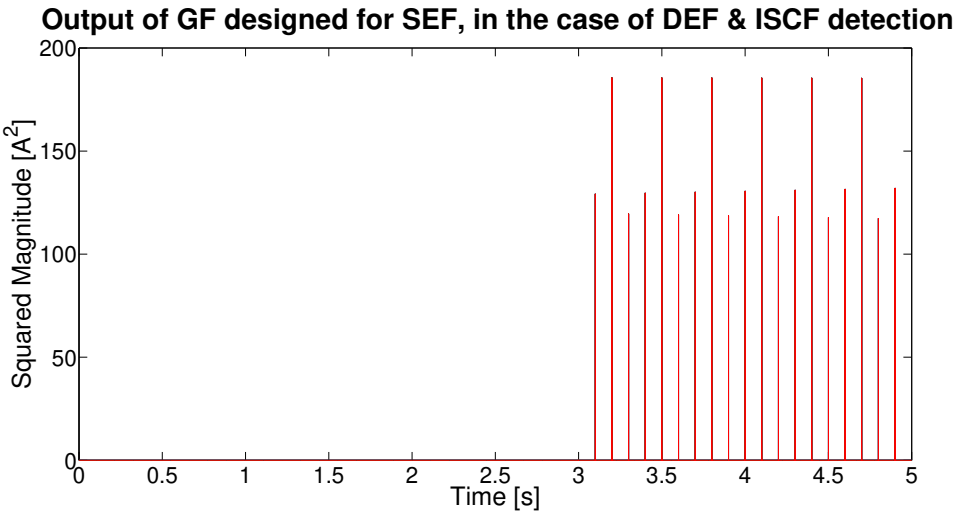

FIGURE 4.19: The output of the GF designed for SEF, when the PMSG is affected by both DEF and ISCF.

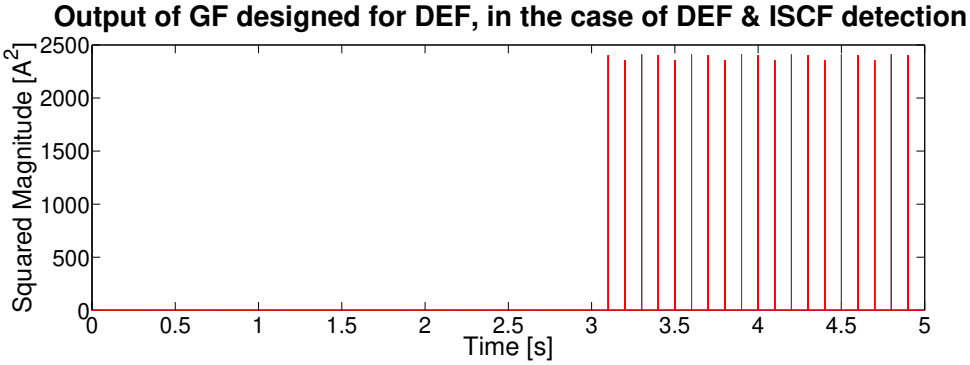

FIGURE 4.20: The output of the GF designed for DEF, when the PMSG is affected by both DEF and ISCF.

Therefore, appropriate thresholds for fault detection are around 1000 for SEF and DEF, and around 100 for ISCF, in the case of these harmonics.

The behavior of the last GF of the bank was peculiar, because it showed a rising trend. The output of the other two seemed constant or near constant. A longer simulation was carried out, in the presence of only the ISCF, as

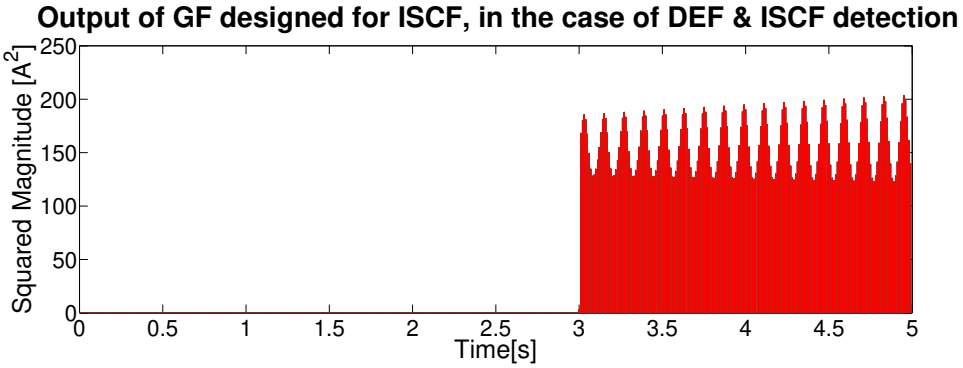

FIGURE 4.21: The output of the GF designed for ISCF, when the PMSG is affected by both DEF and ISCF.

that fault determined an increase in the filter's output. The result of this simulation is presented in Figure 4.22. It seems the output is modulated in amplitude by a sinusoid with a very low frequency. The authors tried to simulate for longer periods of time, to see if this behavior persists, but due to the low sampling frequency, the computer would run out of memory.

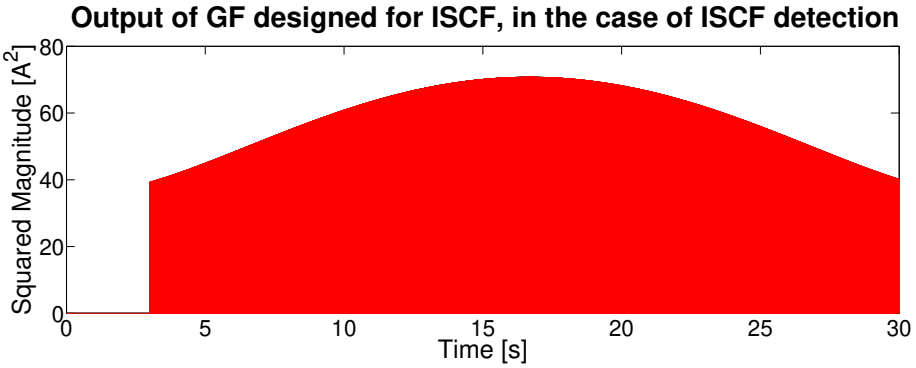

FIGURE 4.22: The output of the GF designed for ISCF, when the PMSG is affected by ISCF.

The mean of the generated voltage can be easily computed over a period of the signal. Because it is not related to the GF and the difficulty is trivial, no simulations are presented. However, it must be considered that this mean can only be known at the end of each period of the signal.

The stimulus signal for the bank of GFs was made of the residuals computed between the simulated currents and an EKF.

4.7 Conclusions

The fault signature matrix of the PMSG was constructed after a survey of the literature. The most common types of faults which affect such a generator are the SEF, DEF, MEF, DMF and ISCF. The DMF and eccentricity-type faults are detectable, but cannot be isolated from each other. The

ISCF can always be isolated. The different faults were simulated using the symptoms described in the literature.

The EKF can be used to compute the residuals between the estimated and the measured stator currents. Thus, the effect of the wind speed is negated. Although there is a slight difference between the spectrums computed at different wind speeds, the order of magnitude is the same - 10^{-14}. This means that global thresholds can be used to detect the faults, and these thresholds are valid for all wind speeds. Moreover, the spectrum of the residuals is close to zero, so all the harmonics introduced by the different faults are noticeable, via the FFT.

The Goertzel Filter was presented as a candidate to replace the FFT in FDI. The algorithm was explained, and it was tested on a simulated DDWT, more specifically on its PMSG. Multiple faults affect this generator, and they introduce different harmonics into the currents. Therefore, a bank of GFs was neccesary, where the first filter looks for the harmonic introduced by SEF, the second one monitors the harmonic introduced by DEF and the third one looks for the harmonic introduced by ISCF.

The simulation results showed that the square magnitude of the different harmonics introduced by the faults may be extracted by the bank of GFs. These outputs can be compared with pre-defined thresholds, and can be used in a FDI algorithm. Such a procedure was presented in this chapter, which can isolate different faults of the PMSG.

The FDI cannot be performed in real-time, i.e., at each sampling moment. The output of each filter and the mean value of the voltage can only be known at certain sampling moments. Therefore, this FDI approach must be implemented using a supervisor.

Although the sampling rate used in the simulations is 1 MHz, the GF can be used for signals sampled less often, e.g. sampling rates of kHz. The 1 MHz frequency was used to assure the stability of the Simscape/Power Systems blocks, namely the PMSG.

Chapter 5

Wireless Communication

5.1 Introduction

MONITORING of Wind Turbines (WTs) is necessary for the control, diagnosis and prognosis. Supervisory Control And Data Acquisition (SCADA) systems are responsible for controlling the power plant, so it may perform as it is expected by the shareholders. Faults are looked for by the Condition Monitoring (CM) or/and Structural Health Monitoring (SHM) systems. The purpose of Fault Detection and Identification (FDI) is to avoid unplanned downtime and the losses associated with it. Prognosis (Nejad et al., 2014) is used to estimate the remaining life-time of the equipment, and to program, in advance, the maintenance operations. Moreover, the equipment would be used for as long as possible, by minimizing the frequency of replacement.

Even if monitoring is crucial, its cost should be as low as possible, as this would encourage investments in the field. The price of wind energy has decreased in recent years, with onshore wind power being as cheap as fossil fuel equivalents. However, the cost of offshore wind power remains high (International Renewable Energy Agency, 2018).

Costs can be lowered by using SCADA data for FDI (Yang et al., 2014). Thus, the need for a dedicated FDI system would disappear, together with its cost. Another approach is to lower the number of signals needed for

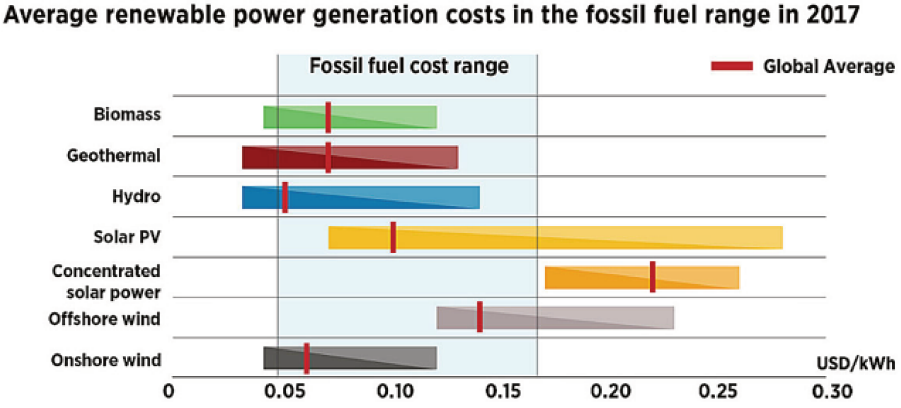

FIGURE 5.1: Prices of different alternative energy sources (International Renewable Energy Agency, 2018)

FDI. In (Deekshit Kompella, Venu Gopala Rao, and Srinivasa Rao, 2017), the generated currents are used to monitor both the generator and its main bearing. Therefore, even the bearing faults could be traced back, possibly to rotor faults.

Costs can also be lowered by eliminating cables. The installation and maintenance of cables is often more expensive than the actual sensors used in a WT. The solution is to use a Wireless Sensor Network (WSN) to monitor the WT, and by extension, the whole Wind Farm (WF) (Gliga, Lupu, et al., 2017).

WSNs are already used in smart cities (e.g. Barcelona, Amsterdam, Singapore and Alba Iulia). A multitude of sensors are used to cover a very large area and to acquire big data. However, in smart cities WSNs are only used to gather data relevant for constructing operational histories of different systems (transport, parking, lightning), for later processing. They are not used for critical real-time applications. This is different from industrial applications, where real-time requirements must be satisfied. WSNs are used in agriculture, to monitor the land and the animal shelters, but, in these cases, the sampling times are so large that the latency is negligible. However, due to advances in wireless communication technology, a WSN may form the backbone of an Industrial Communication System (ICS).

An important technology to consider is the Internet of Things (Jaradat et al., 2015). Companies currently use dedicated networks to connect to the industrial equipment. This means either laying kilometers of cables or using local supervision stations. IoT could help in connecting the local network of the WF (in the case of this work) to the internet, to enable remote operation. Moreover, the WTs could coordinate locally between themselves, if they could communicate in real-time with one another.

In this chapter, WSN technologies are compared to select a most suitable one for the monitoring of a WF. Because different technologies work better in different situations, offshore and onshore installations are considered. The onshore installations are further split into ones residing in rural areas, and others located in cities.

The connection between the WSN and the internet is discussed. The internet connection to the ICS can be a weak point, from a security standpoint. Therefore, security aspects are also presented.

In Section 5.2, the motivation for using a WSN and the IoT, in the case of a WF, is presented. A description of the monitoring requirements for a wind turbine and for a WF are shown in Section 5.3. The different communication technologies are examined in Section 5.4. A possible communication architecture, using LoRa, is shown in Section 5.5. A short review on industrial communication security is presented in Section 5.6. The conclusions close this chapter.

5.2 Motivation for a WSN and IoT in a Wind Farm

5.2.1 Wireless Sensor Networks

In remote WFs, a power cable runs from the farm to the place where it is connected to the grid. Together with the cables for the three phases (or the high voltage direct current in some cases) there is a fiber optic cable, which is used for communication. These remote WFs can be placed both onshore and offshore, so the distances can be great. Moreover, inside any WF, there are kilometers of copper cables connecting each sensor and actuator to the control equipment, located inside the nacelle. All these cables cost money and require a long time to be installed.

The majority of them can be eliminated by using a WSN. Then, the installation and the maintenance of the equipment would be easier, cheaper and faster. Because the data transmission is wireless, it cannot be affected by animals, vehicles and accidents caused by workers.

WSNs have several characteristics, which make them useful in a WF (Z. Liu and He, 2017):

- Low energy nodes would decrease the energy consumption of the whole ICS. More energy could be sold on the electrical energy market, which would increase revenue.
- Self-organization is needed when one or more nodes go offline. If one sensor is faulty and shuts down, the rest of the sensors can still communicate, because the network would re-organize itself without the intervention of the operator.
- The ICS would be scalable, as new sensors could be easily added and the network would self-organize to include them. Thus, sensors could be easily replaced.

The possible disadvantages of WSNs are:

- All the nodes should use the same communication protocol, and even the different versions must be compatible. A node which uses Wi-Fi cannot communicate with a node that only supports Bluetooth. However, this is not a new disadvantage: wired industrial networks are under the same constraint: a Modbus network cannot communicate with another one based on HART, if there is no adapter.
- WSN communication can be influenced by weather conditions and by obstacles (e.g. trees). The sensors should be arranged judiciously or the chosen communication technology should assure interference protection.

5.2.2 Internet of Things

In industrial applications, IoT can be seen as potentially unnecessary, unsecured and unreliable.

Firstly, the IoT can reduce costs. Instead of using a dedicated communication network from the WF to the power plant operator, which is very expensive, the data can be transmitted via wireless to the closest internet gateway. It would then be transmitted through the internet infrastructure. On the other hand, IoT-ready communication infrastructures could be used to transmit the data.

Secondly, such an interconnection between the different wind turbines would grant the WF a local intelligence. This would allow it to quickly reorganize itself automatically, in case of sudden faults or happenings. If a wind turbine would go off-line or lower its production, the others could quickly coordinate to compensate, as in network-controlled systems (Park et al., 2018).

Another advantage of IoT would be the integration of distributed energy resources (Vijitha and Selvan, 2013). Even if WTs would be far apart from each other, they could still be operated as a single WF and they would respond better to the demand.

Because the security aspect is critical for an energy plant, such as a WF, it is thoroughly discussed in Section VI.

5.3 Wind Farm Monitoring Requirements

Both Horizontal Axis Wind Turbines (HAWTs) and Vertical Axis ones (VAWTs) are considered in this work. HAWTs are placed offshore or onshore, but in isolated rural areas. VAWTs are assumed to be placed in cities or other populated areas, namely where there is 4G coverage. These considerations play an important role in choosing the communication technologies. Because 5G networks are just being installed, they are not considered in this work.

Furthermore, both types of WTs are equipped with Permanent Magnet Synchronous Generators (PMSGs), to consider the current trend towards Direct Drive Wind Turbines (DDWTs).

The SCADA, CM and SHM systems are considered to be the same for a HAWT and for a VAWT.

5.3.1 Wind Turbine Monitoring Requirements

The most important systems in a WT, from the point of view of automatic control, are the SCADA, the CM and the SHM systems.

A WT SCADA system samples data at short time intervals and it transmits the information to the control equipment (PLCs or microcontrollers), which is usually located inside the nacelle. A SCADA system also transmits commands for the pitch and yaw motors, power converter transistors, hydraulic brake, etc.

The WT components which are monitored by a CM system are the blades, the main bearing, the main shaft, the generator, the converter, the transformer and the nacelle. Commercially available systems may employ temperature sensors, oil particle counters, accelerometers, ammeters, hall sensors and fiber optic strain gauges.

A SHM system (Adams et al., 2011) oversees the structural elements of the WT, mainly the foundation, the tower and the structural integrity of the nacelle. These are crucial for offshore WTs, especially those which are not anchored to the sea bottom.

Only the results of the data processed by these systems, which are useful for creating a history of the WT, are send further to the WF operator. This design ensures fast data rates and low latency between the WF and the power plant operator, while it also lowers the technical requirements of the ICS. This architecture is well suited for long range communication. The local intelligence autonomously takes care of the WT, and it reports only relevant data to monitor its performance. A WSN can use the same architecture.

The coverage requirements of a WSN can be estimated by considering the worst-case scenario. For the current largest wind turbine, the V164-10.0MW manufactured by Vestas, the length of the nacelle is 20.7 meters, the width is 8.8 m and the height is 9.3 m (Vestas, 2017). If the worst-case scenario is to be assumed, where sensors from opposite ends of the nacelle should communicate, the distance would be 24.35 m. If a WSN would be used to transmit the data, 24.35 m would have to be its minimum coverage (to minimize signal loss) and to allow communication between all sensors.

VAWTs, which are used in cities, are smaller. They can reach heights of around 10 – 15 meters and can sweep an area of 2 – 3 meters. There are very high HAWT designs used in remote areas, but these are still in experimental phases.

The amount of data transmitted from a WT to the operator can be estimated by inspecting the real data acquired from the Haute Borne WF in France (Enjie, 2018). The data is transmitted by a WF with WTs equipped with Doubly-Fed Induction Generators (DFIGs). For the purpose of this work, all the data acquired from the gearbox, together with the rotor currents and voltages, is ignored. The remaining information are all floating-point numbers which indicate the reactive power, wind speed and its direction (a set for each of the two anemometers and wind vanes of each WT), temperature of the generator stator, outdoor temperature, temperature of

the nacelle, grid frequency and its voltage, torque of the shaft, angular velocity of the shaft, yaw angle, pitch angle, temperature of the hub, active power, power factor, temperatures of the main bearing (measured in two different locations) and the temperature of the rotor's bearing. Control signals are also sent to the WT, like pitch and yaw set points.

The number of signals acquired by a CM system depends on the manufacturer (Yang et al., 2014). For example, a commercial system might use only 8 accelerometers.

All these systems can have very high sampling rates. Data must be continuously transferred between the sensor and the station where it is processed. The sampling rate is in the order of milliseconds.

There are around 50 (also considering the signals necessary for diagnosis and other control signals) floating point numbers to be transmitted to the WF operator. If single precision format is assumed, the size of the data is 100 bytes (assuming a single precision representation of 16 bits). which must be transmitted every 10 minutes to the WF operator. The number of signals that is transferred locally inside a wind turbine can be in the order of hundreds. However, no relevant information could be found in this regard. It is important to acknowledge that some sampling rates are so low (e.g. the commands for the transistors in the power converter are send with a frequency between 10 and 100 kHz) that cannot be realistically supported by current wireless communication.

5.3.2 Extension to a Wind Farm

The size of the WF must also be considered. The largest offshore WF has 175 wind turbines (London Array Limited, 2018) and onshore WFs can have up to 100 wind turbines. The number of VAWTs which might reside in cities is also very high (B. K. Singh et al., 2013).

The current architecture used for the communication infrastructure of a WF is shown in Figure ArchCom. There are three types of communication lanes:

- Very fast communication, where data must be transmitted every several microseconds (μs);
- Fast communication, where sensors acquire the data with sampling periods in the order of milliseconds (ms) to seconds (sec);
- Slow communication, where the data is transmitted at intervals of several minutes (min).

The first two types of lanes are local to each WT. The slow communication takes place between the different WTs, the WF and its operator.

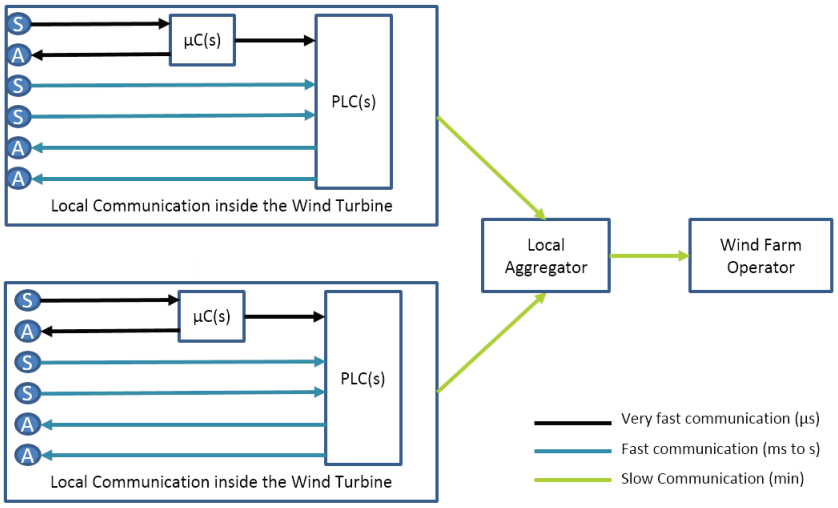

FIGURE 5.2: Architecture of a WF communication system. "S" stands for sensor and "A" for actuator.

5.4 Communication systems

There are several key factors that define a WSN. Among them are the topology and the communication technology which is used.

5.4.1 WSN Topology

The choice of a WSN topology depends on the distribution of the sensors, the energy consumption and the redundancy requirements.

The classical network topologies are line (of which point to point is a special case), bus, star, ring and mesh. The most used topologies in Industrial WSNs (IWSNs) are star and mesh. While the fully connected mesh assures the best path redundancy, each node uses more energy to construct and maintain its routing table. A star topology uses less power, but problems can appear when the central node goes offline. Then, the routing paths must be rediscovered.

The WTs in a WF might not lie in a grid, but at different distances from one another. Therefore, WTs can be grouped into clusters, and a star topology can be used for each cluster, and also to group all of them.

At WT-level, there are two different cases. The sensor density in the nacelle is very high, while the sensors which monitor the tower and the blades are far apart. In the first case, either a mesh or a star topology could be used. For the second case, the star topology is better suited.

A partially connected mesh topology could be the best choice for a WSN, for both cases. Nodes can form at least two paths between them to assure redundancy. Moreover, the complexity of the network will remain low, as well as the power consumption.

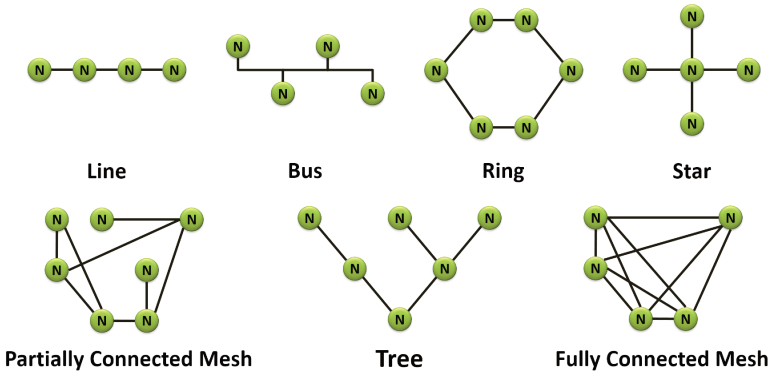

FIGURE 5.3: Network topologies

5.4.2 Communication technologies

There are many wireless communication technologies suited for different implementations. They can be grouped into three categories:

- Long Range Wide Area (LPWA)
- Local Area IoT (LAIoT)
- Cellular

LPWA technologies enable low power communication over very long range (at least a few kilometers), while LAIoT ones offer high data rates and low latency, but a smaller coverage (up to several hundreds of meters). Thus, LAIoT protocols could be used for WT-level communication, while LPWA transmission could be used to transfer the data from the WF to the power plant operator. The current communication architecture would be maintained, where data is acquired at high sampling rates and is processed locally inside a wind turbine. The wind farm operator would receive relevant data at greater time intervals.

The cellular technologies are 2G, 3G, 4G and 5G. They allow high data rates and wide area coverage, but they consume more power, compared to LPWA ones. Even if a WSN node would not be battery powered, the saved electrical energy would lower the costs. Moreover, high data rates (like the ones for 3G and above) are not necessary for an industrial installation. Furthermore, cellular networks might get crowded because of the large number of users. 2G networks could be used for ICSs. However, they are being decommissioned by mobile carriers, so they are expected to disappear in the future (Y. Hwang, 2017).

Long Range Wide Area Technologies

The different LPWA communication technologies are compared in Table 5.1 (Ali et al., 2017) (Sinha, Wei, and S. H. Hwang, 2017) (Song et al., 2017).

Most LPWA protocols only use the star topology, as it requires less power.

LoRaWAN (Long Range Wide Area Network) is a wireless technology developed by the LoRa Alliance (Silva et al., 2017). LoRa transmits data in the sub 1Ghz unlicensed spectrum bands, so long-distance communication does not require a lot of power and it is resilient against physical obstacles. It also provides very good coverage. LoRa networks support three different classes of devices:

- Class A, or battery powered devices, consume the least amount of power but they have the highest latency. They can be used to transmit data to the wind farm operator, once every ten minutes (as current SCADA data) or when necessary (the alarms from the SCADA or CM systems).
- Class B devices are used for periodic communication. These devices can be used for sensors which do not need to transmit data very often (e.g. accelerometers on the tower and/or foundation of the wind turbine). These devices assure lower latency.
- Class C devices consume the most amount of power, but they offer the lowest latency, as their radio is always turned on.

For securing the communication, LoRa uses:

- Network Session Keys for the communication between the nodes and the network
- Application Session Keys to encrypt the payload using AES (Advanced Encryption Standard) 128bit encryption
- A Device Address for each node, to allow the network to correctly organize and protect itself.

LoRa nodes are relatively cheap, so the infrastructure is not expensive to build. The downside of LoRa is the low data transfer. The maximum latency and quality of service are not assured. Moreover, because it operates in unlicensed bands, LoRa has a duty cycle of only 1% (imposed by EU regulations), so the number of messages which can be transmitted every day is limited. This can be avoided by changing to other sub-bands of the transmission spectrum.

NB-IoT (Sinha, Wei, and S. H. Hwang, 2017), or Narrow Band Internet of Things, is a communication protocol developed by the 3rd Generation Partnership Project. It uses the LTE (Long Term Evolution) infrastructure for the physical layer. It offers very high data rates (both uplink and downlink) and excellent coverage. The devices who use this protocol consume more current, but at the same time the latency is lower, and the data rate is higher

than LoRa. NB-IoT is very well suited for a WSN in places where 4G coverage exists. It uses the existing 4G equipment, so the wind farm operator does not need to concern itself with the communication infrastructure, as this is already installed and operated by a mobile carrier. The security measures are the ones already used for cellular networks (like 4G), which include: message encryption, session authentication and unique identifiers for each device. More security can be added by the mobile carrier. The infrastructure operator may ask for a periodic fee, but the total cost should be much lower than the price of installing and maintaining the equipment necessary for a dedicated network. However, this advantage is quickly turned to a disadvantage when considering WFs located in remote areas, such as rural or offshore. No 4G infrastructure exists there, so it is cheaper to deploy a dedicated LoRa network than a NB-IoT one.

LTE-M (Ali et al., 2017), or Long-Term Evolution for Machines, is another technology developed by the 3GPP, for Machine to Machine (M2M) communication. Compared with the previous ones, it offers lower latency and higher transfer speeds. As NB-IoT, it uses the existing LTE infrastructure and the same security methods. However, the current (and therefore the power) consumption is much higher, so this technology is not suitable for battery powered sensors or low power devices. Again, because it uses the LTE infrastructure, its deployment is not feasible in offshore or rural areas. Urban usage could be limited by the high-power consumption. The data rate is too high for the application discussed in this work, but the latency is low enough for real-time implementations.

Sigfox (Ali et al., 2017) is a proprietary technology developed by the French company with the same name. It was the first LPWA protocol developed for IoT, and it was successfully deployed in many industrial applications. The power consumption is very low. It ensures data security through encryption, session authentication, device authentication and *https* encrypted interfaces. Sigfox is also resistant to interference. However, it has a very low data rate. Even more, Sigfox operates in unlicensed spectrum bands, so it is also limited by the 1% duty cycle ratio imposed by regulations.

EC-GSM-IoT (Ali et al., 2017) is another technology developed by the 3GPP, which is based on the existing GSM network. Instead of using the newer LTE communication network, it uses the old GSM ones (like 2G), so it allows their recycling. There are currently no commercially available modules using this protocol, but it should cover a large area, have low latency and a good data transfer rate. Because it uses the mesh topology, it is expected to use more power than other technologies. It has the same security features found in GSM networks. It may be considered in the future, once deployment starts.

DigiMesh ((Osiegbu2015)) is a proprietary protocol developed for a wide range of applications. It supports very long communication, high speeds and multiple topologies. For close range, the communication speed is good, but the power consumption is high. It has multiple security features like AES128 and 256-bit encryption and network lock-down capabilities. Interference protection differs depending on the operating frequency band: frequency hopping for unlicensed spectrum bands or Direct Sequence Spread Spectrum (DSSS) for the 2.4GHz band. The data rate depends on the frequency band.

Other LPWA protocols are WiMAX, WeightLess (Ali et al., 2017) and RPMA (Ingenu, 2016).

WiMAX (Worldwide Interoperability for Microwave Access) was a competitor against 4G, but it lost. Its usage is limited to some countries, and even there it is dwindling. Because of its deprecating support, it is not recommended for future implementations.

The WeightLess Special Interest Group created three different standards for IoT communication: W, N and P. *WeightLess W* uses the TV white space frequency bands. It was developed by a company named Neul which, in the meantime, was bought by Huawei. Since the acquisition, they are working on technology for NB-IoT. *WeightLess N* was developed by a company called Nwave Technologies, however it was superseded by WeightLess P, developed by a company called Ubiik. Since then, the WeightLess N standard has been rebranded as Nwave (Nwave, 2017), but not sufficient data could be found for a complete characterization. The company uses it for smart parking. The same is applicable to the *WeightLess P*, developed by Ubiik. The WeightLess N and P technologies are supposed to have a coverage of at least several kilometers and to support high data rates. There are claims that they have high levels of security and interference protection.

RPMA (Random Phase Multiple Access) is a proprietary solution of the Ingenu Company. It operates in the 2.4 GHz band and it boasts a coverage of 52.8 square kilometers. It doesn't use an IP address for the devices. It ensures message confidentiality and integrity, replay protection, device anonymity and mutual authentication. However, no more information could be found.

From the previous LPWA protocols, LoRa is recommended for implementation in the case of offshore or onshore, but remote, WFs. A backup solution would be Sigfox. NB-IoT and LTE-M are recommended for areas with 4G coverage. LTE-M can even be used in real-time systems and is best suited for cities. DigiMesh is a jack of all trades, which may be used either for long and short distance communication.

Local Area IoT Technologies

The different LAIoT technologies are compared in Table 5.2.

ANT (Ali et al., 2017) is a communication technology developed by Samsung, while ANT+ is its interoperability function. ANT is mainly used in fitness trackers, healthcare products and is also present in high-end smartphones. It has low power consumption but has very low data rate and relatively low coverage. The protocol was created to transfer data from a sensor to a processing unit, so it does not support downlink communication. Its only security measure is data encryption.

IEEE 802.11b (Ali et al., 2017) is an older standard for Wi-Fi, which can be used for Machine to Machine (M2M) communication. It offers very high data rates and good coverage, but the energy consumption is high. The latency is very low, so it can be used in real-time applications. Even if the data rate is lowered, the energy consumption remains the same, because the radio of the chip is always turned on. Its security should be enhanced if it were to be used in a sensitive application such as a power plant - Wi-Fi network attacks are very common and easy to perform.

Wi-Fi HaLow or *IEEE 802.11ah* (Bankov et al., 2017) is a low-power version of Wi-Fi designed for the IoT. It uses the unlicensed spectrum bands to decrease costs and to improve the interference protection against physical obstacles. Currently, there are no chips for this technology, so the latency and the current consumption cannot be estimated. It is a promising technology, but as it is still not tested, it cannot be recommended for implementation.

BLE version 5 (Collotta et al., 2018) (Bluetooth Low Energy) is a widely used low power communication technology. BLE has very long transmission range, excellent data rate (depending on the selected physical mode) and very low latency, which even allows real-time implementations. It supports different topologies. The chips which implement it use very little power and they are relatively cheap. It has interference protection and it uses encryption, data integrity checks and device trust policies for ensuring the security of the network.

Bluetooth 5 is the “regular power” variant of Bluetooth and the counterpart of BLE. It has good range, very high data rates and low latency. It also consumes very little electrical energy. It is very similar to BLE. However, the low-power version is more suitable for this application because it is more energy efficient and the very high data rates of Bluetooth are not useful.

Zigbee (Ali et al., 2017) is a widely used technology for ICSs. It has good coverage and high data rates. It assures data security (though it was repeatedly cracked in the past). Zigbee PRO also ensures interference protection. Its power consumption is relatively high. Zigbee can use the Message Queuing Telemetry Transport (MQTT) to ensure a reliable communication.

IrDA (Val, Peyrard, and Misson, 2003) is best known for having been used to transfer files between mobile phones before Bluetooth replaced it. It has very high speed, low power consumption and excellent interference protection. However, it requires LOS between devices and the communication range is very small.

NFC (Prauzek et al., 2016) is mostly used for payments or identification. The devices must be in very close proximity (a few centimeters) to communicate between them.

Z-Wave (Ali et al., 2017) is a home automation technology developed by the Z-Wave Alliance. It offers good security features (encryption, device authentication) and it has good range. However, the data rate is relatively low, and its latency is high.

RFID (Khemmar et al., 2014) is a tag based communication system, widely used in product tracking and personal identification documents. Passive or active tags, which can incorporate sensors, are attached to different objects. RFID has good range, good speed but its topology is point to point. The tags do not establish communication links, but they are read, individually, by a dedicated device called a reader. The protocol does not incorporate security – the tags can be read by any reader. Only the data can be encrypted.

DASH7 (Grabia et al., 2017) was developed by the DASH7 Alliance. It has great range and low latency. Its data rate depends on the transmission range. It supports various security measures. It operates in many frequency ranges (depending on the country), and it has interference avoidance mechanisms.

WirelessHART (S. M. Hassan et al., 2017) is one of the oldest wireless communication technologies. It has good range, good transfer speed and low latency. It supports various security mechanisms (data encryption and integrity check, device authentication and failed access attempt notifications) and interference protection through channel hopping. It is a very mature technology which is already used in various real-time applications.

Wireless MBus (Zeman et al., n.d.) is used in smart meters and other monitoring devices. It transmits data using the 169/433/868 frequencies. It utilizes the star topology. The latency cannot be estimated, as all systems using it are closed proprietary solutions.

Another wireless communication system was developed by Nike for its Nike+ sport accessories. It transmits data every 1 s.

Thread (Thread Group, 2017) is a home automation technology developed by a consortium of companies. It is advertised to work in the 2.4 GHz frequency band, and to support mesh topology. However, no more details could be obtained.

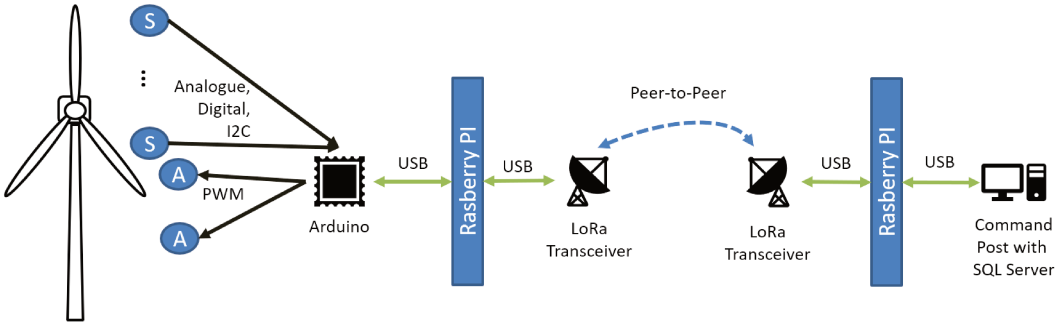

FIGURE 5.4: Possible architecture for LoRa communication

MIWI (Microchip, 2018) is a simplified implementation of ZigBee, developed by Microchip. It is intended for short range communication with low data rates.

Wavenis (Ali et al., 2017) was developed by a company named Coronis. It transmits information over a range of 1 to 4 km but only with LOS. It operates in the sub 1GHz bands. The maximum data rate is 100kbps. It is an ultra-low power technology and has multiple security and interference avoidance features. The exclusive LOS communication prevents its use.

From all the LAIoT protocols, BLE is best suited for this application, because of its high speed, good latency, good coverage and maturity. It is closely followed by Zigbee (due to its maturity), DASH7, WirelessHart and Bluetooth.

5.5 Potential Communication Architecture

A test stand was developed to test the feasibility of a WSN for a wind farm. The chosen communication technology was LoRa. The communication architecture is presented in Figure 5.4.

The WT is simulated by a collection of sensors:

- a weather station, which contains:
  - a temperature sensor;
  - a luminosity sensor;
  - a wind wane;
  - an anemometer;
  - a rain gauge;
  - a humidity sensor;
  - an ID chip which can send the code of the weather station;
- a voltmeter;
- an ammeter.

- an electrical power sensor;

The actuators are two servo-motors. They are used to simulate the yaw system and the mechanical brake of the rotor shaft. The measurements (from the sensors) and control signals (to the motors) were used to test the proof of concept of real-time wireless communication. The wind turbine contains a DC motor. Its rotor is turned by the rotor to generate DC.

All the sensors transmit the data through analogue, digital and Inter-Integrated Circuit (I2C) communication to an Arduino board. Because the board is not designed to handle wireless communication, a Raspberry PI (RPI) (Subhashini and Rao, n.d.) single-board computer is used for this role. The Arduino and the RPI communicate through USB. The Arduino also controls the servomotor, through PWM pulses. It acts similar to the Input/Output (I/O) and control modules of a Programmable Logic Controller (PLC). The RPI can be seen as the communication module of a PLC.

The RPI communicates with a LoRa transceiver, which is a Nemeus MK002-xx-EU USB (Remote) Stick. The transceiver supports both LoRa and Sigfox technologies - the second one can be used as a back-up. The transceiver can be used as a class A or class C LoRa device.

Another LoRa transceiver connects the command post (computer) to the wireless network. This transceiver is connected to the computer through USB. A Web application was developed, which incorporates a Human Machine Interface (HMI), to show the status of the simulated wind turbine. The data received via the LoRa network is transferred to a MySQL database via a JSON file.

As preliminary results, the LoRa transceivers can communicate with one another, over three kilometers, through Radio Frequency (RF) transmission. The Arduino can be used to control the servo-motors. The wind turbine can communicate with the computer every few seconds.

5.6 Industrial Communication Security

In the past, ICSs were not connected to the internet, and they were less common - except in industrial settings. Their security was based on isolation and anonymity. Now, ICSs are everywhere, from cars to air conditioners and homes. Many are connected to the internet through Virtual Private Networks (VPNs) to allow remote monitoring. These VPNs provide a certain degree of protection. But the ICS itself it not secured. And this vulnerability leaves room for attacks.

There have been several high-profile attacks against SCADA systems:

- A disgruntled former employee, which was a software developer, attacked a sewage water treatment plant in Australia, releasing hundreds of thousands of liters of sewage water into rivers and parks.
- An attack in 2009-2010, against Iran, destroyed about 1000 of the centrifuges used to enrich uranium. A worm named Stuxnet (Kushner, 2013) was developed to infect the Siemens Step7 Programmable Logic Controllers (PLCs). The worm used to randomly change the speed of the turbines which were enriching uranium. By increasing and then decreasing the angular velocity, vibrations were induced in the equipment and some of the turbines malfunctioned.
- The cyber-attack on the Ukrainian power grid in 2015 left about 230 000 people without electricity, after attackers shut down multiple distribution stations. Many files stored on the computers of the electrical energy distribution company were erased. A malware named BlackEnergy (Styczynski, Beach-Westmoreland, and Stables, 2016) was used for this attack. It included a Remote Access Terminal (RAT) through which the attackers reprogrammed the firmware of the control equipment of the substations.
- Another attack against a water treatment plant was carried out in Australia. The hackers changed the concentrations of the chemicals used to treat tap water.
- The 2016 cyber-attack against the Ukrainian power grid cut off 20% of the population of Kiev from electrical power. A malware named Industroyer (Cherepanov, 2017) was used in this attack. It targeted ICSs, and the OLE (Object Linking and Embedding) for Process Control Data Access, to hijack the communication network and to send commands to the PLCs.
- An attack took place in December 2017 against Saudi Arabia, where the security systems of several nuclear, oil and gas plants were targeted. At least one plant was shut down.

These attacks targeted industrial facilities, including electrical plants and the power grid itself. With the ever-increasing connectedness between industrial systems and the internet, these attacks will become more common and the risks associated with them will be more severe. Electrical grids and power plants are tempting targets for both lone wolves or groups of hackers who wish to prove themselves. These systems are also a very tempting target for countries. Attacks on the power grid can severely cripple a city or even a country and can produce economic and social problems.

According to (Minhaj Ahmad Khan and Salah, 2018), a network based on IoT should meet the following security requirements:

- The data has to be confidential - the content has to be known only by the WF operator and by authorized third parties. Moreover, the data must not be copied or transferred without the consent of the operator. The content of the data should remain constant from the moment it is acquired until it will be no longer needed.
- Access to the data and to the network must be controlled and verified, through means of authentication. Only authorized personnel should have access. Their usage of the data and of the network resources should be monitored. The same requirements are valid for the different nodes in the network: sensors, gateways, switches, etc. They should use the network resources in a transparent manner (to the operating company) and only for the purposes which they should fulfilled.
- The service, in this case being the supply of electrical energy to the end users, must always be available (when environmental conditions permit).
- Any network should not rely on single points of failure. There must always be a back-up for critical devices (e.g. gateways).

According to (ThreatLabZ, 2017), the most common software vulnerabilities in IoT devices are weak passwords, unencrypted communications (mainly HTTP requests) and outdated firmware (without patches for newly found exploits. Hackers can use the following tools to gain access to a network (Zaabi, 2016):

- Rootkits are software designed to remotely access and control a computer.
- Spyware are used to gather sensitive information (credentials, confidential data, files) which are then transmitted to the attackers.
- Viruses spread by copying themselves and travel by attaching to files, programs and web applications. They are used to steal information, cause damage to computers and networks, etc.
- Worms are like viruses, but they can spread themselves automatically through the network, without the need of human intervention.

Most malware connect to a Command and Control (C&C) center to receive commands, to send reports, and even to update itself.

Malicious software is usually delivered through:

- Trojans, which disguise themselves are legitimate files or programs. They try to trick users into downloading and running them. They grant the attackers a foothold in the system, from where other malware can be installed.

- Exploit kits target vulnerabilities in certain programs (web browsers and their extensions) to gain access to the computer and to deliver their payload (worms, viruses, etc).

5.6.1 Attacks Against ICSs

There are different types of attacks against IoT devices. Depending on the objective, the attacker may try to collect information, gain control of equipment or attempt to render the device unusable.

Man in The Middle attacks (S. S. Hassan et al., 2018) take place when a third party with malicious intents (adversary) has access to the communication channel. It is positioned between the transmitter and the receiver. This third party can read the messages (eavesdropping attacks) or even modify their content (relay attacks). The communicating parties do not know that the attacker is intercepting their communications.

Sinkhole attacks happen when an adversary tricked a great number of network nodes to send their data traffic through it. The data is received, but it is never re-transmitted to the intended receiver.

Denial of Service (DoS) is probably the most well-known attack (S. S. Hassan et al., 2018). The attacker tries to render a device or service unusable. Usually, it is carried out by spamming a target with huge amounts of traffic (requests, messages, etc.). Distributed DoS (DDoS) attacks use many nodes to generate the spam. The attackers first infect the devices with malware, to turn them into bots. The malware either communicates with a C&C center to receive instructions when to start the attack, or the date and time are hardcoded. Then, the devices are used in the actual attack, without the knowledge of their users. DoS attacks can be used to deplete the battery of wireless sensors or render servers unavailable.

Sybil attacks (Bazzi and Konjevod, 2007) are probably one of the most dangerous types of attacks. An adversary presents itself (or his group of bots) as legitimate nodes in a network. The attacker can thus gain access to a network or/and can exert influence in the network (by changing routing paths, data flows, etc.)

Backdoors (S. S. Hassan et al., 2018) are specific vulnerabilities in software, which are usually introduced intentionally either by the developer (for maintenance purposes) or by other entities. They can be used to gain control of the software and act as entry points into secured networks and devices.

Brute-force attacks (Minhaj Ahmad Khan and Salah, 2018) happen when an attacker simply tries all the possible encryption and/or password combinations to get access to a protected network.

Jamming attacks (Tayebi, Berber, and Swain, 2013) can target the different layers of the network. An attacker can use a RF emitter to disrupt the signal between two or more nodes. He can also target the synchronization

signals between the nodes (e.g. the acknowledgement). A jamming attack can also change the bits of data packets.

HELLO flooding (V. P. Singh, Jain, and Singhai, 2010) is carried out when the network is being set up. The nodes send "HELLO" packets to discover their neighbors and to create their routing tables. An adversary node with a high transmission range and high processing power floods the network with "HELLO" messages. It tries to trick the nodes in accepting it into the network, and to slow down the set up. As the nodes have limited processing power, they require a longer time to process the high number of messages.

Node tampering (Becher, Benenson, and Dornseif, 2006) can be dangerous in a WSN because there is no way to know the physical condition of a node, without visual inspection. An attacker can physically access a node and try to hack it to obtain access keys. The network would continue to see the node as trustworthy, while it may duplicate, forward, or even inject data into the network.

5.6.2 Attack vectors

An attack vector is the mean through which an attacker gains access inside a secured network, and the way the attack is carried out afterwards.

According to (European Union Agency for Network and Information Security, 2017), attacks usually commence through an employee of the target company. Either the person is an attacker (an inside attack), or he is a victim (outside attack).

Inside Attacks are very dangerous, and very easy to be carried out. The employee already knows the network infrastructure and the security measures. Most likely, this attacker also has the credentials to bypass any protection. These attacks are very hard to detect and investigate. Possible countermeasures are:

- Users should have unique access credentials, to ensure the traceability of their actions. Each person should hold on to their username and passwords and each employee should be trained to not share them with others.
- Users should be permitted to access the systems on a "need to know" basis.
- After contractors have finished their work in the company, their access rights should be suspended (unless they are responsible for the maintenance of the equipment).
- The company should train the employees to be aware of the security aspects. They should know the possible consequences of security breaches - towards the community, the environment, themselves and

the company). They should be taught basic notions about network security.

- The company should gain the trust of its employees and create a good working environment. No preventive measure can ever be effective if the employees are disgruntled.

External Attacks are much more common, although they are harder to carry out. Attackers usually monitor the enterprise looking for vulnerabilities in the software. When they find weak points, they design a special malware to make use of them. Attackers rely on weak protection of the company's network or on zero-day vulnerabilities in the software. The software designed for the attack must be injected in the network. This can be achieved in two ways:

- The attackers find a person in the organization with a unsafe behaviour on the internet. They design special emails or messages for that person, which contain infected attachments or links to compromised websites. When that employee opens an attachment while being connected to the corporate network, the malware will be set free in the network.
- A malware can be used to retrieve the credentials of at least one employee. Then, the attackers use them to access the network. Again, the targeted employees must have an unsafe behaviour on the internet.

There are protection measures which can help mitigate the risks:

- The users of the company have to be trained to have good habits while on the internet. They not should access suspicious websites, open emails and email attachments from unknown sources.
- The company should invest in malware protection, firewall software, encryption equipment, etc. The operating system and all other software should always be updated to the latest versions.
- The connection between the SCADA systems and the internet must be secure. This connection should never be direct, but through secure applications and software interfaces.

On the hardware side, each device should only have as many ports as needed. The ports should be protected against unauthorized access.

5.7 Conclusions

The standard ICS architecture should be maintained. All the sensors inside a WT should connect to a processing station located in the nacelle of

the WT, to reduce the latency and to increase the reliability and availability of the network. For local communication, the best protocol is BLE, followed by DASH7 and WirelessHART. Zigbee is also suitable.

Data and alarms (especially for SCADA) should also be transmitted to the wind farm operator, to help the company keep track of its assets. The current SCADA implementation which sends data at 10-minute time intervals is appropriate. LoRa can be used for offshore and onshore WTs which are located in areas without 4G coverage, and NB-IoT or LTE-M can be used for turbines which reside in areas covered by a LTE network.

A potential architecture for a communication system based on LoRa was also presented. Data can be acquired and transmitted from the WT at specific time intervals. Commands can also be send to control the test stand.

Attackers can target industrial installations, and the consequences can be severe. Different attacks were presented, to raise awareness about the security requirements of ICSs.

	Maximum overage [km]	Date rate [kbps]	Maximum latency [a] [s]	Topology	Frequency band [MHz]	Peak Current [b] [mA]	Duplex mode	Security	Interference protection
LoRa	15 - 20	0.29 - 50	60	star	433 / 868 / 915	40	Half	Yes	Yes
NB-IoT	35	250	10	star	LTE bands	120 - 300	Half	Yes	Yes
LTE-M	11	1024	0.015	star	LTE bands	500	Half	Yes	Yes
Sigfox	30 - 50 (with LOS [c])	0.3	60	star	868 / 915	51	Half	Yes	Yes
EC-GSM-IoT	15	474	N/A	mesh	900 / 2.4 * 10^3	N/A	Half	Yes	Yes
Digi Mesh	14.5	250	5	mesh	868 / 900 / 2.4 * 10^3	300	Half	Yes	Yes

TABLE 5.1: LPWA Communication Technologies

[a] Estimated from existing implementations.
[b] Estimated from existing implementations
[c] LOS stands for "Line of Sight"

	Maximum overage [km]	Date rate [kbps]	Maximum latency [a] [s]	Topology	Frequency band [MHz]	Peak Current [b] [mA]	Duplex mode	Security	Interference protection
ANT(+)	30	0.02	0	peer to peer / star / mesh	2.4	17	N/A	Yes	Yes
Wi-fi (802.11b)	150	11	1.5	star / tree	2.4	116	half	Yes	No
Wi-fi HaLoW	1000	347	N/A	star / tree	0.9	N/A	half	Yes	Yes
BLE (v. 5)	10 - 600	0.125 - 2	2.5	point to point / mesh	2.4	5.9	half	Yes	Yes
Bluetooth (v. 5)	40 - 400 (with LOS [c])	1 - 3	15	point to point / mesh	2.4	7.5	full	Yes	Yes
Zigbee	250	0.25	20	mesh	2.4	40	half	Yes	Yes
IrDA	1	1024	25	point to point	N/A	10.2	half	Yes	Yes
NFC	0.04	0.424	1000	point to point	0.01356	15	half	No	No
Z-Wave	40	0.04	3000	mesh	0.9	40	half	Yes	Yes
RFID	200	0.64	400	point to point	2.4 / 5	40	half	No	No
DASH7	100 - 5000	0.167 (lower with distance)	15	point to point / star / tree	0.433 / 0.868 / 0.915	160	half	Yes	Yes
Wireless HART	225	0.25	20	mesh	2.4	12	half	Yes	Yes
Wireless M-Bus	2000	0.1	N/A	star	0.169 / 0.433 / 0.868	37	half	Yes	Yes

TABLE 5.2: LAIoT Communication Technologies

[a] Estimated from existing implementations.
[b] Estimated from existing implementations
[c] LOS stands for "Line of Sight"

Chapter 6

General Conclusions and Perspectives

6.1 Conclusions

The objective of this work was the Fault Detection and Identification (FDI) of the different failures which can affect a Permanent Magnet Synchronous Generator (PMSG). This type of electrical machine is used in Direct Drive Wind Turbines (DDWT). The most common impairments of the PMSG, which were considered in this work, are the:

- Static Eccentricity Fault (SEF);
- Dynamic Eccentricity Fault (DEF);
- Mixed Eccentricity Fault (MEF);
- DeMagnetization Fault (DMF);
- Inter-turn Short Circuit Fault (ISCF).

These impairments are found using a mix of methods based on signal processing and state estimators. They are detected and identified by only monitoring the signals which are usually acquired by the SCADA system. In this case, these signals are the generated currents, the voltages of the generated electrical energy and the angular velocity of the rotor shaft.

Between the different tools used in signal processing, the Fast Fourier Transform (FFT) was selected due to its widespread use. However, the spectrum of the generated current changes with the wind speed, and thus it is more difficult to set thresholds for FDI. The Extended Kalman Filter (EKF) is used as a software sensor, to ensure redundancy. A new method to estimate the covariance matrix of the process noise is proposed, which is independent of the EKF. This procedure was compared with other methods from the literature and it was proven to be effective. The spectrum of the residuals computed between the generated currents and the estimated ones is shown to be constant with respect to changes in the wind speed.

The FFT is used to compute the spectrum over all the possible frequencies. However. there is a small number of frequencies of interest. The Goertzel Filter (GF) replaced the FFT, due to its higher efficiency and lower computational requirements. The GF can substitute the FFT only in this case, when the number of frequencies of interest is small. A bank of GFs is used - each one would monitor a certain frequency bin. The obtained results prove the effectiveness of the proposed approach.

Many different wireless communication technologies were compared, to highlight the most suitable ones for a real-time implementation. They can partially replace the wired communication network which exists inside Wind Turbines (WTs), thus lowering the installation and maintenance costs and speeding up the laying out of the cables.

6.2 Perspectives

Sensorless Estimation

The inputs of the first model of the PMSG, presented in Chapter II, are the angular speed of the rotor shaft and the voltages in the dq0 frame. Thus, the only measurements which remain to be used for the state update are the currents. The authors tried to find ways to eliminate the need for current measurement, i.e. to only use the generator speed as an input and the voltages for the state correction. It is possible, but one would have to model the rest of the electrical circuit (back-to-back converter, transformer, the grid-side filter and the infinite bus). The generator would serve a current source and the voltage drop across the rest of the circuit should be calculated and used to estimate the current in the prediction step of the EKF. The measured voltages would then be used in the update step of the filter. However, such a model might be too computationally heavy to be implemented on a microcontroller and/or a PLC, i.e. in a real-time environment. However, a simplified model might be usable.

Elimination of the constraints imposed by the assumptions

The first assumption presented in Chapter III is very restrictive. There are solutions to avoid it, such as using the pseudo-inverse for non-invertible matrices or estimating the Jacobian of nonlinear measurement functions.

The second assumption is also restrictive, as the system must have a high observability index.

The assumption should be changed to allow the usage of this method even for less observable systems. Possible solutions will be the focus of future research.

Covariance Estimation

The method proposed in Chapter III requires knowledge about the covariance matrix of the measurement noise. This necessity can be eliminated by combining the proposed method with the one from (Akhlaghi, Zhou, and Huang, 2017). The covariance matrix of the measurement noise could be estimated with the method presented in (Akhlaghi, Zhou, and Huang, 2017), and the process noise covariance matrix may be evaluated as it was proposed in Chapter III (or vice-versa). So, no a priori knowledge of any noise would be necessary. Moreover, the complexity of the method from (Akhlaghi, Zhou, and Huang, 2017) would decrease, without sacrificing precision. Nevertheless, the resulting procedure would be tied to the EKF.

Method Stability for LTV Systems

The inductances and the resistances of the different stator phases can change in the case of inter-turn short circuit faults. A study of the resulting system, i.e. its stability, should be conducted to check if the proposed method could be used for systems with time-varying parameters.

Isolation of DEF and SEF from each other

To ensure the isolability of DEF and SEF, the magnitude of the Side-Band Components (SBCs) of the harmonics, introduced by the impairments, must be monitored. The speed with which this magnitude changes can be used to isolate one fault from the other Ebrahimi et al., 2014.

Fault Tree Analysis for the Generator

The GF will be used in a FDI algorithm based on Fault Tree Analysis (FTA) Ruijters and Stoelinga, 2015, to look for the specific cause of a fault. E.g., for ISCF, this new algorithm should point to the affected phase of the current and, if possible, to the pole pair which is affected by the fault.

Scientific Production

Papers published in international journals:

- L. I. Gliga, H. Chafouk, D. Popescu, and C. Lupu, "A method to estimate the process noise covariance for a certain class of nonlinear systems," In: Mechanical Systems and Signal Processing, IF 5.005, vol. 131, pp. 381–393, Sep. 2019.

Papers submitted to international journals:

- L. I. Gliga, B. D. Ciubotaru, H. Chafouk, D. Popescu and C. Lupu, "Diagnosis of a PMSG Using Machine Current Signature Analysis," In: ISA Transactions, IF 4.343;
- L. I. Gliga, R. Khemmar, H. Chafouk, D. Popescu and C. Lupu, "A Survey of Wireless Communication Technologies for an IoT-connected Wind Farm", In: Mobile Networks and Applications, IF 2.39.

Papers presented in international conferences:

- A. Abdelkarim, H. Chafouk, L. I. Gliga, and D. Popescu, “Diagnosis of a NPC inverter using Goertzel Filters,” In: 23rd International Conference on System Theory, Control and Computing (ICSTCC), 2019, pp. 803–808.
- A. Abdelkarim, L. I. Gliga, H. Chafouk, and D. Popescu, “A Novel Approach for Model-based Diagnosis of a Three-Level Three-Phase NPC Inverter,” In 4th Conference on Control and Fault Tolerant Systems (SysTol), 2019, pp. 300–305.
- L. I. Gliga, B. D. Ciubotaru, H. Chafouk, D. Popescu and C. Lupu, "Fault Diagnosis of a Direct Drive Wind Turbine Using a Bank of Goertzel Filters," In: 6th International Conference on Control, Decision and Information Technology (CoDIT), Paris, Apr. 2019;
- L. I. Gliga, H. Chafouk, D. Popescu, and C. Lupu, "Comparison of State Estimators for a Permanent Magnet Synchronous Generator," In: 22nd

International Conference on System Theory, Control and Computing (ICSTCC), 2018, pp. 474–479;

- L. I. Gliga, H. Chafouk, D. Popescu, and C. Lupu, "Diagnosis of a Permanent Magnet Synchronous Generator using the Extended Kalman Filter and the Fast Fourier Transform," In: 7th International Conference on Systems and Control (ICSC), 2018, pp. 65–70;
- L. I. Gliga, C. Lupu, H. Chafouk, and D. Popescu, "Innovations in fault detection and tolerant control for a wind farm, using Wireless Sensor Networks," In: 18th International Carpathian Control Conference (ICCC), 2017, pp. 332–336.

Oral presentations in local scientific events:

- L. I. Gliga, "Diagnostic of a Wind Turbine, Using Wireless Sensor Networks," In: 11th PhD Students of ED MIIS et PSIME Day, UFR des Sciences et Techniques, Saint Etienne du Rouvray, Jun. 2019;
- L. I. Gliga, "Diagnosis and Fault Tolerant Control of a Wind Farm, using IoT," In: PhD Students of IRSEEM Day, ESIGELEC, Saint Etienne du Rouvray, Mar. 2019.

Appendix A

Simulation Parameters

A.1 Parameters of the Wind Energy Conversion Chain

TABLE A.1: Wind Turbine Parameters

Parameter	Notation	Value	Unit
Radius of the propeller	R	21	m
Air Density	ρ_{air}	1.225	$\mathrm{kg/m^3}$
Stator dq Resistance	R_s	0.4418	Ω
Stator dq Inductance	L_s	$1.4 \cdot 10^{-5}$	H
Flux Linkage	ϕ	1.0118^{-11}	$\mathrm{V \cdot s}$
Moment of Inertia	J	0.0295	$\mathrm{kg/m^2}$
Viscous Damping	B	0.0004924	N/m/s
Number of Pole Pairs	n_P	6	N/A
Fundamental frequency	f_s	50	Hz
Generator-side Capacitor	C_{gen}	0.001	F
PWM Frequency	f_{PSM}	100 000	Hz
DC-link Capacitor	C_{DC}	30	F
RL Filter Resistance	R_{RL}	0.4418	Ω
RL Filter Inductance	L_{RL}	0.0017	H
Grid Voltage	V_{grid}	230	V
Grid Frequency	f_{grid}	50	Hz

The values of the parameters of the generator were initially taken from (Alameh, 2017). Some were modified later, after repeated simulations.

The values of the parameters of the electrical chain (e.g. IGBT bridge snubber resistance) were the default values from Matlab.

Appendix B

Model of the Mechanical Part of the Wind Turbine

B.1 Mechanical Model of the Wind Turbine

The mechanical model of the Wind Turbine (WT) was simulated using the equations from (Pintea, Popescu, and Borne, 2010) and (Rolan et al., 2009). According to these publications, the mechanical torque (T_m) generated by the rotor is

$$T_m = \frac{P_m}{\omega_m} = \frac{0.5 \cdot \rho_{air} \cdot \pi \cdot R^2 \cdot v_{wind} \cdot C_p}{\omega_m}, \tag{B.1}$$

where P_m is the mechanical power of the WT (in $N \cdot m$), ω_m is the angular velocity of the rotor shaft (in rpm), ρ_{air} is the density of air (in kg/m^3), R is the radius of the propeller (in m), v_{wind} is the speed of the wind (in m/s) and C_p is the power coefficient of the WT.

The power coefficient is computed as

$$C_p(\lambda, \beta) = c_1 \cdot \left(\frac{c_2}{\lambda_i} - c_3 \cdot \beta - c_4 \right) \cdot e^{\frac{-c_5}{\lambda_i}} + c_6 \cdot \lambda \tag{B.2}$$

where the coefficients $c_i, i = \overline{1,6}$, have the values $c_1 = 0.5175$, $c_2 = 116$, $c_3 = 0.4$, $c_4 = 5$, $c_5 = 21$, $c_1 = 0.0068$ and β is the pitch angle. λ is the tip-speed ratio

$$\lambda = \frac{\omega_m \cdot R}{v_{wind}}, \tag{B.3}$$

and λ_i is computed using

$$\frac{1}{\lambda_i} = \frac{1}{\lambda + 0.08 \cdot \beta} - \frac{0.035}{\beta^3 + 1}. \tag{B.4}$$

Appendix C

Useful Transforms

C.1 The Clarke Transform

The Clarke, also called alpha-beta, transform is used to convert three-phase AC currents/voltages into two-phase AC ones (Mohan, 2012). The mathematical relation that describes the power invariant Clarke Transform (which preserves the values of the active and reactive powers in both systems) is

$$\begin{bmatrix} i_\alpha(t) \\ i_\beta(t) \\ i_0(t) \end{bmatrix} = \sqrt{\frac{2}{3}} \cdot \begin{bmatrix} 1 & -\frac{1}{2} & -\frac{1}{2} \\ 0 & \frac{\sqrt{3}}{2} & -\frac{sqrt3}{2} \\ \frac{1}{\sqrt{2}} & \frac{1}{\sqrt{2}} & \frac{1}{\sqrt{2}} \end{bmatrix} \begin{bmatrix} i_a(t) \\ i_b(t) \\ i_c(t) \end{bmatrix}, \tag{C.1}$$

where $i_\alpha(t), i_\beta(t), i_0(t)$ are the currents in the two-phase alpha-beta frame and $i_a(t), i_b(t), i_c(t)$ are the currents in the three-phase abc frame. In a balanced system, $i_0(t) = 0$, hence the name.

The the power invariant version of the Inverse Clarke Transform, is

$$\begin{bmatrix} i_a(t) \\ i_b(t) \\ i_c(t) \end{bmatrix} = \sqrt{\frac{2}{3}} \cdot \begin{bmatrix} 1 & 0 & \frac{1}{\sqrt{2}} \\ -\frac{1}{\sqrt{2}} & \frac{\sqrt{3}}{2} & \frac{1}{\sqrt{2}} \\ -\frac{1}{2} & -\frac{sqrt3}{2} & \frac{1}{\sqrt{2}} \end{bmatrix} \begin{bmatrix} i_\alpha(t) \\ i_\beta(t) \\ i_0(t) \end{bmatrix}. \tag{C.2}$$

The Clarke Transform and its inverse can be deduced geometrically. The alpha axis should be aligned with the a axis, while the beta axis is perpendicular on the alpha one. The transforms are deduced through projecting the phasor, in the abc system, on the alpha-beta axes.

C.2 The Park Transform

The Park, also called direct-quadrature, transform is used to convert three-phase AC currents/voltages into two-phase DC ones (Mohan, 2012). The mathematical relation that describes the power invariant Park Transform (which preserves the values of the active and reactive powers in both

systems) is

$$\begin{bmatrix} i_d \\ i_q \\ i_0 \end{bmatrix} = \sqrt{\frac{2}{3}} \cdot \begin{bmatrix} sin\left(\theta\right) & sin\left(\theta - \frac{2\pi}{3}\right) & sin\left(\theta + \frac{2\pi}{3}\right) \\ cos\left(\theta\right) & cos\left(\theta - \frac{2\pi}{3}\right) & cos\left(\theta + \frac{2\pi}{3}\right) \\ \sqrt{\frac{1}{2}} & \sqrt{\frac{1}{2}} & \sqrt{\frac{1}{2}} \end{bmatrix} \begin{bmatrix} i_a(t) \\ i_b(t) \\ i_c(t) \end{bmatrix}, \tag{C.3}$$

where i_d, i_q, i_0 are the currents in the dq0 frame and θ is the angle between the phasor, in the abc frame, and the a axis.

The power invariant version of the Inverse Park Transform, is

$$\begin{bmatrix} i_a(t) \\ i_b(t) \\ i_c(t) \end{bmatrix} = \sqrt{\frac{2}{3}} \cdot \begin{bmatrix} sin\left(\theta\right) & cos\left(\theta\right) & \sqrt{\frac{1}{2}} \\ sin\left(\theta - \frac{2\pi}{3}\right) & cos\left(\theta - \frac{2\pi}{3}\right) & \sqrt{\frac{1}{2}} \\ sin\left(\theta + \frac{2\pi}{3}\right) & cos\left(\theta + \frac{2\pi}{3}\right) & \sqrt{\frac{1}{2}} \end{bmatrix} \begin{bmatrix} i_d \\ i_q \\ i_0 \end{bmatrix}. \tag{C.4}$$

The Park and Inverse Park Transforms previously presented can be deduced geometrically. The dq axes rotate in the abc frame. The projections of the three-phase currents/voltages phasor on the dq axis are computed using the previous equations.

Appendix D

Matlab Code and Simulink Schematics

D.1 Matlab Code

The implementation of the Goertzel Filter for Static Eccentricity Fault Detection:

```
function Amp  = myGoertzel(u)
persistent N Q1 Q2 coeff Fs Ft k
if isempty(N)
    N = 0;      %frequency resolution
    Q1 = [0; 0; 0];
    Q2 = [0; 0; 0];
    Fs = 1000000;   %sampling frequency
    Ft = 25;        %target grequency
    k = round(0.5 + 100000 * Ft / Fs);
    coeff = 2 * cos(2 * pi * k / 100000);
end
Q0 = coeff * Q1 - Q2 + u;
Q2 = Q1;
Q1 = Q0;
if N == 100000
    Amp = sqrt(Q1 .^ 2 + Q2 .^ 2 - Q1 .* Q2 * coeff);
    N = -1;
    Q1 = [0; 0; 0];
    Q2 = [0; 0; 0];
else
    Amp = [0; 0; 0];
end
N = N + 1;
end
```

D.2 Simulink Schematics

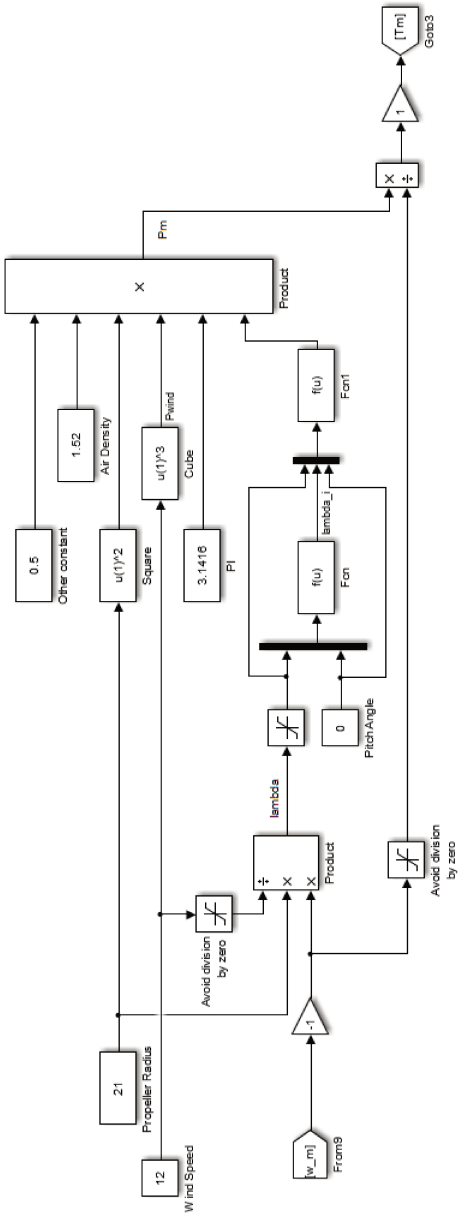

FIGURE D.1: The Simulink schematic of the mechanical part of the WT.

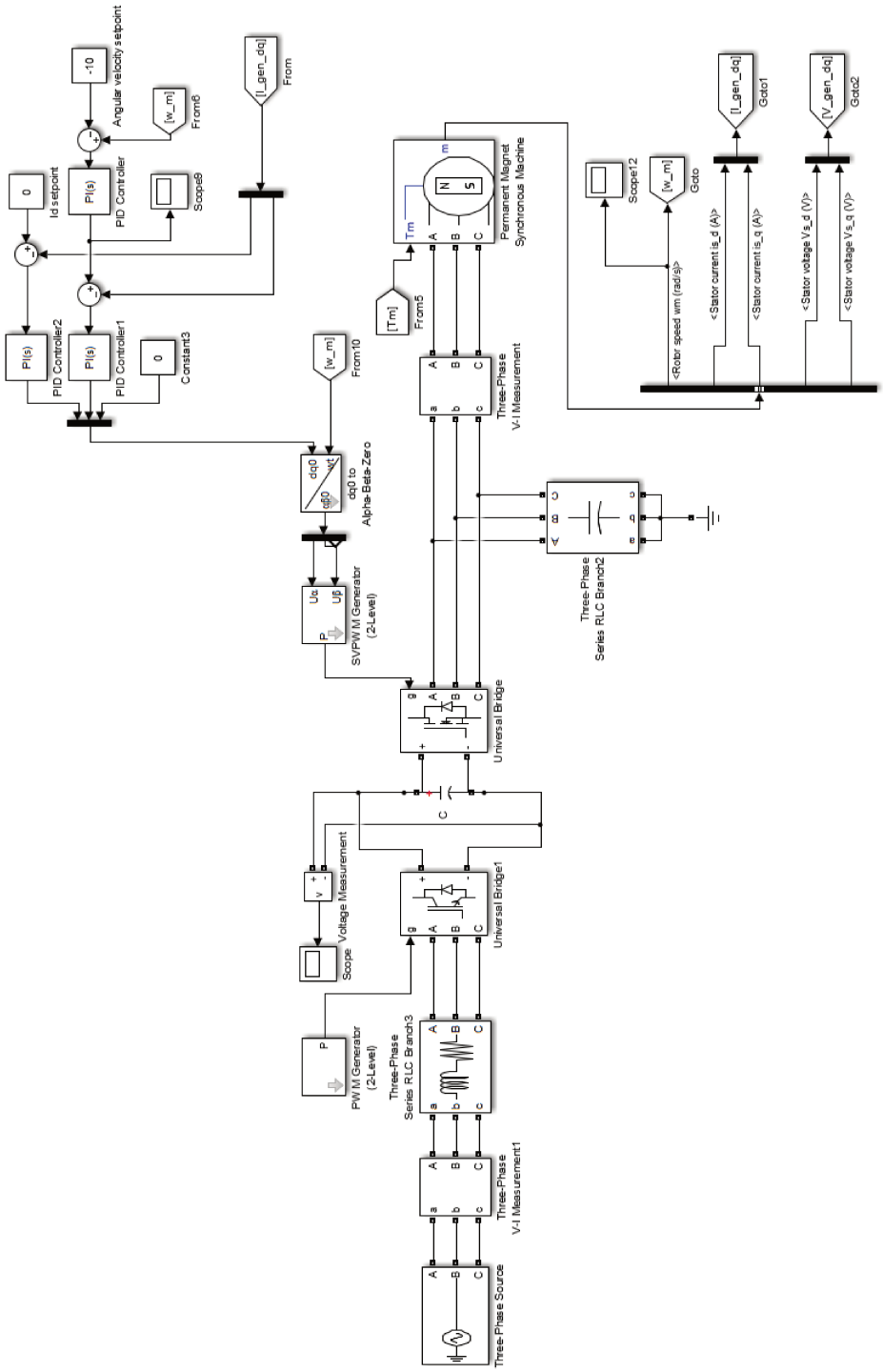

FIGURE D.2: The Simulink schematic of the nominal control of the WT.

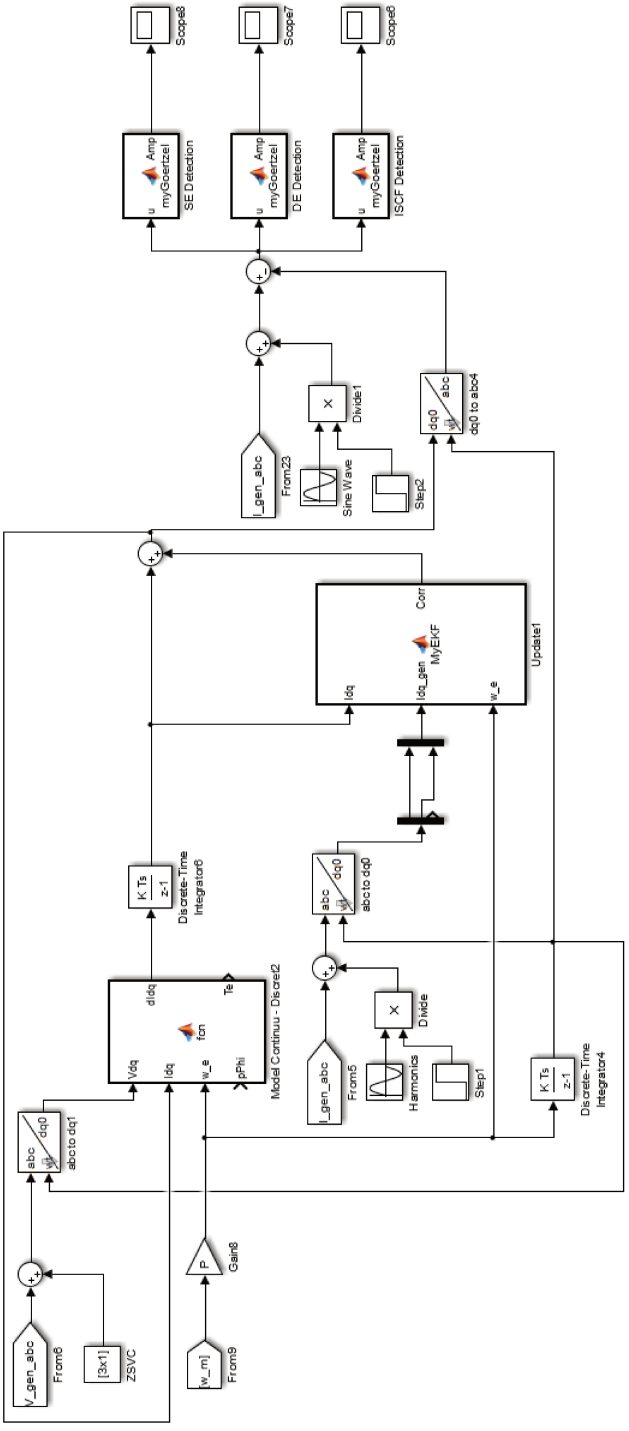

FIGURE D.3: The Simulink schematic of the fault diagnosis using the Extended Kalman Filter and the Goertzel Filters.

Appendix E

Summary in English

Context

WIND Farm (WF) numbers are on the rise in the European Union. From the potential electrical energy generation capacity, using wind power, of about 500GW, only 178.8GW are currently harvested using Wind Energy Conversion Systems (WECS) (Walsh and Pineda, 2019). Wind Turbines (WTs) are expected to become the primary source of electrical energy in the EU by 2019. They offer a very good combination between power generation capacity and cost. Therefore, they are attractive to investors. With this future growth in perspective, there are certain challenges that still need to be solved.

There are different types of WTs, depending on the generator type and on the presence or lack of a gearbox. Direct Drive Wind Turbines (DDWTs) are considered in this work. They do not have a gearbox and are usually equipped with Permanent Magnet Synchronous Generators (PMSG). They are widely used in offshore installations and their market share is increasing in both offshore and onshore WFs, due to their higher energy yield and reliability (Carroll, McDonald, and McMillan, 2015).

Monitoring of WFs is not trivial. Offshore WFs can lie several kilometers away from the shore and they can be made of hundreds of WTs. The largest offshore WF in the world, which is currently under extension, is the Walney Offshore WF, in the United Kingdom. It comprises 189 WTs which cover an area of around $73km^2$ (Ørsted, 2017). The largest onshore WF is the Gansu WF in China, which comprises around 7000 WTs (Vyas, 2018).

Usually, a WT is equipped with a Supervisory Control and Data Acquisition (SCADA) system. It can also be monitored using Condition Monitoring (CM) and/or Structural Health Monitoring (SHM) systems. The data acquired and sent by these systems is usually transmitted through copper cables, inside each WT. Although no official statistic could be found, it can be reasonably assumed that the number of signals transmitted inside each WT is, at least, in the order of hundreds. Therefore, when considering the

number of WTs of the previously mentioned WFs, the cost generated by the installation and maintenance of the cables becomes significant.

Moreover, WF operators need to remotely monitor their assets. Thus, fiber-optic cables are laid between the different WTs in a WF, and from the gateway of the WF to the operator. These data transmission lines run along the three-phase power cables (in case of AC transmission) which are laid from the WF to the grid. The dedicated line used for the communication between the dispatch center and the WF is maintained by a separate company, for a fee. This tax is relatively high, and depending on the availability and redundancy requirements, it can amount to tens of thousands of euros per year.

Although DDWTs are more reliable nowadays than those in previous generations, they can still break down, so they require automatic diagnosis systems. The different components which can fail in a DDWT are the blades, the generator, the main shaft, the hydraulic systems, etc., (Qiao and Lu, 2015a). These impairments can lead to lower power generation, asset damage and even downtime. The generator is considered in this work, as it is responsible for almost 25% of the total downtime of a DDWT.

Objectives

The objective of this work is the Fault Diagnosis and Identification (FDI) of the different faults which can affect a PMSG. The most common faults, which can affect the PMSG, are (Alameh et al., 2015):

- Static eccentricity fault;
- Dynamic eccentricity fault;
- Mixed eccentricity fault;
- Demagnetization fault;
- Inter-turn short-circuit fault.

These impairments should be detected as early as possible, even in incipient stages. The Fault Detection and Identification (FDI) tools should be precise, but also simple to use and implement. Therefore, the accent should lie on simpler methods which can be understood and utilized by engineers with only bachelor-level studies.

The feasibility of using Wireless Sensor Networks (WSNs), to eliminate the wired communication network, should be investigated. The current communication architecture of a WT should be studied, together with different wireless communication technologies. A short guide should be developed, to help choose a suitable wireless protocol for a given application.

Description of the Chapters

The state of the art, related to the diagnosis and to surveys of wireless communication, is presented in Chapter I.

The mathematical model of the PMSG is presented in Chapter II. Its mathematical model is continuous and non-linear, therefore it is difficult to discretize. A comparison is made between different discretization techniques. A continuous model with a discrete integrator is shown to be the best solution. Then, the nominal closed-loop control of the WT is presented.

In Chapter III, there is presented a new method to compute the covariance matrix of the process noise. This procedure is shown in the context of an Extended Kalman Filter (EKF). However, it does not use any of the matrices of the filter and is therefore independent of it. The method uses a constant covariance matrix for the measurement noise and, at each iteration, it re-computes the values of the process noise covariance matrix. The proposed method and two other ones, selected from the scientific literature, are tested to estimate the current generated by the PMSG. All three methods are tested in the context of the EKF. The obtained results are compared and discussed to highlight the strengths and weaknesses of the proposed approach. Then, the Kalman Filter (KF), the Extended Kalman Filter (EKF) and the Unscented Kalman Filter (UKF) are compared. The results are presented and it is shown that the EKF is the most suitable one for this application. This is followed by a discussion regarding the behavior of the filters, where all are shown to act like proportional controllers.

The different faults which can affect a PMSG are shown in Chapter IV. The most common ones are the rotor demagnetization, eccentricity (static, dynamic and mixed) and inter-turn short circuit. Their effect is noticeable on the spectrum of the stator currents, which is computed using the Fast Fourier Transform (FFT). However, for a WT, the spectrum of the currents changes with the wind speed. Therefore, the obtained results may not be accurate. In this chapter, the residuals, computed using the currents estimated with the EKF and the measured ones, are proposed to be used for FDI, together with the FFT. The spectrum of the residuals is invariant to changes in the wind speed, but sensitive to faults. However, the FFT computes the whole spectrum, while the number of possible faults and the number of introduced harmonics is very low. The Goertzel Algorithm (GA), implemented as a filter - the Goertzel Filter (GF), is also presented in this chapter as a more efficient alternative to the FFT. The GF was tested and simulation results prove that it can return the squared magnitude of these harmonics. This information can be used to set thresholds for fault detection, within a FDI algorithm.

WFs can be located in isolated areas, or the WTs may be distributed

geographically. Therefore, the necessary communication infrastructure can be expensive to install and maintain. In Chapter V, WSNs and the Internet of Things (IoT) are presented as solutions for these problems. WSNs are quick to install, easy to maintain and they scale up easily. The requirements for a potential WSN, for both a WT and a WF, are studied in this chapter. Different wireless communication technologies are thoroughly compared. Both long-range low-power protocols and short-range high-speed ones are considered. A possible LoRa-based architecture of a WF communication system is presented. The integration of a power generation facility in the IoT raises security concerns. Potential dangers and vulnerabilities are listed, to increase awareness of the necessity of security in Industrial Communication Systems (ICS).

Conclusions

These impairments were found using a mix of methods based on signal processing and state estimators. They were detected and identified by only monitoring the signals which are usually acquired by the SCADA system. In this case, these signals are the generated currents, the voltages of the generated electrical energy and the angular velocity of the rotor shaft.

Between the different tools used in signal processing, the Fast Fourier Transform (FFT) was selected due to its widespread use. However, the spectrum of the generated current changes with the wind speed, and thus it is more difficult to set thresholds for FDI. The Extended Kalman Filter (EKF) is used as a software sensor, to ensure redundancy. A new method to estimate the covariance matrix of the process noise is proposed, which is independent of the EKF. This procedure was compared with other methods from the literature and it was proven to be effective. The spectrum of the residuals computed between the generated currents and the estimated ones is shown to be constant with respect to changes in the wind speed.

The FFT is used to compute the spectrum over all the possible frequencies. However. there is a small number of frequencies of interest. The Goertzel Filter (GF) replaced the FFT, due to its higher efficiency and lower computational requirements. The GF can substitute the FFT only in this case, when the number of frequencies of interest is small. A bank of GFs is used - each one would monitor a certain frequency bin. The obtained results prove the effectiveness of the proposed approach.

Many different wireless communication technologies were compared, to highlight the most suitable ones for a real-time implementation. They can partially replace the wired communication network which exists inside Wind Turbines (WTs), thus lowering the installation and maintenance costs and speeding up the laying out of the cables.

Appendix F

Résumé en Français

Contexte

Le secteur de l'énergie éolienne en Union Européenne (UE) est en forte croissance depuis quelques années. La capacité potentielle de production d'énergie électrique à partir de l'énergie éolienne est d'environ 500 GW, dont 178,8 GW sont actuellement exploités par des systèmes de conversion de l'énergie éolienne (SCEE) (Walsh and Pineda, 2019). Cette énergie devraient devenir la principale source d'énergie électrique dans l'UE, devançant ainsi le charbon, le nucléaire puis le gaz. Elle est une énergie renouvelable et elle offre une très bonne combinaison entre la capacité de production d'électricité et le coût, ce qui rend ce secteur plus attrayant pour les investisseurs. Le secteur de l'éolien est en plein développement mais il reste encore certains défis à relever.

Il existe différents types de Turbines Éoliennes(TEs), en fonction du type de générateur et de la présence ou non d'une boîte de vitesses. Les Turbines Éoliennes à Entraînement Direct (TEED) sont considérées dans ce travail. Elles n'ont pas de boîte de vitesses et sont généralement équipées de générateurs synchrones á aimants permanents (GSAP). Elles sont largement utilisées dans les installations offshore et onshore, en raison de leur rendement énergétique et de leur fiabilité plus élevée (Carroll, McDonald, and McMillan, 2015).

La surveillance des Parcs Éoliens (PEs) n'est pas facile. Ceux qui sont offshore peuvent se trouver à plusieurs kilomètres de la côte et peuvent être constitués de centaines des éoliennes. Le plus grand PE offshore du monde, actuellement en cours d'extension, est l'Offshore Walney, au Royaume-Uni. Il comprend 189 TEs qui couvrent une surface d'environ $73km^2$ (Ørsted, 2017). Le plus grande PE onshore est celui de Gansu en Chine, qui comprend environ 7000 éoliennes (Vyas, 2018).

En général, une TE est équipée d'un système SCADA (Supervisory Control and Data Acquisition). Elle peut également être surveillé à l'aide de systèmes de Condition Monitoring (CM) et/ou de Structural Health Monitoring (SHM). Les données acquises et envoyées par ces systèmes sont

généralement transmises par des câbles en cuivre, à l'intérieur de chaque turbine. Bien qu'aucune statistique officielle n'ait pu être trouvée, on peut raisonnablement supposer que le nombre de signaux transmis à l'intérieur de chaque TE est, au moins, de l'ordre de centaines. Par conséquent, si on considère le nombre de TEs des PEs, le coût généré par l'installation et l'entretien des câbles devient significatif.

De plus, les opérateurs d'un PÉ doivent surveiller leurs actifs à distance. Ainsi, des câbles en fibre optique sont installées entre les différentes TEs d'un PE, et de la passerelle du réseau du PE vers l'opérateur. Ces lignes de transmission de données longent les câbles d'alimentation triphasés (dans le cas d'une transmission CA) qui sont posés du PE vers le réseau. La ligne spécialisée utilisée pour la communication entre le centre de surveillance et le parc est maintenue par une société lucrative distincte. La taxe est relativement élevée et, selon les besoins de disponibilité et de redondance, elle peut s'élever à des dizaines de milliers d'euros par an.

Bien que les TEED soient aujourd'hui plus fiables que celles des générations précédentes, elles peuvent encore tomber en panne et nécessitent donc des systèmes de diagnostic automatique. Les différents composants qui peuvent tomber en panne dans une TEED sont les pales, le générateur, l'arbre principal, les systèmes hydrauliques, etc. (Qiao and Lu, 2015a). Ces déficiences peuvent entraîner une baisse de la production d'électricité, des dommages aux biens et même des temps d'arrêt. Le générateur est considéré dans ce travail, car il est responsable de près de 25% du temps d'arrêt total d'une TEED.

Objectifs

L'objectif de ce travail est la Détection et l'Identification des Défauts (DID) des différentes défaillances qui peuvent affecter un GSAP. Ce type de machine électrique est utilisé dans les Éoliennes à Entraînement Direct (EED). Les déficiences les plus courantes du GSAP, sont le (Alameh et al., 2015) :

- Défaut d'excentricité statique ;
- Défaut d'excentricité dynamique ;
- Défaut d'excentricité mixte ;
- Défaut de désaimantation ;
- Défaut court-circuit inter-tour.

Ces déficiences doivent être détectées le plus tôt possible. Les outils de détection et d'identification des défaillances doivent être précis, mais aussi simples à utiliser et à mettre en œuvre. Par conséquence, l'accent devrait

être mis sur des méthodes plus simples qui peuvent être comprises et utilisées par les ingénieurs qui n'ont que des études de niveau licence.

La faisabilité de l'utilisation de Réseaux de Capteurs sans Fil (RCF), pour éliminer le réseau de communication filaire, devrait être étudiée. L'architecture de communication d'une TE devrait être étudiée, ainsi que les différentes technologies de communication sans fil. Un petit guide devrait être élaboré pour aider à choisir un protocole sans fil adapté à une application donnée.

Description du Chapitres

L'état de l'art en matière de diagnostic et d'enquêtes sur les communications sans fil est présenté au Chapitre I.

Le modèle mathématique du GSAP est présenté au Chapitre II. Son modèle mathématique est continu et non linéaire - il est donc difficile de discrétiser. Une comparaison est faite entre les différentes techniques de discrétisation. Un modèle continu avec un intégrateur discret s'avère être la meilleure solution. Ensuite, la régulation nominale du TEED est présentée.

Le Chapitre III présente une nouvelle méthode de calcul de la matrice de covariance du bruit du processus. Cette procédure est illustrée par la mise en œuvre du filtre de Kalman étendu (FKE). Cependant, elle n'utilise aucune des matrices du filtre et est donc indépendante de celle-ci. La méthode utilise une matrice de covariance constante pour la mesure du bruit et, à chaque itération, elle recalcule les valeurs de la matrice de covariance du bruit de processus. La méthode proposée et deux autres, sélectionnées de la littérature scientifique, sont testées pour estimer le courant généré par le GSAP. Les trois méthodes sont testées dans le cadre du FKE. Les résultats obtenus sont comparés et discutés afin de mettre en évidence les forces et les faiblesses de l'approche proposée. Ensuite, le Filtre de Kalman (FK), Filtre de Kalman Étendu (FKE) et le Filtre de Kalman (FKU) sont comparés. Les résultats sont présentés, et il est démontré que le FKE est la méthode la plus appropriée pour cette application. Ceci est suivi d'une discussion sur le comportement des filtres, où il est prouvé que tous agissent comme des régulateurs proportionnels.

Les différents défauts qui peuvent affecter un GSAP sont présentés en Chapitre IV. Les plus courantes sont la démagnétisation du rotor, l'excentricité (statique, dynamique et mixte) et le court-circuit inter-tour. Leur effet est visible sur le spectre des courants statoriques, qui est calculé à l'aide de la Transformée de Fourier Rapide (TFR). Cependant, pour une TE, le spectre des courants change avec la vitesse du vent. Par conséquence, les résultats obtenus peuvent ne pas être précis. Dans ce chapitre, il est proposé d'utiliser les résidus, calculés à l'aide des courants estimés avec l'FKE et ceux mesurés, pour le DID, conjointement avec la TFR. Le spectre des

résidus est invariant aux changements de la vitesse du vent, mais sensible aux défauts. Cependant, la TFR calcule l'ensemble du spectre, tandis que le nombre de défauts possibles et le nombre d'harmoniques introduites sont très faibles. L'Algorithme de Goertzel (AG), est mis en œuvre comme un filtre - le Filtre de Goertzel (FG), est également présenté dans ce chapitre comme une alternative plus efficace au TFR. Le FG a été testé et les résultats de la simulation prouvent qu'il peut restituer la magnitude de ces harmoniques, au carré. Ces informations peuvent être utilisées pour définir des seuils de détection de défauts, dans le cadre d'un algorithme de DID.

Les PEs peuvent être situées dans des zones isolées, ou les TEs peuvent être distribués géographiquement. Par conséquent, l'infrastructure de communication nécessaire peut être coûteuse à installer et à entretenir. En Chapitre V, les Réseaux des Capteurs sans Fil (RCFs) et l'Internet des Objets (IdO) sont présentés comme des solutions à ces problèmes. Les RCFs sont rapides à installer, faciles à entretenir et à mettre à l'échelle facilement. Les exigences d'une éventuelle RCF, tant pour une TE que pour un PE, sont étudiées dans ce chapitre. Différentes technologies de communication sans fil sont comparées. Les protocoles à longue-portée et à faible consommation d'énergie, ainsi que les protocoles à courte portée et à haute vitesse sont considérés. Une architecture possible basée sur la technologie LoRa est présentée. L'intégration d'une installation de production d'électricité dans l'IdO pose des problèmes de sécurité. Les dangers potentiels et les vulnérabilités sont répertoriés, afin de sensibiliser à la nécessité de la sécurité dans les Systèmes de Communication Industrielle (SCI).

Conclusions

Les déficiences ont été constatées à l'aide d'une combinaison de méthodes basées sur le traitement du signal et des estimateurs d'état. Elles ont été détectés et identifiés en surveillant uniquement les signaux généralement acquis par le système SCADA. Dans ce cas, ces signaux étaient les courants générés, les tensions de l'énergie électrique générée et la vitesse angulaire de l'arbre du rotor.

Parmi les différents outils utilisés dans le traitement du signal, la Transformée de Fourier Rapide (TFR) a été choisie en raison de son utilisation généralisée. Toutefois, le spectre du courant généré change en fonction de la vitesse du vent, et il est donc plus difficile de fixer des seuils pour les DID. Le Filtre de Kalman Étendu (FKE) est utilisé comme capteur logiciel pour assurer la redondance. Une nouvelle méthode d'estimation de la matrice de covariance du bruit du processus est proposée, qui est indépendante du FKE. Cette procédure a été comparée à d'autres méthodes de la littérature et s'est révélée efficace. Le spectre des résidus calculés entre les courants

générés et les courants estimés s'avère constant par rapport aux variations de la vitesse du vent.

La TFR est utilisée pour calculer le spectre sur toutes les fréquences possibles. Cependant, il y a un petit nombre de fréquences d'intérêt. Le Filtre de Goertzel (FG) a remplacé la TFR, en raison de son efficacité plus élevée et de ses exigences de calcul plus faibles. Le FG ne peut substituer la TFR que lorsque le nombre de fréquences d'intérêt est faible. Une banque de FGs est utilisée - chacun d'eux surveillerait un certain intervalle de fréquence. Les résultats obtenus prouvent l'efficacité de l'approche proposée.

De nombreuses technologies de communication sans fil différentes ont été comparées, afin de mettre en évidence les plus appropriées pour une mise en œuvre en temps-réel. Ils peuvent remplacer partiellement le réseau de communication filaire qui existe à l'intérieur des éoliennes, réduisant ainsi les coûts d'installation et de maintenance, et accélérant la pose des câbles.

Bibliography

Adams, Douglas et al. (2011). "Structural health monitoring of wind turbines: Method and application to a HAWT". In: *Wind Energy* 14.4, pp. 603–623. ISSN: 10954244. DOI: 10.1002/we.437. arXiv: arXiv:1006.4405v1. URL: https://onlinelibrary.wiley.com/doi/abs/10.1002/we.437.

Ahmed, Arif and Ejaz Ahmed (Jan. 2016). "A survey on mobile edge computing". In: *10th International Conference on Intelligent Systems and Control (ISCO)*. IEEE, pp. 1–8. ISBN: 978-1-4673-7807-9. DOI: 10.1109/ISCO.2016.7727082. URL: http://ieeexplore.ieee.org/document/7727082/.

Ahmed, Mohamed A. and Young Chon Kim (2014). "Communication network architectures for smart-wind power farms". In: *Energies* 7.6, pp. 3900–3921. ISSN: 19961073. DOI: 10.3390/en7063900. URL: https://www.mdpi.com/1996-1073/7/6/3900.

Akhlaghi, Shahrokh, Ning Zhou, and Zhenyu Huang (July 2017). "Adaptive adjustment of noise covariance in Kalman filter for dynamic state estimation". In: *IEEE Power & Energy Society General Meeting*. IEEE, pp. 1–5. ISBN: 978-1-5386-2212-4. DOI: 10.1109/PESGM.2017.8273755. URL: http://ieeexplore.ieee.org/document/8273755/.

Alahakoon, Sanath et al. (Feb. 2013). "Unknown input sliding mode functional observers with application to sensorless control of permanent magnet synchronous machines". In: *Journal of the Franklin Institute* 350.1, pp. 107–128. ISSN: 0016-0032. DOI: 10.1016/J.JFRANKLIN.2012.10.012. URL: https://www.sciencedirect.com/science/article/pii/S0016003212002621.

Alameh, Kawthar (Dec. 2017). "Contribution au diagnostic et a l'analyse de défauts d'une machine synchrone à aimants permanents." PhD thesis. Normandy University. URL: https://tel.archives-ouvertes.fr/tel-01700940/.

Alameh, Kawthar et al. (Jan. 2015). "Vibration-based Fault Diagnosis Approach for Permanent Magnet Synchronous Motors". In: *IFAC-PapersOnLine* 48.21, pp. 1444–1450. ISSN: 2405-8963. DOI: 10.1016/J.IFACOL.2015.09.728. URL: https://www.sciencedirect.com/science/article/pii/S2405896315018571.

Ali, Anum et al. (Apr. 2017). "Technologies and challenges in developing Machine-to-Machine applications: A survey". In: *Journal of Network and Computer Applications* 83, pp. 124–139. ISSN: 10958592. DOI: 10.1016/j.jnca.2017.02.002. URL: http://www.sciencedirect.com/science/article/pii/S1084804517300620.

Althof, Rudimar Baesso and Moises Ferber (Apr. 2017). "Efficient uncertainty analysis of wind farms in the time domain using the Unscented Transform". In: *8th International Symposium on Power Electronics for Distributed Generation Systems (PEDG)*. Florianopolis: IEEE, pp. 1–4. ISBN: 978-1-5090-5339-1. DOI: 10.1109/PEDG.2017.7972467. URL: http://ieeexplore.ieee.org/document/7972467/.

Badoud, Abd Essalam et al. (May 2014). "Bond Graph Algorithms for Fault Detection and Isolation in Wind Energy Conversion". In: *Arabian Journal for Science and Engineering* 39.5, pp. 4057–4076. ISSN: 1319-8025. DOI: 10.1007/s13369-014-1044-4. URL: http://link.springer.com/10.1007/s13369-014-1044-4.

Bankov, Dmitry et al. (May 2017). "Fast centralized authentication in Wi-Fi HaLow networks". In: *International Conference on Communications (ICC)*. IEEE, pp. 1–6. ISBN: 978-1-4673-8999-0. DOI: 10.1109/ICC.2017.7996510. URL: http://ieeexplore.ieee.org/document/7996510/.

Bazzi, Rida A. and Goran Konjevod (Feb. 2007). "On the establishment of distinct identities in overlay networks". In: *Distributed Computing* 19.4, pp. 267–287. ISSN: 0178-2770. DOI: 10.1007/s00446-006-0012-y. URL: http://link.springer.com/10.1007/s00446-006-0012-y.

Becher, Alexander, Zinaida Benenson, and Maximillian Dornseif (2006). "Tampering with Motes: Real-World Physical Attacks on Wireless Sensor Networks". In: *International Conference on Security in Pervasive Computing (SPC)*. Springer, Berlin, Heidelberg, pp. 104–118. DOI: 10.1007/11734666_9. URL: http://link.springer.com/10.1007/11734666%7B%5C_%7D9.

Bin, Qin et al. (May 2014). "The maximum power control of direct-drive wind turbine". In: *26th Chinese Control and Decision Conference (2014 CCDC)*. IEEE, pp. 4834–4839. ISBN: 978-1-4799-3708-0. DOI: 10.1109/CCDC.2014.6853039. URL: http://ieeexplore.ieee.org/document/6853039/.

Blesa, Joaquim, Pedro Jimenez, et al. (2014). "An Interval NLPV Parity Equations Approach for Fault Detection and Isolation of a Wind Farm". In: *IEEE Transactions on Industrial Electronics*, pp. 1–1. ISSN: 3794-3805. DOI: 10.1109/TIE.2014.2386293. URL: http://ieeexplore.ieee.org/document/6998858/.

Blesa, Joaquim, Fatiha Nejjari, et al. (Oct. 2013). "Robust fault detection and isolation of wind turbines using interval observers". In: *Conference*

on Control and Fault-Tolerant Systems (SysTol). IEEE, pp. 353–358. ISBN: 978-1-4799-2855-2. DOI: 10.1109/SysTol.2013.6693854. URL: http://ieeexplore.ieee.org/document/6693854/.

Bocca, Maurizio et al. (Apr. 2011). "Structural Health Monitoring in Wireless Sensor Networks by the Embedded Goertzel Algorithm". In: *ACM Second International Conference on Cyber Physical Systems*, pp. 206–214. DOI: 10.1109/ICCPS.2011.19.

Borcehrsen, Anders Bech, Jesper Abildgaard Larsen, and Jakob Stoustrup (Jan. 2014). "Fault Detection and Load Distribution for the Wind Farm Challenge". In: *IFAC Proceedings Volumes* 47.3, pp. 4316–4321. ISSN: 1474-6670. DOI: 10.3182/20140824-6-ZA-1003.00704. URL: https://www.sciencedirect.com/science/article/pii/S1474667016422779.

Burkholder, Joshua (2013). *Online Covariance*. URL: https://joshuaburkholder.com/wordpress/2013/10/26/%7B%5C%%7D0Aonline-covariance/ (visited on 07/15/2018).

Carroll, James, Alasdair McDonald, and David McMillan (2015). "Reliability Comparison of Wind Turbines with DFIG and PMG Drive Trains". In: *IEEE Transactions on Energy Conversion* 30.2, pp. 663–670. ISSN: 0885-8969. DOI: 10.1109/TEC.2014.2367243.

Cherepanov, Anton (2017). "WIN32/INDUSTROYER: A new threat for industrial control systems". In: *Eset*, pp. 1–17. URL: https://www.welivesecurity.com/wp-content/uploads/2017/06/Win32%7B%5C_%7DIndustroyer.pdf (visited on 03/17/2019).

Chouiref, Houda et al. (Dec. 2015). "LPV model-based fault detection: Application to wind turbine benchmark". In: *7th International Conference on Modelling, Identification and Control (ICMIC)*. IEEE, pp. 1–5. ISBN: 978-0-9567-1575-3. DOI: 10.1109/ICMIC.2015.7409464. URL: http://ieeexplore.ieee.org/document/7409464/.

Collotta, Mario et al. (July 2018). "Bluetooth 5: A Concrete Step Forward toward the IoT". In: *IEEE Communications Magazine* 56.7, pp. 125–131. ISSN: 15581896. DOI: 10.1109/MCOM.2018.1700053. arXiv: 1711.00257. URL: https://ieeexplore.ieee.org/document/8419192/.

Culiță, Janetta and Dan Ștefănoiu (2008). *Modelare Analitică și Experimentală a Sistemelor*. București: PRINTECH. ISBN: 978-973-718-987-5.

Ed-dahmani, Chafik et al. (May 2018). "FPGA Based Variable Structure Control of Direct Drive Permanent Magnet Synchronous Generator Wind Power". In: *SSRN Electronic Journal*. ISSN: 1556-5068. DOI: 10.2139/ssrn.3185348. URL: https://www.ssrn.com/abstract=3185348.

Damiano, Alfonso et al. (June 2012). "A multi-phase PM synchronous generator torque control for direct-drive wind turbines". In: *International*

Symposium on Power Electronics Power Electronics, Electrical Drives, Automation and Motion. IEEE, pp. 962–968. ISBN: 978-1-4673-1301-8. DOI: 10.1109/SPEEDAM.2012.6264614. URL: http://ieeexplore.ieee.org/document/6264614/.

Deekshit Kompella, K. C., Mannam Venu Gopala Rao, and Rayapudi Srinivasa Rao (2017). "Bearing fault detection in a 3 phase induction motor using stator current frequency spectral subtraction with various wavelet decomposition techniques". In: *Ain Shams Engineering Journal*. ISSN: 20904479. DOI: 10.1016/j.asej.2017.06.002. URL: http://www.sciencedirect.com/science/article/pii/S2090447917300771.

Dhaouadi, Rached, Ned Mohan, and Lars E. Norum (July 1991). "Design and implementation of an extended Kalman filter for the state estimation of a permanent magnet synchronous motor". In: *IEEE Transactions on Power Electronics* 6.3, pp. 491–497. ISSN: 08858993. DOI: 10.1109/63.85891. URL: http://ieeexplore.ieee.org/document/85891/.

DNV GL (2015). *ISO 9001:2015 Quality Management Systems- Requirements*. Tech. rep. URL: https://www.dnvgl.be/publications/%7B%5C%%7D0Athe-new-iso-9001-2015-63171.

Duviella, Eric, Lisa Serir, and Moamar Sayed-Mouchaweh (Oct. 2013). "An evolving classification approach for fault diagnosis and prognosis of a wind farm". In: *Conference on Control and Fault-Tolerant Systems (SysTol)*. IEEE, pp. 377–382. ISBN: 978-1-4799-2855-2. DOI: 10.1109/SysTol.2013.6693940. URL: http://ieeexplore.ieee.org/document/6693940/.

Ebrahimi, Bashir Mahdi et al. (Apr. 2014). "Advanced Eccentricity Fault Recognition in Permanent Magnet Synchronous Motors Using Stator Current Signature Analysis". In: *IEEE Transactions on Industrial Electronics* 61.4, pp. 2041–2052. ISSN: 0278-0046. DOI: 10.1109/TIE.2013.2263777. URL: http://ieeexplore.ieee.org/document/6523080/.

Echavarria, E. et al. (2008). "Fault diagnosis system for an offshore wind turbine using qualitative physics". In: *Wind Energy Conference & Exhibition (EWEC)*. Ed. by Takis Chaviaropoulos. Brussel: EWEA, pp. 1–10. URL: http://citeseerx.ist.psu.edu/viewdoc/download?doi=10.1.1.462.2623%7B%5C&%7Drep=rep1%7B%5C&%7Dtype=pdf.

Enjie (2018). *ENGIE France Renewable Energy open data site — Engie France Renewable Energy open data site*. URL: https://opendata-renewables.engie.com/pages/home/ (visited on 01/20/2019).

Errami, Youssef et al. (May 2018). "Power Extraction Control of Variable Speed Wind Turbine Systems Based on Direct Drive Synchronous Generator in All Operating Regimes". In: *Journal of Electrical and Computer Engineering* 2018, pp. 1–17. ISSN: 2090-0147. DOI: 10.1155/2018/

3837959. URL: https://www.hindawi.com/journals/jece/2018/3837959/.

Espinosa, Antonio Garcia et al. (June 2010). "Fault Detection by Means of Hilbert–Huang Transform of the Stator Current in a PMSM With Demagnetization". In: *IEEE Transactions on Energy Conversion* 25.2, pp. 312–318. ISSN: 0885-8969. DOI: 10.1109/TEC.2009.2037922. URL: http://ieeexplore.ieee.org/document/5404255/.

European Union Agency for Network and Information Security (2017). *Communication network dependencies for ICS/SCADA Systems*. February. Athens, Greece: European Union Agency For Network and Information Security, p. 80. ISBN: 9789292041922. DOI: 10.2824/397676. URL: https://www.enisa.europa.eu/publications/ics-scada-dependencies.

Faiz, Jawad and Hossein Nejadi-Koti (Apr. 2016). "Demagnetization Fault Indexes in Permanent Magnet Synchronous Motors—An Overview". In: *IEEE Transactions on Magnetics* 52.4, pp. 1–11. ISSN: 0018-9464. DOI: 10.1109/TMAG.2015.2480379. URL: http://ieeexplore.ieee.org/document/7273933/.

Feng, Bo et al. (Nov. 2014). "Kalman Filter With Recursive Covariance Estimation—Sequentially Estimating Process Noise Covariance". In: *IEEE Transactions on Industrial Electronics* 61.11, pp. 6253–6263. ISSN: 0278-0046. DOI: 10.1109/TIE.2014.2301756. URL: http://ieeexplore.ieee.org/document/6719478/.

Feng, Yong et al. (Sept. 2009). "Hybrid Terminal Sliding-Mode Observer Design Method for a Permanent-Magnet Synchronous Motor Control System". In: *IEEE Transactions on Industrial Electronics* 56.9, pp. 3424–3431. ISSN: 0278-0046. DOI: 10.1109/TIE.2009.2025290. URL: http://ieeexplore.ieee.org/document/5089428/.

Fernandez-Canti, Rosa M. et al. (Dec. 2013). "Nonlinear set-membership identification and fault detection using a Bayesian framework: Application to the wind turbine benchmark". In: *52nd IEEE Conference on Decision and Control*. IEEE, pp. 496–501. ISBN: 978-1-4673-5717-3. DOI: 10.1109/CDC.2013.6759930. URL: http://ieeexplore.ieee.org/document/6759930/.

Foo, Gilbert Hock Beng, Xinan Zhang, and D. M. Vilathgamuwa (Aug. 2013). "A Sensor Fault Detection and Isolation Method in Interior Permanent-Magnet Synchronous Motor Drives Based on an Extended Kalman Filter". In: *IEEE Transactions on Industrial Electronics* 60.8, pp. 3485–3495. ISSN: 0278-0046. DOI: 10.1109/TIE.2013.2244537. URL: http://ieeexplore.ieee.org/document/6428675/.

Foo, Gilbert Hock Beng, Xinan Zhang, and Mahinda D. Vilathgamuwa (Aug. 2013). "A Sensor Fault Detection and Isolation Method in Interior

Permanent-Magnet Synchronous Motor Drives Based on an Extended Kalman Filter". In: *IEEE Transactions on Industrial Electronics* 60.8, pp. 3485–3495. ISSN: 0278-0046. DOI: 10.1109/TIE.2013.2244537. URL: http://ieeexplore.ieee.org/document/6428675/.

Gao, Zhen et al. (Jan. 2014). "A fault tolerant implementation of the Goertzel algorithm". In: *Microelectronics Reliability* 54.1, pp. 335–337. ISSN: 0026-2714. DOI: 10.1016/J.MICROREL.2013.08.012. URL: https://www.sciencedirect.com/science/article/pii/S0026271413003235.

Gliga, Lavinius Ioan, Houcine Chafouk, et al. (May 2017). "Fault Detection and Identification for Fire and Explosion Detection". In: *21st International Conference on Control Systems and Computer Science (CSCS)*. IEEE, pp. 43–50. ISBN: 978-1-5386-1839-4. DOI: 10.1109/CSCS.2017.13. URL: http://ieeexplore.ieee.org/document/7968541/.

— (Oct. 2018a). "Comparison of State Estimators for a Permanent Magnet Synchronous Generator". In: *22nd International Conference on System Theory, Control and Computing (ICSTCC)*. IEEE, pp. 474–479. ISBN: 978-1-5386-4444-7. DOI: 10.1109/ICSTCC.2018.8540746. URL: https://ieeexplore.ieee.org/document/8540746/.

— (Oct. 2018b). "Diagnosis of a Permanent Magnet Synchronous Generator using the Extended Kalman Filter and the Fast Fourier Transform". In: *7th International Conference on Systems and Control (ICSC)*. IEEE, pp. 65–70. ISBN: 978-1-5386-8537-2. DOI: 10.1109/ICoSC.2018.8587632. URL: https://ieeexplore.ieee.org/document/8587632/.

Gliga, Lavinius Ioan, Ciprian Lupu, et al. (May 2017). "Innovations in fault detection and tolerant control for a wind farm, using Wireless Sensor Networks". In: *18th International Carpathian Control Conference (ICCC)*. Sinaia: IEEE, pp. 332–336. ISBN: 978-1-5090-4862-5. DOI: 10.1109/CarpathianCC.2017.7970421. URL: http://ieeexplore.ieee.org/document/7970421/.

Gliga, Lavinius Ioan, Cosmin - Constantin Mihai, et al. (June 2015). "Adaptive - Robust control a computational efficient real time simulation". In: *2015 13th International Conference on Engineering of Modern Electric Systems (EMES)*. IEEE, pp. 1–4. ISBN: 978-1-4799-7649-2. DOI: 10.1109/EMES.2015.7158403. URL: http://ieeexplore.ieee.org/document/7158403/.

— (Jan. 2017). "Real Time & Power Efficient Adaptive - Robust Control". In: *Journal of Physics: Conference Series* 783.1. ISSN: 1742-6588. DOI: 10.1088/1742-6596/783/1/012034. URL: http://stacks.iop.org/1742-6596/783/i=1/a=012034?key=crossref.9eeeb6545f971049af748b39363c4d00.

Goertzel, Gerald (1958). "An Algorithm for the Evaluation of Finite Trigonometric Series". In: *The American Mathematical Monthly* 65.1, pp. 34–35.

ISSN: 0002-9890. DOI: 10.2307/2310304. URL: https://www.jstor.org/stable/2310304.

Grabia, Michal et al. (2017). "Design of a DASH7 low power wireless sensor network for Industry 4.0 applications". In: *International Conference on RFID Technology and Application (RFID-TA 2017)*, pp. 254–259. ISBN: 9781538618332. DOI: 10.1109/RFID-TA.2017.8098904.

Gritli, Yasser et al. (Sept. 2012). "Demagnetizations diagnosis for Permanent Magnet Synchronous Motors based on advanced Wavelet Analysis". In: *20th International Conference on Electrical Machines*. IEEE, pp. 2397–2403. ISBN: 978-1-4673-0142-8. DOI: 10.1109/ICElMach.2012.6350219. URL: http://ieeexplore.ieee.org/document/6350219/.

Hang, Jun et al. (Dec. 2015). "Online Interturn Fault Diagnosis of Permanent Magnet Synchronous Machine Using Zero-Sequence Components". In: *IEEE Transactions on Power Electronics* 30.12, pp. 6731–6741. ISSN: 0885-8993. DOI: 10.1109/TPEL.2015.2388493. URL: http://ieeexplore.ieee.org/document/7004080/.

Hassan, Sabo Miya et al. (Jan. 2017). "Application of Wireless Technology for Control: A WirelessHART Perspective". In: *Procedia Computer Science* 105, pp. 240–247. ISSN: 1877-0509. DOI: 10.1016/J.PROCS.2017.01.217. URL: https://www.sciencedirect.com/science/article/pii/S1877050917302405.

Hassan, Shaikh Shahriar et al. (2018). "Security threats in Bluetooth technology". In: *Computers and Security* 74, pp. 308–322. ISSN: 01674048. DOI: 10.1016/j.cose.2017.03.008. URL: http://www.sciencedirect.com/science/article/pii/S0167404817300615.

Hwang, Yitaek (2017). *The 2G Sunset and What it Means for IoT*. URL: https://www.leverege.com/blogpost/2g-sunset-iot (visited on 11/30/2017).

Idrissi, Imane, Rachid El bachtiri, and Houcine Chafouk (Dec. 2017). "A Bank of Kalman Filters for Current Sensors Faults Detection and Isolation of DFIG for Wind Turbine". In: *International Renewable and Sustainable Energy Conference (IRSEC)*. IEEE, pp. 1–6. ISBN: 978-1-5386-2847-8. DOI: 10.1109/IRSEC.2017.8477263. URL: https://ieeexplore.ieee.org/document/8477263/.

Ingenu (2016). *HOW RPMA WORKS: The Making of RPMA*. Ed. by •. Ingenu, p. 92. URL: http://www.ingenu.com/get-started/resources/.

International Renewable Energy Agency (2018). *Onshore Wind Power Now as Affordable as Any Other Source, Solar to Halve by 2020*. URL: /newsroom/pressreleases/2018/Jan/Onshore-Wind-Power-Now-as-Affordable-as-Any-%7B%5C%%7D5C%7B%5C%%7D5COther-Source (visited on 03/15/2019).

Jaradat, Manar et al. (2015). "The internet of energy: Smart sensor networks and big data management for smart grid". In: *Procedia Computer Science*. 10th International Conference on Future Networks and Communications (FNC) / 12th International Conference on Mobile Systems and Pervasive Computing (MobiSPC) 56.1, pp. 592–597. ISSN: 18770509. DOI: 10.1016/j.procs.2015.07.250. arXiv: 1801.07731. URL: http://www.sciencedirect.com/science/article/pii/S1877050915017317.

Kang, Jichuan, Liping Sun, and Carlos Guedes Soares (Apr. 2019). "Fault Tree Analysis of floating offshore wind turbines". In: *Renewable Energy* 133, pp. 1455–1467. ISSN: 0960-1481. DOI: 10.1016/J.RENENE.2018.08.097. URL: https://www.sciencedirect.com/science/article/pii/S0960148118310474.

Khan, Minhaj Ahmad and Khaled Salah (2018). "IoT security: Review, blockchain solutions, and open challenges". In: *Future Generation Computer Systems* 82, pp. 395–411. ISSN: 0167739X. DOI: 10.1016/j.future.2017.11.022. arXiv: 1705.08230. URL: http://www.sciencedirect.com/science/article/pii/S0167739X17315765.

Khemmar, Redouane et al. (2014). "The Application of RFID Technology in a Port". In: *International Journal of Computer Application* 86.7, pp. 41–50. ISSN: 09758887. DOI: 10.5120/15001-3249. URL: http://research.ijcaonline.org/volume86/number7/pxc3893249.pdf.

Koziy, Kostyantyn, Gou Bei, and Joel Aslakson (July 2013). "A Low-Cost Power-Quality Meter With Series Arc-Fault Detection Capability for Smart Grid". In: *IEEE Transactions on Power Delivery* 28.3, pp. 1584–1591. ISSN: 0885-8977. DOI: 10.1109/TPWRD.2013.2251753. URL: http://ieeexplore.ieee.org/document/6502756/.

Kulikov, Gennady Y. and Maria V. Kulikova (July 2017). "Do the Cubature and Unscented Kalman Filtering Methods Outperform Always the Extended Kalman Filter ?" In: *IFAC-PapersOnLine* 50.1, pp. 3762–3767. ISSN: 2405-8963. DOI: 10.1016/J.IFACOL.2017.08.478. URL: https://www.sciencedirect.com/science/article/pii/S2405896317308418.

Kushner, David (2013). *The Real Story of Stuxnet*. URL: https://spectrum.ieee.org/telecom/security/the-real-story-of-stuxnet (visited on 09/08/2018).

LEM (2013). *Voltage transducer DVL 500*. Tech. rep., p. 8. URL: https://www.lem.com/sites/default/files/products%7B%5C_%7Ddatasheets/dvl%7B%5C_%7D500.pdf.

— (n.d.). *Current Transducer HAIS 50..400-P and HAIS 50..100-TP*. Tech. rep., p. 3. URL: http://www.farnell.com/datasheets/1681212.pdf.

Levy, Simon D. (2016). *The Extended Kalman Filter: An Interactive Tutorial for Non-Experts*. URL: https://home.wlu.edu/%7B~%7Dlevys/kalman%7B%5C_%7Dtutorial/ (visited on 03/15/2018).

Liu, Zhentong and Hongwen He (Jan. 2017). "Sensor fault detection and isolation for a lithium-ion battery pack in electric vehicles using adaptive extended Kalman filter". In: *Applied Energy* 185, pp. 2033–2044. ISSN: 0306-2619. DOI: 10.1016/J.APENERGY.2015.10.168. URL: https://www.sciencedirect.com/science/article/pii/S0306261915014105.

London Array Limited (2018). *The Project*. URL: http://www.londonarray.com/the-project-3/ (visited on 04/28/2019).

Lopez Pulgarin, Erwin Jose and Jorge Ivan Sofrony Esmeral (Sept. 2016). "Data-driven FDI for wind farms using W-SVM". In: *2016 IEEE International Symposium on Intelligent Control (ISIC)*. IEEE, pp. 1–6. ISBN: 978-1-5090-2051-5. DOI: 10.1109/ISIC.2016.7579979. URL: http://ieeexplore.ieee.org/document/7579979/.

Lyons, Richard G. (2010). *Understanding Digital Signal Processing*. 3rd. Vol. 1. Prentice Hall. ISBN: 978-0-13-702741-5.

Lyons, Rick (2015). *Correcting an Important Goertzel Filter Misconception*. URL: https://www.dsprelated.com/showarticle/796.php (visited on 12/05/2018).

Mahmood, Anzar, Nadeem Javaid, and Sohail Razzaq (2015). "A review of wireless communications for smart grid". In: *Renewable and Sustainable Energy Reviews* 41, pp. 248–260. ISSN: 13640321. DOI: 10.1016/j.rser.2014.08.036. URL: https://linkinghub.elsevier.com/retrieve/pii/S1364032114007126.

Marché, Vincent (2017). *Electric Rotating Machine Eccentricities Faults Analysis with Flux*. URL: https://insider.altairhyperworks.com/electric-motor-static-dynamic-and-mixed-eccentricities-analysis-in-flux-finite-element-software/ (visited on 07/25/2019).

MathWorks (2018). *Choose a Solver*. URL: https://fr.mathworks.com/help/simulink/ug/%7B%5C%%7D0Atypes-of-solvers.html?searchHighlight%7B%5C%%7D5C=choose%7B%5C%%7D5C%20a%7B%5C%%7D5C%7B%5C%%7D0A%20solver%7B%5C%%7D5C%7B%5C&%7Ds%7B%5C_%7Dtid%7B%5C%%7D5C=doc%7B%5C%%7D5C%7B%5C_%7Dsrchtitle (visited on 07/20/2018).

Meng, Yanjing and Wenzhan Gong (2012). "Design of SCADA System Based on Wireless Communication for Offshore Wind Farm". In: *Recent Advances in Computer Science and Information Engineering* 4, pp. 347–352. DOI: 10.1007/978-3-642-25769-8_50. URL: https://link.springer.com/chapter/10.1007/978-3-642-25769-8%7B%5C_%7D50.

Microchip (2018). *MiWi Protocol*. URL: https://www.microchip.com/design-centers/wireless-connectivity/embedded-wireless%7B%5C%%7D5C%7B%5C%%7D5C/802-15-4/software/miwi-protocol (visited on 05/24/2018).

Mohan, Ned (2012). *Electric power systems : a first course*. John Wiley & Sons, p. 243. ISBN: 9781118074794.

Moness, Mohammed and Ahmed Mahmoud Moustafa (Apr. 2016). "A Survey of Cyber-Physical Advances and Challenges of Wind Energy Conversion Systems: Prospects for Internet of Energy". In: *IEEE Internet of Things Journal* 3.2, pp. 134–145. ISSN: 23274662. DOI: 10.1109/JIOT.2015.2478381.

Morel, Florent et al. (July 2009). "A Comparative Study of Predictive Current Control Schemes for a Permanent-Magnet Synchronous Machine Drive". In: *IEEE Transactions on Industrial Electronics* 56.7, pp. 2715–2728. ISSN: 0278-0046. DOI: 10.1109/TIE.2009.2018429. URL: http://ieeexplore.ieee.org/document/4812111/.

Napolitano, Antonio (Mar. 2016). "Cyclostationarity: New trends and applications". In: *Signal Processing* 120, pp. 385–408. ISSN: 0165-1684. DOI: 10.1016/J.SIGPRO.2015.09.011. URL: https://www.sciencedirect.com/science/article/pii/S0165168415003138.

Nejad, Amir Rasekhi et al. (2014). "A prognostic method for fault detection in wind turbine drivetrains". In: *Engineering Failure Analysis* 42, pp. 324–336. ISSN: 13506307. DOI: 10.1016/j.engfailanal.2014.04.031. URL: https://www.sciencedirect.com/science/article/abs/pii/S1350630714001459.

Niu, Gang and Senyi Liu (Mar. 2018). "Demagnetization monitoring and life extending control for permanent magnet-driven traction systems". In: *Mechanical Systems and Signal Processing* 103, pp. 264–279. ISSN: 0888-3270. DOI: 10.1016/J.YMSSP.2017.10.003. URL: https://www.sciencedirect.com/science/article/pii/S0888327017305290.

Nwave (2017). *Smart Parking Technology That Will Change The World*. URL: https://www.nwave.io/ (visited on 10/30/2018).

Ogidi, Oladapo Omotade, Paul S. Barendse, and Mohamed A. Khan (July 2016). "Fault diagnosis and condition monitoring of axial-flux permanent magnet wind generators". In: *Electric Power Systems Research* 136, pp. 1–7. ISSN: 03787796. DOI: 10.1016/j.epsr.2016.01.018. URL: https://www.sciencedirect.com/science/article/abs/pii/S0378779616300049.

Oppenheim, Alan V., Ronald W. Schafer, and John R. Buck (1999). *Discrete-time signal processing*. 2nd. Upper Saddle River, N.J.: Prentice Hall. ISBN: 978-0-13-754920-7.

Ørsted (2017). *Walney Extension Wind Farm*. Tech. rep. URL: https://walneyextension.co.uk/-/media/WWW/Docs/Corp/UK/Walney-extension/180822%7B%5C_%7DWalney-Extension-Project-Summary-V4.ashx?la=en%7B%5C&%7Dhash=4F8D0C0F6EE86D9300B36D2DEFB3462DA4A9C419 (visited on 05/17/2019).

Park, Pangun et al. (2018). "Wireless Network Design for Control Systems: A Survey". In: *IEEE Communications Surveys and Tutorials* 20.2, pp. 978–1013. ISSN: 1553877X. DOI: 10.1109/COMST.2017.2780114. arXiv: 1708.07353.

Pillay, Pragasen and Ramu Krishnan (1989). "Modeling, simulation, and analysis of permanent-magnet motor drives. I. The permanent-magnet synchronous motor drive". In: *IEEE Transactions on Industry Applications* 25.2, pp. 265–273. ISSN: 00939994. DOI: 10.1109/28.25541. URL: http://ieeexplore.ieee.org/document/25541/.

Pinar Pérez, Jesús María et al. (July 2013). "Wind turbine reliability analysis". In: *Renewable and Sustainable Energy Reviews* 23, pp. 463–472. ISSN: 1364-0321. DOI: 10.1016/J.RSER.2013.03.018. URL: https://www.sciencedirect.com/science/article/pii/S1364032113001779.

Pintea, Andreea, Dumitru Popescu, and Pierre Borne (June 2010). "Robust control for wind power systems". In: *18th Mediterranean Conference on Control and Automation, MED'10*. IEEE, pp. 1085–1091. ISBN: 978-1-4244-8091-3. DOI: 10.1109/MED.2010.5547647. URL: http://ieeexplore.ieee.org/document/5547647/.

Popescu, Dumitru et al. (2006). *Automatică Industrială*. București: Agir, p. 384. ISBN: 973-720093-4.

Prauzek, Michal et al. (2016). "NFC Interface for Standalone Data Acquisition Device". In: *IFAC-PapersOnLine*. 14th IFAC Conference on Programmable Devices and Embedded Systems (PDES) 49.25, pp. 437–441. ISSN: 24058963. DOI: 10.1016/j.ifacol.2016.12.051. URL: http://www.sciencedirect.com/science/article/pii/S2405896316326878.

Qiao, Wei and Dingguo Lu (Oct. 2015a). "A Survey on Wind Turbine Condition Monitoring and Fault Diagnosis—Part I: Components and Subsystems". In: *IEEE Transactions on Industrial Electronics* 62.10, pp. 6536–6545. ISSN: 0278-0046. DOI: 10.1109/TIE.2015.2422112. URL: http://ieeexplore.ieee.org/document/7084135/.

— (Oct. 2015b). "A Survey on Wind Turbine Condition Monitoring and Fault Diagnosis—Part II: Signals and Signal Processing Methods". In: *IEEE*

Transactions on Industrial Electronics 62.10, pp. 6546–6557. ISSN: 0278-0046. DOI: 10.1109/TIE.2015.2422394. URL: http://ieeexplore.ieee.org/document/7084650/.

Qiu, Zhenbing, Huaming Qian, and Guoqing Wang (Apr. 2018). "Adaptive robust cubature Kalman filtering for satellite attitude estimation". In: *Chinese Journal of Aeronautics* 31.4, pp. 806–819. ISSN: 1000-9361. DOI: 10.1016/J.CJA.2018.01.023. URL: https://www.sciencedirect.com/science/article/pii/S1000936118300414.

Queiroz, Diego V. et al. (Nov. 2017). "Survey and systematic mapping of industrial Wireless Sensor Networks". In: *Journal of Network and Computer Applications* 97, pp. 96–125. ISSN: 1084-8045. DOI: 10.1016/J.JNCA.2017.08.019. URL: https://www.sciencedirect.com/science/article/pii/S1084804517302771.

Reddi, Sashank J., Satyen Kale, and Sanjiv Kumar (Apr. 2019). "On the Convergence of Adam and Beyond". In: arXiv: 1904.09237. URL: http://arxiv.org/abs/1904.09237.

Reljic, Dejan, Josif Tomic, and Zeljko Kanovic (2015). "Application of the Goertzel's algorithm in the airgap mixed eccentricity fault detection". In: *Serbian Journal of Electrical Engineering* 12.1, pp. 17–32. ISSN: 1451-4869, 2217-7183. DOI: 10.2298/SJEE1501017R. URL: http://www.doiserbia.nb.rs/Article.aspx?ID=1451-48691501017R.

Riera-Guasp, Martin, Jose A. Antonino-Daviu, and Gerard-Andre Capolino (Mar. 2015). "Advances in Electrical Machine, Power Electronic, and Drive Condition Monitoring and Fault Detection: State of the Art". In: *IEEE Transactions on Industrial Electronics* 62.3, pp. 1746–1759. ISSN: 0278-0046. DOI: 10.1109/TIE.2014.2375853. URL: http://ieeexplore.ieee.org/document/6975204/.

Rolan, Alejandro et al. (July 2009). "Modeling of a variable speed wind turbine with a Permanent Magnet Synchronous Generator". In: *IEEE International Symposium on Industrial Electronics*. IEEE, pp. 734–739. ISBN: 978-1-4244-4347-5. DOI: 10.1109/ISIE.2009.5218120. URL: http://ieeexplore.ieee.org/document/5218120/.

Roux, Wiehan le, Ronald G Harley, and Thomas G Habetler (Jan. 2007). "Detecting Rotor Faults in Low Power Permanent Magnet Synchronous Machines". In: *IEEE Transactions on Power Electronics* 22.1, pp. 322–328. ISSN: 0885-8993. DOI: 10.1109/TPEL.2006.886620. URL: http://ieeexplore.ieee.org/document/4052417/.

Ruijters, Enno and Mariëlle Stoelinga (Feb. 2015). "Fault tree analysis: A survey of the state-of-the-art in modeling, analysis and tools". In: *Computer Science Review* 15-16, pp. 29–62. ISSN: 1574-0137. DOI: 10.1016/J.COSREV.2015.03.001. URL: https://www.sciencedirect.com/science/article/pii/S1574013715000027.

Sahraoui, Mohamed et al. (Sept. 2014). "Detection of inter-turn short-circuit in induction motors using Park–Hilbert method". In: *International Journal of System Assurance Engineering and Management* 5.3, pp. 337–351. ISSN: 0975-6809. DOI: 10.1007/s13198-013-0173-6. URL: http://link.springer.com/10.1007/s13198-013-0173-6.

Sapena-Bano, Angel et al. (2018). "Using the Goertzel Algorithm Over Disjoint Narrow Frequency Bands for Fault Diagnosis of Induction Motors". In: *13th International Conference on Electrical Machines ICEM*, pp. 1965–1971. DOI: 10.1109/ICELMACH.2018.8506967.

Schlechtingen, Meik, Ilmar Ferreira Santos, and Sofiane Achiche (Jan. 2013). "Wind turbine condition monitoring based on SCADA data using normal behavior models. Part 1: System description". In: *Applied Soft Computing* 13.1, pp. 259–270. ISSN: 1568-4946. DOI: 10.1016/J.ASOC.2012.08.033. URL: https://www.sciencedirect.com/science/article/pii/S1568494612003821.

Shahriari, Sayyed Ali Akbar et al. (Oct. 2016). "Dynamic state estimation of a permanent magnet synchronous generator-based wind turbine". In: *IET Renewable Power Generation* 10.9, pp. 1278–1286. ISSN: 1752-1416. DOI: 10.1049/iet-rpg.2015.0502. URL: https://digital-library.theiet.org/content/journals/10.1049/iet-rpg.2015.0502.

Silva, Jonathan de Carvalho et al. (2017). "LoRaWAN - A Low Power WAN Protocol for Internet of Things: a Review and Opportunities". In: *2nd International Multidisciplinary Conference on Computer and Energy Science (SpliTech)*, pp. 1–6. ISBN: 9781538605516. DOI: 10.1109/ATSIP.2017.8075570. URL: https://ieeexplore.ieee.org/abstract/document/8019271.

Simani, Silvio, Saverio Farsoni, and Paolo Castaldi (June 2015). "Fault Diagnosis of a Wind Turbine Benchmark via Identified Fuzzy Models". In: *IEEE Transactions on Industrial Electronics* 62.6, pp. 3775–3782. ISSN: 0278-0046. DOI: 10.1109/TIE.2014.2364548. URL: http://ieeexplore.ieee.org/lpdocs/epic03/wrapper.htm?arnumber=6933934.

Singh, Brajendra Kumar et al. (2013). "Survey on communication architectures for wind energy integration with the smart grid". In: *International Journal of Environmental Studies* 70.5, pp. 765–776. ISSN: 00207233. DOI: 10.1080/00207233.2013.798501. URL: http://www.tandfonline.com/doi/abs/10.1080/00207233.2013.798501.

Singh, Virendra Pal, Sweta Jain, and Jyoti Singhai (2010). "Hello Flood Attack and its Countermeasures in Wireless Sensor Networks". In: *International Journal of Computer Science Issues* 7.11. ISSN: 1694-0814. URL: www.IJCSI.org.

Sinha, Rashmi Sharan, Yiqiao Wei, and Seung Hoon Hwang (2017). "A survey on LPWA technology: LoRa and NB-IoT". In: *ICT Express* 3.1, pp. 14–21. ISSN: 24059595. DOI: 10.1016/j.icte.2017.03.004. URL: http://www.sciencedirect.com/science/article/pii/S2405959517300061.

Song, Yonghua et al. (Aug. 2017). "An Internet of Energy Things Based on Wireless LPWAN". In: *Engineering* 3.4, pp. 460–466. ISSN: 20958099. DOI: 10.1016/J.ENG.2017.04.011. URL: http://www.sciencedirect.com/science/article/pii/S2095809917306057.

Staggs, Jason, David Ferlemann, and Sujeet Shenoi (2017). "Wind farm security: attack surface, targets, scenarios and mitigation". In: *International Journal of Critical Infrastructure Protection* 17, pp. 3–14. ISSN: 18745482. DOI: 10.1016/j.ijcip.2017.03.001. URL: http://www.sciencedirect.com/science/article/pii/S1874548217300434.

Ștefănoiu, Dan and Janetta Culiță (Mar. 2009). "Kalman Filtering of Distributed Time Series". In: *17th International Conference on Control Systems and Computer Science (CSCS)*. Bucharest, pp. 101–108. DOI: 10.1007/978-1-4615-0931-8_7. arXiv: 1703.07194. URL: http://arxiv.org/abs/1703.07194.

Styczynski, Jake, Nate Beach-Westmoreland, and Scott Stables (2016). "Industrial Cybersecurity Threat Briefing". In: URL: https://cdn2.hubspot.net/hubfs/407136/PDFs/Booz%7B%5C_%7DAllen/Industrial%7B%5C_%7DCybersecurity%7B%5C_%7D%7B%5C%%7D5C%7B%5C%%7D5CThreat%7B%5C_%7DBriefing.pdf?t%7B%5C%%7D5C=1473881858278 (visited on 06/10/2019).

Subhashini, M. and Venkateswara A. Rao (n.d.). "Internet based sensor networking & home automation using cortex processor on Linux platform (Raspberry Pi2)". In: *International Conference on Signal Processing, Communication, Power and Embedded System, SCOPES 2016 - Proceedings*, pp. 456–460. ISBN: 9781509046201. DOI: 10.1109/SCOPES.2016.7955872.

Sysel, Petr and Pavel Rajmic (2012). "Goertzel algorithm generalized to non-integer multiples of fundamental frequency". In: *EURASIP Journal on Advances in Signal Processing* 2012.1. ISSN: 1687-6180. DOI: 10.1186/1687-6180-2012-56. URL: https://asp-eurasipjournals.springeropen.com/articles/10.1186/1687-6180-2012-56.

Tayebi, Arash, Setevan Berber, and Akshya Swain (2013). "Wireless Sensor Network attacks: An overview and critical analysis". In: *Proceedings of the International Conference on Sensing Technology, ICST*, pp. 97–102. ISBN: 9781467352215. DOI: 10.1109/ICSensT.2013.6727623.

Teng, Wei et al. (2016). "Detection and Quantization of Bearing Fault in Direct Drive Wind Turbine via Comparative Analysis". In: *Shock and Vibration* 2016, pp. 1–12. ISSN: 1070-9622. DOI: 10.1155/2016/2378435. URL: http://www.hindawi.com/journals/sv/2016/2378435/.

Terejanu, Gabriel A. (2008). *Unscented Kalman Filter Tutorial*. Tech. rep. Buffalo, New York, Web: Department of Computer Science and Engineering, University at Buffalo, p. 6. URL: https://cse.sc.edu/%7B~%7Dterejanu/files/tutorialUKF.pdf.

Thread Group (2017). *What is Thread Thread Benefits*. URL: https://www.threadgroup.org/What-is-Thread%7B%5C#%7DThreadbenefits (visited on 11/26/2018).

ThreatLabZ (2017). *Mid-year Threat Research Report*.

TransÉnergie Technologies Inc (2003). *User's Guide For Use with Simulink ®*. Tech. rep. MathWorks. URL: https://www.mathworks.com/help/releases/R13sp2/pdf%7B%5C_%7Ddoc/physmod/powersys/powersys.pdf (visited on 09/14/2018).

Val, Thierry, Fabrice Peyrard, and Michel Misson (2003). "Study and simulation of the infrared WLAN IrDA: An alternative to the radio". In: *Computer Communications*. Ubiquitous {Computing} 26.11, pp. 1210–1218. ISSN: 01403664. DOI: 10.1016/S0140-3664(02)00255-4. URL: http://www.sciencedirect.com/science/article/pii/S0140366402002554.

Van der Merwe, R. and Eric A. Wan (2001). "The square-root unscented Kalman filter for state and parameter-estimation". In: *International Conference on Acoustics, Speech, and Signal Processing (ICASSP)*. Vol. 6. Salt Lake City: IEEE, pp. 3461–3464. ISBN: 0-7803-7041-4. DOI: 10.1109/ICASSP.2001.940586. URL: http://ieeexplore.ieee.org/document/940586/.

Venkatasubramanian, Venkat, Raghunathan Rengaswamy, and Surya N. Kavuri (2003). "A review of process fault detection and diagnosis: {Part} {II}: {Qualitative} models and search strategies". In: *Computers & Chemical Engineering* 27.3, pp. 313–326. ISSN: 0098-1354. DOI: 10.1016/S0098-1354(02)00161-8. URL: http://www.sciencedirect.com/science/article/pii/S0098135402001618.

Venkatasubramanian, Venkat, Raghunathan Rengaswamy, Surya N. Kavuri, and Kewen Yin (2003). "A review of process fault detection and diagnosis: {Part} {III}: {Process} history based methods". In: *Computers & Chemical Engineering* 27.3, pp. 327–346. ISSN: 0098-1354. DOI: 10.1016/S0098-1354(02)00162-X. URL: http://www.sciencedirect.com/science/article/pii/S009813540200162X.

Venkatasubramanian, Venkat, Raghunathan Rengaswamy, Kewen Yin, et al. (2003). "A review of process fault detection and diagnosis: {Part} {I}:

{Quantitative} model-based methods". In: *Computers & Chemical Engineering* 27.3, pp. 293–311. ISSN: 0098-1354. DOI: 10.1016/S0098-1354(02)00160-6. URL: http://www.sciencedirect.com/science/article/pii/S0098135402001606.

Vestas (2017). *Innovations Offshore Wind Turbines*. URL: http://www.mhivestasoffshore.com/innovations/ (visited on 03/12/2019).

Vijitha, K. and Manickavasagam Parvathy Selvan (2013). "Performance analysis of distribution network with optimally sized WTGS based DGs considering wind speed variation". In: *2013 Annual IEEE India Conference, INDICON 2013*, pp. 1–6. ISBN: 9781479922758. DOI: 10.1109/INDCON.2013.6725962.

Vyas, Kashyap (2018). *The 11 Biggest Wind Farms and Wind Power Constructions That Reduce Carbon Footprint*. URL: https://interestingengineering.com/the-11-biggest-wind-farms-and-wind-power-constructions-that-reduce-carbon-footprint (visited on 07/31/2019).

Walsh, Colin and Ivan Pineda (2019). "Wind energy in Europe in 2018". In: URL: https://windeurope.org/wp-content/uploads/files/about-wind/statistics/WindEurope-Annual-Statistics-2018.pdf (visited on 07/24/2019).

Wang, Shuangyuan et al. (Nov. 2016). "Wind turbines abnormality detection through analysis of wind farm power curves". In: *Measurement* 93, pp. 178–188. ISSN: 0263-2241. DOI: 10.1016/J.MEASUREMENT.2016.07.006. URL: https://www.sciencedirect.com/science/article/pii/S0263224116303657.

Xi, Yanhui et al. (May 2018). "Detection of power quality disturbances using an adaptive process noise covariance Kalman filter". In: *Digital Signal Processing* 76, pp. 34–49. ISSN: 1051-2004. DOI: 10.1016/J.DSP.2018.01.013. URL: https://www.sciencedirect.com/science/article/pii/S1051200418300253.

Xiao, Mengli et al. (Apr. 2018). "An adaptive three-stage extended Kalman filter for nonlinear discrete-time system in presence of unknown inputs". In: *ISA Transactions* 75, pp. 101–117. ISSN: 00190578. DOI: 10.1016/j.isatra.2018.02.007. URL: http://www.ncbi.nlm.nih.gov/pubmed/29471968%20https://linkinghub.elsevier.com/retrieve/pii/S0019057818300661.

Xingzhen, Bai et al. (Sept. 2008). "Design of Wireless Sensor Network in SCADA system for wind power plant". In: *International Conference on Automation and Logistics*. IEEE, pp. 3023–3027. ISBN: 978-1-4244-2502-0. DOI: 10.1109/ICAL.2008.4636697. URL: http://ieeexplore.ieee.org/document/4636697/.

Yan, Jianhu et al. (June 2014). "Control of a grid-connected direct-drive wind energy conversion system". In: *Renewable Energy* 66, pp. 371–380. ISSN: 0960-1481. DOI: 10.1016/J.RENENE.2013.12.037. URL: https://www.sciencedirect.com/science/article/pii/S0960148114000081.

Yang, Wenxian et al. (May 2014). "Wind turbine condition monitoring: technical and commercial challenges". In: *Wind Energy* 17.5, pp. 673–693. ISSN: 10954244. DOI: 10.1002/we.1508. URL: http://doi.wiley.com/10.1002/we.1508.

Yassa, Nacera and M'hemed Rachek (May 2018). "Modeling and detecting the stator winding inter turn fault of permanent magnet synchronous motors using stator current signature analysis". In: *Mathematics and Computers in Simulation*. ISSN: 0378-4754. DOI: 10.1016/J.MATCOM.2018.04.012. URL: https://www.sciencedirect.com/science/article/abs/pii/S0378475418300983.

Zaabi, Khulood Al (June 2016). "Android device hacking tricks and countermeasures". In: *International Conference on Cybercrime and Computer Forensic (ICCCF)*. IEEE, pp. 1–10. ISBN: 978-1-5090-6096-2. DOI: 10.1109/ICCCF.2016.7740441. URL: http://ieeexplore.ieee.org/document/7740441/.

Zeman, Krystof et al. (n.d.). "Wireless M-BUS in Industrial IoT: Technology Overview and Prototype Implementation". In: *23th European Wireless Conference*, pp. 1–6.

Zhang, Qing, Luyao Tan, and Guanghua Xu (Feb. 2018). "Evaluating transient performance of servo mechanisms by analysing stator current of PMSM". In: *Mechanical Systems and Signal Processing* 101, pp. 535–548. ISSN: 0888-3270. DOI: 10.1016/J.YMSSP.2017.09.011. URL: https://www.sciencedirect.com/science/article/pii/S0888327017304879.

Zhifu, Wang et al. (Aug. 2014). "A review of Permanent Magnet Synchronous Motor fault diagnosis". In: *2014 IEEE Conference and Expo Transportation Electrification Asia-Pacific (ITEC Asia-Pacific)*. IEEE, pp. 1–5. ISBN: 978-1-4799-4239-8. DOI: 10.1109/ITEC-AP.2014.6940870. URL: https://ieeexplore.ieee.org/document/6940870/.

Abstract: Direct Drive Wind Turbines (DDWTs) are equipped with Permanent Magnet Synchronous Generators (PMSGs). Their three most common failures are demagnetization, eccentricity (static, dynamic and mixed) and inter-turn short circuit. Machine Current Signature Analysis is often used to look for generator problems, as these impairments introduce additional harmonics into the generated currents. The Fast Fourier Transform (FFT) is utilized to compute the spectrum of the currents. However, the FFT calculates the whole spectrum, while the number of possible faults and the number of introduced harmonics is low. The Goertzel algorithm, implemented as a filter (the Goertzel filter), is presented as a more efficient alternative to the FFT. The spectrum of the currents changes with the wind speed, and thus the detection is made more difficult. The Extended Kalman Filter (EKF) is proposed as a solution. The spectrum of the residuals, computed between the estimated and the generated current, is constant, regardless of the wind speed. However, the effect of the faults is visible in the spectrum. When using the EKF, one challenge is to find out the covariance matrix of the process noise. A new method was developed in this regard, which does not use any of the matrices of the filter. DDWTs are either placed in remote areas or in cities. For the monitoring of a DDWT, tens or hundreds of kilometers of cables are necessary. Wireless Sensor Networks (WSNs) are suited to be used in the communication infrastructure of DDWTs. WSNs have lower initial and maintenance costs, and they are quickly installed. Moreover, they can complement wired networks. Different wireless technologies are compared - both wide area ones, as well as short range technologies which support high data rates.
Keywords: Direct Drive Wind Turbines; Permanent Magnet Synchronous Generator; Extended Kalman Filter; Process Covariance Estimation; Fast Fourier Transform; Goertzel Filter; Wireless Sensor Networks.

Résume: Les Éoliennes à Entraînement Direct (ÉED) sont équipées de Générateurs Synchrones à Aimants Permanents (GSAP). Leurs trois plus courantes défaillances sont la démagnétisation, l'excentricité (statique, dynamique et mixte) et le court-circuit inter-tour. L'analyse de la signature du courant de la machine est souvent utilisée pour rechercher des problèmes du générateur, car ces altérations introduisent des harmoniques supplémentaires dans les courants générés. La Transformée de Fourier Rapide (TFR) est utilisée pour calculer le spectre des courants. Cependant, la TFR permet de calculer l'ensemble du spectre, tandis que le nombre de défauts possible et le nombre d'harmoniques introduites sont faibles. L'algorithme de Goertzel, mis en œuvre sous forme de filtre (le filtre de Goertzel), est présenté comme une alternative plus efficace au TFR. Le spectre des courants change avec la vitesse du vent, ce qui rend la détection plus difficile. Le Filtre de Kalman Étendu (FKÉ) est proposé comme solution. Le spectre de résidus, calcule entre les courants estimés et les courants générés, est constant, quelle que soit la vitesse du vent. Cependant, l'effet des défauts est visible dans leur spectre. Lors de l'utilisation de l'FKÉ, un défi consiste à estime la matrice de covariance pour le bruit du processus. Une nouvelle méthode était développée pour ça, qui n'utilise aucune de maîtrise du filtre. Les ÉED sont placés soit dans des zones éloignées, soit dans des villes. Pour la surveillance des ÉED, des dizaines ou des centaines de kilomètres de câbles sont nécessaires. Les Réseaux de Capteurs sans Fil (RCF) sont bien adaptés pour être utilisés dans l'infrastructure de communication des ÉED. RCF ont des coûts initiaux et d'entretien plus faibles et leurs installations sont rapides. De plus, ils peuvent compléter les réseaux câblés. Différentes technologies sans fil sont comparées : les technologies à grande surface, ainsi que les technologies à courte portée qui supportent des débits de données élevés.
Mots clé: Éoliennes à Entraînement Direct; Générateur Synchrones à Aimants Permanents; Filtre de Kalman Étendu; Estimation du Covariance du Bruit du Processus; Transformée de Fourier; Filtre de Goertzel; Réseaux de Capteurs sans Fil.

Rezumat: Turbinele Eoliene cu Acționare Directă (TEAD) sunt echipate cu Generatoare Sincrone cu Magneți Permanenți (GSMP). Cele mai comune defecte ale acestora sunt demagnetizarea, excentricitatea (statică, dinamică și mixtă) și scurtcircuitul inter spire. Analiza Semnăturii Curenților Mașinii (ASCM) este deseori folosită pentru a căuta probleme ale generatorului, deoarece aceste defecte introduc armonici suplimentare în curenții generați. Transformarea Fourier Rapidă (TFR) este utilizată pentru a calcula spectrul curenților. Dar, TFR calculează întregul spectru, pe când numărul de defecte posibile, și numărul de armonici introduse, este mic. Algoritmul lui Goertzel, implementat ca un filtru (filtrul Goetzel), este presentat ca o alternativă mai eficientă la TFR. Spectrul curenților se schimbă cu viteza vântului, iar detecția este mai dificilă. Filtrul Kalman Extins (FKE) este propus ca o soluție. Spectrul reziduurilor, calculat între curenții estimați și cei generați, este constant, indiferent de viteza vântului. Totuși, efectul defectelor este vizibil în acest spectru. O provocare, în utilizarea FKE-ului, este aflarea matricei de covarianță a zgomotului de proces. O nouă metodă a fost concepută în acest sens, care nu utilizează niciuna dintre matricele filtrului. TEAD sunt amplasate în zone rurale sau în orașe. Pentru monitorizare unor TEAD, sunt necesari zeci sau sute de kilometrii de cabluri. Rețelele de Sensori fără Fir (RSF) sunt adecvate pentru a fi folosite în infrastructura de comunicație a unor TEAD. RSF au costuri inițiale și de instalare sunt mai mici, și pot fi rapid instalate. Mai mult, ele pot complementa rețelele cu fir. Diferite tehnologii fără fir sunt comparate - atât cele cu acoperire mare, cât și cele care oferă viteze mari dar acoperire mai mică.
Cuvinte cheie: Turbine Eoliene cu Acționare Directă; Generator Sincron cu Magneți Permanenți; Filtrul Kalman Extins; Estimarea Covarianței Procesului; Transformarea Fourier Rapidă; Filtrul Goertzel; Rețele de Senzori fără Fir.